Muhammad Qazi Adil

Volume Integral Equations for the Study of Electromagnetic Scattering by Bi-anisotropic Objects

School of Electrical Engineering

Thesis submitted for examination for the degree of Master of Science in Technology.

Espoo, September 28, 2013

Thesis supervisor:

Prof. Ari Sihvola

Thesis instructors:

Ph.D., Docent Pasi Ylä-Oijala

D.Sc. Johannes Markkanen

Aalto University
School of Electrical
Engineering

AALTO UNIVERSITY
SCHOOL OF ELECTRICAL ENGINEERING

ABSTRACT OF THE
MASTER'S THESIS

Author: Muhammad Qazi Adil

Title: Volume Integral Equations for the Study of Electromagnetic Scattering by Bi-anisotropic Objects

Date: September 28, 2013 Language: English Number of pages:10+63

Department of Radio Science and Engineering

Professorship: Electromagnetics Code: S-96

Supervisor: Prof. Ari Sihvola

Instructors: Ph.D., Docent Pasi Ylä-Oijala, D.Sc. Johannes Markkanen

In this Master's thesis volume integral equations based on polarization current densities and potentials, i.e. JM-formulation and AVFU-formulation are developed for bianisotropic scatterers. The volume integral equations are discretized and converted into a system of linear equations using the method of moments. The system of equations for the JM-formulation is solved using the generalized minimal residual method (GMRES) and multilevel fast multipole algorithm (MLFMA) is also applied. Whereas the AVFU-formulation is still under development and GMRES and MLFMA are not implemented; thereby limiting the problem domain that can be analysed. Numerical results are compared to existing model problems solved using either the volume integral equations for the fields, i.e. the EH-formulation, flux densities, i.e. the DB-formulation or the Mie series solutions. The scattering cross-section of simple scatterers like an isotropic sphere to complex scatterers like double negative chiral and metamaterial spheres is investigated.

From the numerical point of view the essence of JM- and AVFU- formulation is discretization using low order basis functions. The polarization current densities in the JM-formulation are expanded using piecewise constant basis functions and Galerkin's technique is applied to test the equations. The scalar and vector potentials in the AVFU-formulation are expanded using the scalar interpolatory nodal basis functions and point-matching technique is applied to test the equations.

An important purpose of the Master's thesis is to provide an academic document that can be easily followed to formulate and numerically implement volume integral equations based on fields, flux densities, polarization current densities or potentials. To achieve this goal the overall implementation from scratch is presented for the AVFU-formulation.

Keywords: Bi-anisotropic scatterers, GMRES, MLFMA, MoM, polarization current density, volume integral equation methods

Preface

I would like to express my gratitude to my supervisor Prof. Ari Sihvola and instructors Ph.D. Docent Pasi Ylä-Oijala and Ph.D. Johannes Markkanen for being supportive, kind, and patient with my work on the master thesis. It was a great opportunity and learning experience working in the group. I would also like to thank Ph.D. Seppo Järvenpää for his support in getting acquainted with the MoM solver for the JM-formulation.

I am also thankful to my family and friends for being supportive and cheerful.

Contents

List of Abbreviations and Symbols

Symbols

$\boldsymbol{a}$	vector
$\bar{\bar{\boldsymbol{a}}}$	dyad
A^i	incident potential
A^s	scattered potential
$\boldsymbol{A}^i$	incident vector
$\boldsymbol{B}$	magnetic flux density
c	speed of light
$\boldsymbol{D}$	electric flux density
$\boldsymbol{E}$	electric field intensity
G	Green's function
$\boldsymbol{H}$	magnetic field intensity
j	imaginary unit
$\boldsymbol{J}_V$	equivalent volume electric current density
$\boldsymbol{J}_s$	surface electric current density
k	wavenumber
$\boldsymbol{M}_V$	equivalent volume magnetic current density
$\boldsymbol{M}_s$	surface magetic current density
$\boldsymbol{n}$	outward unit normal
$N_{n,l}$	triangle element T_n from the vertex of $\boldsymbol{p}_l$ associated with shape function
$\boldsymbol{p}_{n,l}$	triangle element T_n vertex
$\bar{\bar{P}}$	material dyadic
Q_{sca}	scattering efficiency
$\boldsymbol{r}$	position vector, field point
$\boldsymbol{r'}$	position vector,source point
T_n	triangle element
ρ_s	electric charge density
ξ	magnetoelectric parameter, charility
ζ	magnetoelectric parameter
χ	magnetoelectric parameter
κ	magnetoelectric parameter
ϵ	permittivity
μ	permeability
ω	radian frequency
σ	surface charge density
λ	wavelength
(x, y, z)	cartesian coordinates
(r, θ, ϕ)	spherical coordinates
(ρ, ϕ)	polar coordinates

Operators

$\boldsymbol{A} \cdot \boldsymbol{B}$	dot product of vectors $\boldsymbol{A}$ and $\boldsymbol{B}$
$\boldsymbol{A} \times \boldsymbol{B}$	cross product of vectors $\boldsymbol{A}$ and $\boldsymbol{B}$
$\nabla \times \boldsymbol{A}$	curl of a vector $\boldsymbol{A}$
$\nabla \cdot \boldsymbol{A}$	divergence of a vector $\boldsymbol{A}$
∇A	gradient of a scalar A
∇^2	Laplacian operator
D^c	complement of domain D
$\frac{\mathrm{d}}{\mathrm{d}t}$	derivative w.r.t t
∂D	boundary of domain D
$\frac{\partial}{\partial t}$	paartial derivative w.r.t t
Ω_D	relative solid angle on a boundry surface of domain D
$\sum_j$	sum over index j
$\boldsymbol{\mathcal{F}}$	mapping from refrence tetrahederon $\hat{E}_e$ to real tetrahederon E_e
$J_{\boldsymbol{\mathcal{F}}}$	Jacobian of mapping $\boldsymbol{\mathcal{F}}$
$\Re(f)$	real part of a function f
$\Im(f)$	imaginary part of a function f
$\bar{\bar{I}}$	identity dyadic
$\boldsymbol{\mathcal{K}}_s$	surface integral operator
$\boldsymbol{\mathcal{K}}$	volume integral operator
$L(f)$	linear operator over function f
$\boldsymbol{\mathcal{L}}$	surface integral operator
N^e	shape function of a tetrahederon E_e
$\hat{N}^e$	shape function of reference tetrahederon $\hat{E}_e$
$\boldsymbol{\mathcal{S}}$	volume integral operator
$\boldsymbol{\mathcal{S}}_s$	surface integral operator
$\boldsymbol{\mathcal{S}}_V$	volume integral operator

Abbreviations

BEM	Boundary element method
CEM	Computational electromagnetics
GMRES	Generalized Minimum Residual Method
MLMFA	Multi-level Fast Multipole Algorithm
MoM	Method of Moments
PEC	Perfect Electric Conductor
PVIE	Potential volume integral equation
PMC	Perfect Magnetic conductor
SCS	Scattering cross section
RWG	Rao, Wilton, Glisson
VIE	Volume integral equation

List of Figures

List of Tables

1 Introduction

1.1 Motivation

Study of bi-anisotropic materials, their properties and electromagnetic scattering - which is one of the basic problems in the study of interaction between electromagnetic waves and material objects, has been focus of study for many decades. A rigorous solution of scattered fields by spheres can be obtained by using the Mie theory. However, if the structures of complex media are not in canonical geometries, the analytical analysis is limited and not capable then. So, there arises the need of using numerical methods to deal with such problems. However, standard numerical methods tend to lose their efficiency when a scatterer is characterized with complicated constitutive relations.

Advances in the material technology has raised the demand for application of complex materials. Complex structures are being investigated for applications such as antennas, radomes, waveguides, microstrips, substrates for microstrip antennas, MMICs, and electromagnetic absorbers in the anechoic chambers, etc.

Integral equation (IE) methods are important in modelling arbitrary shaped structures and satisfying, automatically, the radiation boundary condition. IE methods are efficient and provide good flexibility and accuracy. The IE methods can be divided into surface and volume integral equation methods.

Volume integral equation methods are indispensable for the electromagnetic modelling of structures involving inhomogeneous materials or a number of many different homogeneous domains. Volume integral equations can be formulated in terms of electric and magnetic field intensities, flux densities, current densities or scalar and vector potentials. In the past, volume integral equations have been formulated for the most general linear media in electromagnetics, i.e. a bi-anisotropic medium in terms of electric and magnetic field intensities (EH-formulation) and flux densities (DB-formulation) [1] and [2], respectively. In [3], the volume integral equations based on equivalent polarization currents, i.e. the JM-formulation is presented in the case of extremely anisotropic parameters and it is shown that the JM-formulation is accurate and stable in terms of the conditioning of the system in a wide range of uniaxially anisotropic medium parameters. The EH-formulation and DB-formulation suffer breakdown when some component of permittivity or permeability dyadic is large in magnitude or close to zero, respectively. Volume integral equations based on potentials, i.e. AVFU-formulation has not been inspected very

thoroughly and there has been a very limited research that is merely limited to simple scatterers [4], [5] and [6].

The equivalent volume current densities have no continuities and simple piecewise constant basis functions can be used to expand the unknown current densities. This leads to simpler numerical implementation and lower requirements for the required computational power. The potentials are continuous functions in space, a set of potential volume integral equations can be formulated by expanding the unknown potentials with scalar linear nodal basis functions and point-matching technique can be used. The use of volume equivalence theorem and Lorenz gauge [6] simplifies the potential formulation and the evaluation of surface integrals is eliminated; moreover, there are no hyper-singular integrals involved. Due to the simplicity and use of low-profile basis function for the expansion of unknown current densities or potentials, the number of unknowns involved is significantly reduced and this leads to significant speed-up in the computational time.

1.2 Objective of the Master Thesis

There is an urgent need to develop an electromagnetic field solver that can handle all kinds of complex media. The objectives of the master thesis are therefore defined as follows;

- to validate the JM-formulation developed for the bi-anisotropic media,
- to formulate and implement volume integral equations for scalar and vector potentials, i.e. to develop the AVFU-formulation,
- To study the numerical properties (solution accuracy as a function of size and material parameters, conditioning of the system matrices etc.) of the JM- and AVFU-formulations,
- to produce a document that can easily followed to formulate and numerically implement volume integral equations based on fields, flux densities, current densities or potentials.

1.3 Organization of the Master Thesis

The organization of the thesis is as follows;

- **Chapter 2** gives a literature overview of electromagnetics in general and computational electromagnetics in particular. The problem of electromagnetic scattering is presented and the terminologies associated with electromagnetic scattering are defined.

- **Chapter 3** presents a brief overview of surface integral equations and a detailed description of the volume integral formulations for the fields, flux densities, current densities and potentials.

- **Chapter 4** gives the numerical implementation of the JM- and AVFU- formulations.

- **Chapter 5** discusses the numerical results and limitations of the proposed formulations.

2 Computational Electromagnetics

Electromagnetic analysis involves solving Maxwell's equations to obtain a better understanding of a complex system. In the beginning electromagnetic analysis was limited to the classical method of solving with pencil and paper. Thus, the solution to Maxwell's equations using the analytical methods was available only for simple problems and some canonical geometries. In the current applied electromagnetic research, the problems of interest involve arbitrary geometries and many different application domains such as antenna design, remote sensing, surface sensing, electromagnetic compatibility (EMC) analysis, RF and microwave analysis and design etc. This has been possible with the advent of computer and numerical methods; the numerical approximation to the system of equations (developed using the Maxwell's equations and applying the appropriate boundary conditions) by utilizing the computational resources provided by the modern computer technology has given birth to the field of *computational electromagnetics* (CEM) [7]. "CEM is a multidisciplinary field and its core disciplines are electromagnetic theory and numerical methods, but for useful implementations, geometric modeling and visualization, and ingenuity in computational algorithms all have important roles to play" [8].

CEM techniques can be classified based on the problem type or application domain such as, propagation, radiation and scattering problems. Propagation problems involve determining the fields distant from a known source, radiation means to determine the originating sources of a field and scattering refers to the finding of scattered fields from an obstacle when the incident fields are known. The scope of any problem is limited by the properties like solution domain/space, dimensionality, and electrical or spacial description.To solve a problem in CEM, a physical domain is to be specified and the electrical characteristics of the domain defined, then the relationship between the input and output depends on the mathematical description used to describe it. This mathematical description can be in terms of integral or differential equations, modal expansions, or an optical description. The mathematical model based on integral equations requires the specification of Green's function which is an exact propagator. The integral equation model includes an explicit radiation condition and is specified over the source function making it indispensable for radiation or scattering problems. The differential equation model is less complicated then an integral equation model and can handle medium inhomogeneities, non-linearities, and time variations in a better fashion then an integral equation model. But the differential operator is local, therefore, the whole space needs to be modeled to determine the field variations. This means that the computational domain is to be terminated by some absorb-

ing boundary condition or perfectly matched layer. With model expansion, the aim is to find the solution to Maxwell's equations in a particular coordinate system by describing the source-field relationship in terms of well-known analytical functions instead of the Green's function. Some examples of these analytical functions are circular harmonics, Hankel functions, Legendre polynomials etc. The field propagation using an optical description is a high frequency concept involving rays, diffraction coefficients, shadowing and other terminologies used in optics and is more generally known as the geometrical theory of diffraction (GTD).

In order to develop a CEM model, the first step is to lay down the observation and analysis in terms of elementary physical principles (Maxwell's equations, the associated boundary conditions and the constitutive relations of matter) and their mathematical description. Next, the problem is formulated in a way that it can be implemented with a computer code. This involves converting the equations of field theory to mathematical equations by using techniques such as the Method of Moments (MoM) (section 4.1). The formulated problem is then numerically implemented by transforming into a computer code. The model is then validated by obtaining quantitative results with the implemented code. These results are compared to analytical solutions or to the results obtained using another CEM model or are verified experimentally [9].

2.1 Maxwell's Equations

The relations that describe the variations of the electric and magnetic fields, charges, and currents connected with electromagnetic waves are governed by physical laws that are known as Maxwell's equations. These laws were put together by James Clerk Maxwell, a Scottish physicist and mathematician. Below are given the differential and integral forms of Maxwell's equations. The differential form of Maxwell's equations describe and relate the field vectors, current densities, and charge densities at any point in space at any time, provided that the field vectors are single-valued, bounded, continuous functions of position and time and have continuous derivatives. The integral form of Maxwell's equations describe the relations of the field vectors, charge densities, and current densities over an extended region of space and are utilized to solve electromagnetic boundary-value problems. A complete description of the field vectors at any point at any time requires Maxwell's equations, the associated boundary conditions that describe the abrupt changes in charges and currents that usually occur when there are discrete changes in the electrical

parameters across an interface and the constitutive relations of matter.

$$\nabla \times \boldsymbol{E} = -\boldsymbol{M} - j\omega\boldsymbol{B} \quad \oint_C \boldsymbol{E} \cdot d\boldsymbol{l} = \iint_S \boldsymbol{M} \cdot d\boldsymbol{s} - j\omega\boldsymbol{\phi} \quad \text{Faraday's law} \tag{1}$$

$$\nabla \times \boldsymbol{H} = \boldsymbol{J} + j\omega\boldsymbol{D} \quad \oint_C \boldsymbol{H} \cdot d\boldsymbol{l} = I + j\omega \iint_S \boldsymbol{D} \cdot d\boldsymbol{s} \quad \text{Maxwell-Ampere law} \tag{2}$$

$$\nabla \cdot \boldsymbol{D} = \rho_e \quad \oint_S \boldsymbol{D} \cdot d\boldsymbol{s} = q_e \quad \text{Gauss's Law} \tag{3}$$

$$\nabla \cdot \boldsymbol{B} = \rho_m \quad \oint_S \boldsymbol{B} \cdot d\boldsymbol{s} = q_m \quad \text{Gauss's Law - magnetic} \tag{4}$$

All these field quantities - $\boldsymbol{E}, \boldsymbol{H}, \boldsymbol{D}, \boldsymbol{B}, \boldsymbol{J}, \boldsymbol{M}, I, \phi$ and q are assumed to be time-varying, and each is a function of the space coordinates and time, i.e. $(\boldsymbol{r}; t)$. Moreover, the variation in time of each of the quantities is harmonic and since time-harmonic quantities satisfy

$$\frac{\partial \boldsymbol{F}(\boldsymbol{r})}{\partial t} e^{j\omega t} = j\omega \boldsymbol{F}(\boldsymbol{r}) e^{j\omega t}$$

Therefore, the time factor $e^{j\omega t}$ is suppressed from Maxwell's equations.
The definition and units of the quantities in Maxwell's equations are

$$\begin{aligned}
\boldsymbol{E} &= \text{electric field intensity (volts/meter)} \\
\boldsymbol{H} &= \text{magnetic field intensity (amperes/meter)} \\
\boldsymbol{D} &= \text{electric flux density (coulombs/square meter)} \\
\boldsymbol{B} &= \text{magnetic flux density (webers/square meter)} \\
\phi &= \iint_S \boldsymbol{B} \cdot d\boldsymbol{s}, \text{ magnetic flux (webers)} \\
\boldsymbol{J} &= \boldsymbol{J}_c + \boldsymbol{J}_i, \text{ electric current density (amperes/square meter)} \\
\boldsymbol{J}_i &= \text{impressed (source) electric current density (amperes/square meter)} \\
\boldsymbol{J}_c &= \text{conduction electric current density (amperes/square meter)} \\
j\omega\boldsymbol{D} &= \boldsymbol{J}_d, \text{ displacement electric current density (amperes/square meter)}
\end{aligned}$$

$$\begin{aligned}
\boldsymbol{M}_i &= \text{impressed (source) magnetic current density (volts/square meter)} \\
\boldsymbol{M}_c &= \text{conduction magnetic current density (volts/square meter)} \\
j\omega\boldsymbol{B} &= \boldsymbol{M}_d, \text{ displacement magnetic current density (volts/square meter)} \\
I &= \iint_S \boldsymbol{J} \cdot d\boldsymbol{s}, \text{ electric current (amperes)} \\
\rho_e &= \text{electric charge density (coulombs/cubic meter)} \\
\rho_m &= \text{magnetic charge density (webers/cubic meter)} \\
q_e &= \iiint_V \rho_e \, dV, \text{ electric charge (coulomb)} \\
q_m &= \iiint_V \rho_m \, dV, \text{ magnetic charge (weber)}
\end{aligned}$$

Implicit in the Maxwell's equation is the continuity equation that relates the net flow of current out of a small volume (in the limit, a point) to the rate of decrease of charge [10] [11], i.e.

$$\nabla \cdot \boldsymbol{J} = -j\omega\rho_e \tag{5}$$

$$\nabla \cdot \boldsymbol{M} = -j\omega\rho_m \tag{6}$$

2.2 Constitutive Relations and Parameters for Bi-anisotropic Medium

Bi-anisotropic or magnetoelectric medium is the most general linear medium in electromagnetics and a class of the commonly known metamaterials defined as media whose properties are emergent from their structural details instead of simple averages of the constituents. A bianisotropic medium gets electrically excited by a magnetic field, and vice versa - meaning that when placed in an electric or magnetic field, a bi-anisotropic medium becomes both polarized and magnetized. For a bi-anisotropic medium the electric and magnetic flux densities $\boldsymbol{D}$ and $\boldsymbol{B}$ are related to the electric and magnetic field intensities $\boldsymbol{E}$ and $\boldsymbol{H}$ by the constitutive relations [12],

$$\boldsymbol{D} = \varepsilon_0\bar{\bar{\varepsilon}}_r \cdot \boldsymbol{E} + \sqrt{\varepsilon_0\mu_0}\bar{\bar{\xi}}_r \cdot \boldsymbol{H} \tag{7}$$

$$\boldsymbol{B} = \sqrt{\varepsilon_0\mu_0}\bar{\bar{\zeta}}_r \cdot \boldsymbol{E} + \mu_0\bar{\bar{\mu}}_r \cdot \boldsymbol{H} \tag{8}$$

And the electric and magnetic current densities are related to the electric and magnetic field intensities by;

$$\boldsymbol{J}_c = \bar{\bar{\sigma}}\boldsymbol{E} \tag{9}$$

$$\boldsymbol{M}_c = \bar{\bar{\sigma}}_m\boldsymbol{H} \tag{10}$$

Here the material parameter dyadics are permittivity $\bar{\bar{\varepsilon}}(\varepsilon_0\bar{\bar{\varepsilon}}_r)$ and permeability $\bar{\bar{\mu}}(\mu_0\bar{\bar{\mu}}_r)$, and two magnetoelectric dyadics $\bar{\bar{\xi}}(\sqrt{\varepsilon_0\mu_0}\bar{\bar{\xi}}_r)$ and $\bar{\bar{\zeta}}(\sqrt{\varepsilon_0\mu_0}\bar{\bar{\zeta}}_r)$ (each of these dyadics contain 9 independent parameters). $\varepsilon_0(= 8.854 \times 10^{-12}$ Farads/meter) is the permittivity of free-space, $\mu_0(= 4\pi \times 10^{-7}$ henrys/meter) is the free-space permeability, σ (siemens/meter) is the electric current conductivity, and σ_m (ohms/meter) is the magnetic current conductivity. The above defined parameters are referred to as the constitutive parameters of a medium, and based on their spatial or frequency dependence, the medium can be characterized as linear or non-linear, homogeneous or inhomogeneous, dispersive or non-dispersive, and isotropic, anisotropic, bi-isotropic, or bi-anisotrpic [14].

If the medium does not have any preferred direction, it is bi-isotropic, and all four dyadics are multiples of the unit dyadic. If on the other hand $\bar{\bar{\xi}}$ and $\bar{\bar{\zeta}}$ are zero, and $\bar{\bar{\varepsilon}}$ and $\bar{\bar{\mu}}$ are non-zero scalars, the medium is simply an isotropic medium, and $\boldsymbol{E}$ is parallel to $\boldsymbol{D}$ and $\boldsymbol{H}$ is parallel to $\boldsymbol{B}$. Hence all linear (constitutive parameters are independent of the field intensities) and stationary media, isotropic or anisotropic, bi-isotropic or bi-anisotropic, can be treated as bi-anisotropic or special cases of bi-anisotropic media. The most general bi-anisotropic material requires 36 parameters in its full constitutive electromagnetic description. These 36 parameters, however, may not be chosen arbitrarily and in realistic "physical" medium the number of free parameters may be smaller. But in fact there is a greater complexity involved with problems involving bi-anisotropic materials in comparison to isotropic, bi-isotropic and anisotropic materials requiring respectively 2, 4 and 18 parameters in their full constitutive electromagnetic description [13].

2.3 Boundary Conditions

At an interface where the media involved exhibit discontinuities, i.e. contiguous regions have different constitutive parameters or there exists sources along the boundaries separating these media, the field vectors are discontinuous and there behavior across the boundaries is described by boundary conditions. Boundary conditions are derived by applying the integral form of Maxwell's equations (1,2,3,4) to a small region at an interface of the two media, e.g. the application of the integral form a curl equation to a flat closed

path at an interface with top and bottom sides in the two touching media gives the boundary conditions for the tangential components; and the application of the integral form of a divergence equation to a shallow pillbox at an interface with the top and bottom faces in the two contiguous media gives the boundary conditions for the normal components [11].

The boundary conditions for the tangential components of $\boldsymbol{E}$ and $\boldsymbol{H}$ and normal components of $\boldsymbol{D}$ and $\boldsymbol{B}$ are summarized in Table 1:

Table 1: Summary of boundary conditions

Boundary Conditions	**Description**
$\boldsymbol{n}_2 \times (\boldsymbol{E}_2 - \boldsymbol{E}_1) = \boldsymbol{M}_s$	The tangential component of $\boldsymbol{E}$ is discontinuous across an interface where an impressed surface magnetic current exists.
$\boldsymbol{n}_2 \times (\boldsymbol{H}_1 - \boldsymbol{H}_2) = \boldsymbol{J}_s$	The tangential component of $\boldsymbol{H}$ is discontinuous across an interface where a surface electric current exists.
$\boldsymbol{n}_2 \cdot (\boldsymbol{D}_1 - \boldsymbol{D}_2) = \rho_{es}$	The normal component of $\boldsymbol{D}$ is discontinuous across an interface where a surface electric charge exists.
$\boldsymbol{n}_2 \cdot (\boldsymbol{B}_1 - \boldsymbol{B}_2) = \rho_{ms}$	The normal component of $\boldsymbol{B}$ is discontinuous across an interface where a surface magnetic charge exists.

The normal components of the electric field intensity ($\boldsymbol{E}$) and magnetic field intensity ($\boldsymbol{H}$) are discontinuous across an interface.

2.4 The Problem of Electromagnetic Scattering

When an electromagnetic wave is incident on an object it introduces currents on the surface of the object[1]. These surface currents which can be purely electrical in case of perfect electric conductor, purely magnetic in case of a perfect magnetic conductor and both electric and magnetic in case of dielectric material, radiate and produce the scattered fields.

The fundamental scattering problem is as follows: Given an object of specified size, shape and material parameters that is illuminated by a plane electromagnetic wave with specified characteristics (frequency, direction, polarization, etc.), determine the electromagnetic field at all points in the object and at all points of the homogeneous medium in which the object is embedded [15], [16].

The field inside the object is $(\boldsymbol{E}_2, \boldsymbol{H}_2)$; the field $(\boldsymbol{E}_1, \boldsymbol{H}_1)$ outside the object is the superposition of the incident field $(\boldsymbol{E}^i, \boldsymbol{H}^i)$ and the scattered field $(\boldsymbol{E}^s, \boldsymbol{H}^s)$ (Fig. 1):

[1] If the object is homogeneous then the surface currents are used to find the scattered fields. For inhomogeneous domains, volume currents are used to describe the scattered fields. If the Green's function or Green's dyadic of the inhomogeneous medium is known, it is possible to formulate the problem of electromagnetic scattering in terms of surface currents.

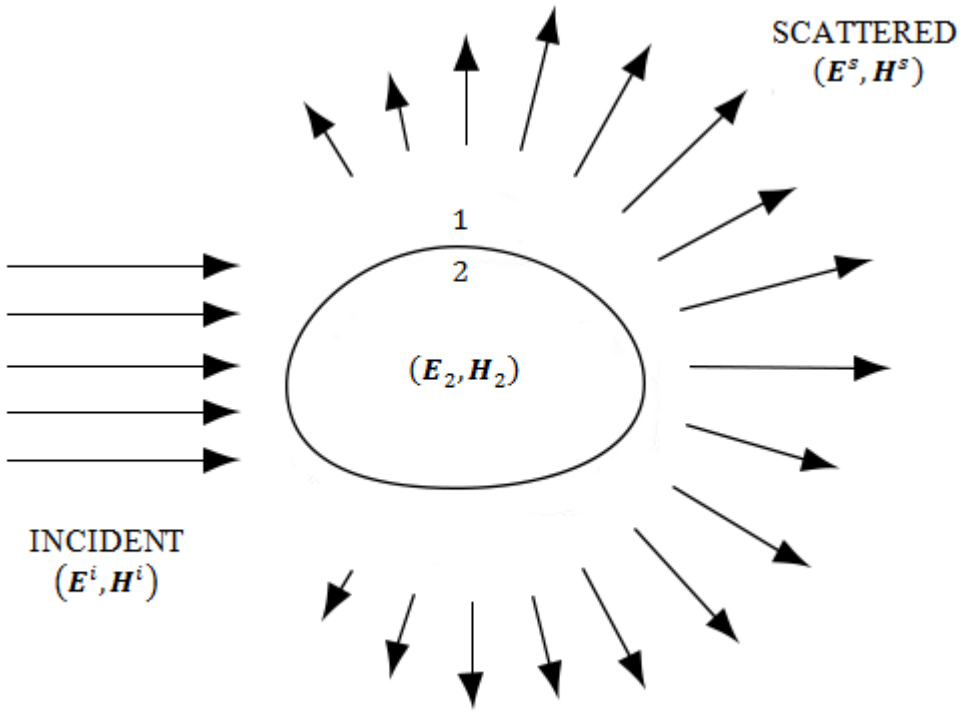

Figure 1: The incident field $(\boldsymbol{E}^i, \boldsymbol{H}^i)$ gives rise to a field $(\boldsymbol{E}_2, \boldsymbol{H}_2)$ inside the object and a scattered field $(\boldsymbol{E}^s, \boldsymbol{H}^s)$ in the medium surrounding the object [15]

$$\boldsymbol{E}_1 = \boldsymbol{E}^i + \boldsymbol{E}^s, \qquad \boldsymbol{H}_1 = \boldsymbol{H}^i + \boldsymbol{H}^s \tag{11}$$

where

$$\boldsymbol{E}^i = \boldsymbol{E}_0 e^{j(\omega t - \boldsymbol{k}\cdot\boldsymbol{r})}, \qquad \boldsymbol{H}^i = \boldsymbol{H}_0 e^{j(\omega t - \boldsymbol{k}\cdot\boldsymbol{r})} \tag{12}$$

and $\boldsymbol{k}$ is the wave vector appropriate to the medium surrounding the obstacle.

Once the equivalent currents on the surface of the scatterer $(\boldsymbol{J}_s, \boldsymbol{M}_s)$ defined using the Surface Equivalence Principle (3.1) or the polarization currents representing the scatterer $(\boldsymbol{J}_V, \boldsymbol{M}_V)$ defined using the Volume Equivalence Principle (3.2) are known, the scattered fields in the far-filed $(\boldsymbol{r} \to \infty)$ can be calculated using [17],

$$\boldsymbol{E}^s(\boldsymbol{r}) \approx \frac{e^{-jkr}}{4\pi r} \int_\Omega \left\{ j\omega\mu \hat{\boldsymbol{r}} \times [\hat{\boldsymbol{r}} \times \boldsymbol{J}(\boldsymbol{r}')] + jk\hat{\boldsymbol{r}} \times \boldsymbol{M}(\boldsymbol{r}') \right\} e^{jk\hat{\boldsymbol{r}}\cdot\boldsymbol{r}'} \, d\Omega', \tag{13}$$

$$\boldsymbol{H}^s(\boldsymbol{r}) \approx \frac{e^{-jkr}}{4\pi r} \int_\Omega \left\{ j\omega\varepsilon \hat{\boldsymbol{r}} \times [\hat{\boldsymbol{r}} \times \boldsymbol{M}(\boldsymbol{r}')] - jk\hat{\boldsymbol{r}} \times \boldsymbol{J}(\boldsymbol{r}') \right\} e^{jk\hat{\boldsymbol{r}}\cdot\boldsymbol{r}'} \, d\Omega' \tag{14}$$

$\boldsymbol{J}$ and $\boldsymbol{M}$ in equation's (13) and (14) are either surface or volume currents.

2.5 Scattering Cross Section

Scattering Cross Section (SCS) is a parameter that characterizes the scattering by an object. It is defined in the three-dimensional case as,

$$\begin{aligned}\sigma(\theta,\varphi,\theta^i,\varphi^i) &= \lim_{r\to\infty} 4\pi r^2 \frac{\left|\boldsymbol{E}^s(r,\theta,\varphi)\right|^2}{\left|\boldsymbol{E}^i(\theta^i,\varphi^i)\right|^2} \\ &= \lim_{r\to\infty} 4\pi r^2 \frac{\left|\boldsymbol{H}^s(r,\theta,\varphi)\right|^2}{\left|\boldsymbol{H}^i(\theta^i,\varphi^i)\right|^2} \end{aligned} \tag{15}$$

where $(\boldsymbol{E}^s, \boldsymbol{H}^s)$ denote the scattered field observed in the direction (θ, φ) and $(\boldsymbol{E}^i, \boldsymbol{H}^i)$ denote the incident field from the direction (θ^i, φ^i). σ is called the monostatic or backscatter scattering cross section when the incident and observation directions are the same; otherwise, it is referred to as the bistatic scattering cross section.

The scattering cross section is often normalized to either square of the wavelength (λ^2) or area (m^2). The unit for σ/λ^2 is dBsw and for σ/m^2 is dBsm. To include information about polarization, the scattering cross section is defined as [17]

$$\sigma_{pq}(\theta,\varphi,\theta^i,\varphi^i) = \lim_{r\to\infty} 4\pi r^2 \frac{\left|\boldsymbol{E}_p^s(r,\theta,\varphi)\right|^2}{\left|\boldsymbol{E}_q^i(\theta^i,\varphi^i)\right|^2} \tag{16}$$

where p and q represent either θ or ϕ. $\sigma_{\theta\theta}$ is the co-polarized SCS in the $\phi = 0^0$ or E-plane and $\sigma_{\theta\phi}$ is the cross-polarized SCS in the $\phi = 0^0$ or E-plane. Likewise, $\sigma_{\phi\phi}$ is the co-polarized SCS in the $\phi = 90^0$ or H-plane and $\sigma_{\phi\theta}$ is the cross-polarized SCS in the $\phi = 90^0$ or H-plane.

3 Integral Equation Methods

Integral equation methods are important in the numerical analysis of certain boundary-value problems, such as, scattering, radiation etc. In electromagnetic integral equation methods the original boundary value problems for Maxwell's equations are reformulated as integral equations over the boundary interfaces of homogeneous domains or integral equations over the entire volume of the object are considered if the object is inhomogeneous. Thus in the special case of a homogeneous medium the problem involving whole of the domain is reduced to one involving only its boundaries, this means that the dimension of the problem is reduced by one. In the case of exterior problems, where the region of interest is of infinite extent, an integral equation formulation is virtually indispensable [18].

Although, the integral equation methods are in many cases flexible and efficient methods for solving various electromagnetic problems, an additional numerical difficulty arises from the singular integrals when the observation point is in the source region. The inconvenience due to singular kernels cannot be eliminated but reduction in integrand's singularity is desired for achieving higher accuracy in numerical computations involving such integrals.

3.1 Surface Equivalence Theorem

The statement of the surface equivalence theorem follows directly from uniqueness theorem [19] that says: "a harmonic field $(\boldsymbol{E}, \boldsymbol{H})$ in a source-free region D can be uniquely determined if the tangential fields are known on an virtual surface S bounding D".

Consider a source free domain D with a known Green's dyadic $\bar{\bar{\boldsymbol{\mathcal{G}}}}$ and surface S enclosing the source domain as illustrated in Figure 2, 3. Then the fields inside the domain D

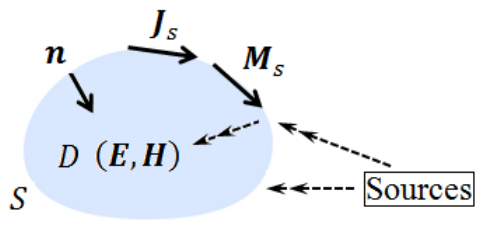

Figure 2: (a) Bounded (interior) regions

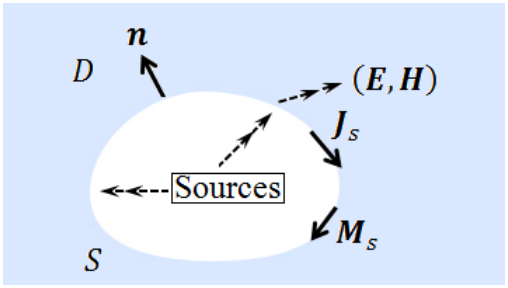

Figure 3: (b) Unbounded (exterior) regions

can be determined by equivalent surface polarization current densities defined as;

$$\boldsymbol{J}_s = \hat{\boldsymbol{n}} \times \boldsymbol{H} \tag{17}$$

$$\boldsymbol{M}_s = -\hat{\boldsymbol{n}} \times \boldsymbol{E} \tag{18}$$

where $\hat{\boldsymbol{n}}$ is unit normal on S pointing into D. $\boldsymbol{J}_s$ and $\boldsymbol{M}_s$ are called equivalent surface polarization current densities since they do not necessarily agree with the the physical current densities (surface S can be a virtual surface).Thus the tangential boundary values of the fields on S can be used to uniquely determine the fields inside D. This holds for both bounded and unbounded regions and in unbounded regions the fields must satisfy the radiation condition,

$$\lim_{|r|\to\infty} |\boldsymbol{r}| \left[\sqrt{\mu}\boldsymbol{H}^s \frac{\boldsymbol{r}}{|\boldsymbol{r}|} - \sqrt{\varepsilon}\boldsymbol{E}^s \right] = 0 \tag{19}$$

The fields can be expressed mathematically as,

$$\chi(\boldsymbol{r})\boldsymbol{E}(\boldsymbol{r}) = \boldsymbol{E}^i + j\omega\mu\boldsymbol{\mathcal{S}}_s(\boldsymbol{J}_s)(\boldsymbol{r}) - \boldsymbol{\mathcal{K}}_s(\boldsymbol{M}_s)(\boldsymbol{r}) \tag{20}$$

$$\chi(\boldsymbol{r})\boldsymbol{H}(\boldsymbol{r}) = \boldsymbol{H}^i + j\omega\varepsilon\boldsymbol{\mathcal{S}}_s(\boldsymbol{M}_s)(\boldsymbol{r}) + \boldsymbol{\mathcal{K}}_s(\boldsymbol{J}_s)(\boldsymbol{r}) \tag{21}$$

$\boldsymbol{\mathcal{S}}_s(\boldsymbol{F})(\boldsymbol{r})$ and $\boldsymbol{\mathcal{K}}_s(\boldsymbol{F})(\boldsymbol{r})$ are surface integral operators defined as;

$$\boldsymbol{\mathcal{S}}_s(\boldsymbol{F})(\boldsymbol{r}) = \int_S \bar{\bar{\boldsymbol{\mathcal{G}}}}(\boldsymbol{r}, \boldsymbol{r}') \cdot \boldsymbol{F}(\boldsymbol{r}')\, dS' \tag{22}$$

$$\boldsymbol{\mathcal{K}}_s(\boldsymbol{F})(\boldsymbol{r}) = \nabla \times \boldsymbol{\mathcal{S}}_s(\boldsymbol{F})(\boldsymbol{r}) \tag{23}$$

$\boldsymbol{E}^i$ and $\boldsymbol{H}^i$ are the primary fields generated by a current source $(\boldsymbol{J}_i, \boldsymbol{M}_i)$ in D (if it exists), $\bar{\bar{\boldsymbol{\mathcal{G}}}}(\boldsymbol{r}, \boldsymbol{r}')$ is the Green's dyadic and $\chi(\boldsymbol{r})$ is the characteristic function of D (D^c is the complement of D).

$$\chi(\boldsymbol{r}) = \begin{cases} 1 & \boldsymbol{r} \,\epsilon\, D \\ 1/2 & \boldsymbol{r} \,\epsilon\, S \\ 0 & \boldsymbol{r} \,\epsilon\, D^c \end{cases} \tag{24}$$

$$\bar{\bar{\boldsymbol{\mathcal{G}}}}(\boldsymbol{r}, \boldsymbol{r}') = \left(\frac{1}{k^2} \nabla\nabla + \bar{\bar{I}} \right) G(\boldsymbol{r}, \boldsymbol{r}') \tag{25}$$

and

$$\boldsymbol{E}^i = j\omega\mu \int\limits_{spt(\boldsymbol{J}_i)} \bar{\bar{\boldsymbol{\mathcal{G}}}}(\boldsymbol{r},\boldsymbol{r}') \cdot \boldsymbol{J}_i(\boldsymbol{r}')\, dr' \tag{26}$$

$$\boldsymbol{H}^i = \nabla \times \int\limits_{spt(\boldsymbol{J}_i)} \bar{\bar{\boldsymbol{\mathcal{G}}}}(\boldsymbol{r},\boldsymbol{r}') \cdot \boldsymbol{J}_i(\boldsymbol{r}')\, dr' \tag{27}$$

where,

$$G(\boldsymbol{r},\boldsymbol{r}') = \frac{e^{-jkr}}{4\pi r}$$

is the homogeneous-space Green's function and

$$k = \omega\sqrt{\mu\varepsilon}$$

is the homogeneous-space wave number.

3.2 Volume Equivalence Theorem

The volume equivalence theorem states that *the field disturbances due the presence of a material body can be described by some prescribed equivalent polarization currents that are a function of the constituent parameters of the material body and the domain in which the body is embedded, and the fields*.

Consider time-harmonic sources radiating in the presence of a general material structure,

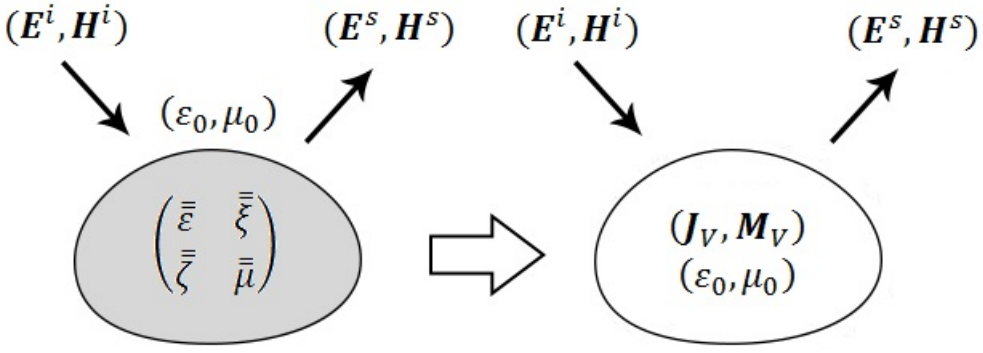

Figure 4: Volume equivalence theorem [14]

Fig 4. The incident fields $(\boldsymbol{E}^i, \boldsymbol{H}^i)$ on interaction with the object give rise to scatered fields $(\boldsymbol{E}^s, \boldsymbol{H}^s)$. Since the fields penetrating the object are not equal to the incident fields, the generation of the scattered fields is necessary to ensure continuity of fields across

boundary surface to full-fill the boundary conditions. According to the volume equivalence theorem these scattered fields can be thought of as originating from equivalent polarization currents defined in the case of the most general linear medium in electromagnetics, i.e. a bi-anisotropic medium as,

$$\boldsymbol{J}_V = j\omega(\bar{\bar{\varepsilon}} - \varepsilon_0\bar{\bar{I}}) \cdot \boldsymbol{E} + j\omega\bar{\bar{\xi}} \cdot \boldsymbol{H} \tag{28}$$

$$\boldsymbol{M}_V = j\omega(\bar{\bar{\mu}} - \mu_0\bar{\bar{I}}) \cdot \boldsymbol{H} + j\omega\bar{\bar{\zeta}} \cdot \boldsymbol{E} \tag{29}$$

Thus, the scattered fields are then defined as,

$$\boldsymbol{E}^s(\boldsymbol{r}) = -j\omega\mu_1 \int_D \bar{\bar{\boldsymbol{\mathcal{G}}}}_1(\boldsymbol{r},\boldsymbol{r}') \cdot \boldsymbol{J}_V(\boldsymbol{r}')\, dV' - \nabla \times \int_D \bar{\bar{\boldsymbol{\mathcal{G}}}}_1(\boldsymbol{r},\boldsymbol{r}') \cdot \boldsymbol{M}_V(\boldsymbol{r}')\, dV' \tag{30}$$

$$\boldsymbol{H}^s(\boldsymbol{r}) = -j\omega\varepsilon_1 \int_D \bar{\bar{\boldsymbol{\mathcal{G}}}}_1(\boldsymbol{r},\boldsymbol{r}') \cdot \boldsymbol{M}_V(\boldsymbol{r}')\, dV' + \nabla \times \int_D \bar{\bar{\boldsymbol{\mathcal{G}}}}_1(\boldsymbol{r},\boldsymbol{r}') \cdot \boldsymbol{J}_V(\boldsymbol{r}')\, dV' \tag{31}$$

where $\bar{\bar{\boldsymbol{\mathcal{G}}}}_2$ is the dyadic Green's function of the background medium.
Alternatively, the scattered fields can be written according to the volume equivalence principle as,

$$\boldsymbol{E}^s(\boldsymbol{r}) = \frac{1}{j\omega\varepsilon_1}\left(\nabla\nabla\cdot + k_1^2\right)\boldsymbol{\mathcal{S}}_V(\boldsymbol{J}_V)(\boldsymbol{r}) - \nabla \times \boldsymbol{\mathcal{S}}_V(\boldsymbol{M}_V)(\boldsymbol{r}) \tag{32}$$

$$\boldsymbol{H}^s(\boldsymbol{r}) = \frac{1}{j\omega\mu_1}\left(\nabla\nabla\cdot + k_1^2\right)\boldsymbol{\mathcal{S}}_V(\boldsymbol{M}_V)(\boldsymbol{r}) + \nabla \times \boldsymbol{\mathcal{S}}_V(\boldsymbol{J}_V)(\boldsymbol{r}) \tag{33}$$

where $\boldsymbol{\mathcal{S}}_V$ is a volume integral operator defined as,

$$\boldsymbol{\mathcal{S}}_V(\boldsymbol{F})(\boldsymbol{r}) = \int_D G_1(\boldsymbol{r},\boldsymbol{r}')\boldsymbol{F}(\boldsymbol{r}')\, dV' \tag{34}$$

with the scalar Green's function of the exterior $G_1(\boldsymbol{r},\boldsymbol{r}')$. By adding primary fields $(\boldsymbol{E}^p, \boldsymbol{H}^p)$ to both sides of the representation of the scattered fields we get the volume integral equations for the total fields,

$$\boldsymbol{E}(\boldsymbol{r}) = \frac{1}{j\omega\varepsilon_1}\boldsymbol{\mathcal{L}}(\boldsymbol{J}_V)(\boldsymbol{r}) - \boldsymbol{\mathcal{K}}(\boldsymbol{M}_V)(\boldsymbol{r}) + \boldsymbol{E}^i \tag{35}$$

$$\boldsymbol{H}(\boldsymbol{r}) = \frac{1}{j\omega\mu_1}\boldsymbol{\mathcal{L}}(\boldsymbol{M}_V)(\boldsymbol{r}) + \boldsymbol{\mathcal{K}}(\boldsymbol{J}_V)(\boldsymbol{r}) + \boldsymbol{H}^i \tag{36}$$

and

$$\boldsymbol{E} = \boldsymbol{E}^i + \boldsymbol{E}^s \qquad \text{and} \qquad \boldsymbol{H} = \boldsymbol{H}^i + \boldsymbol{H}^s \tag{37}$$

The integral operators are defined as,

$$\boldsymbol{\mathcal{L}}(\boldsymbol{F})(\boldsymbol{r}) = \left(\nabla\nabla\cdot + k_1^2\right)\boldsymbol{\mathcal{S}}_V(\boldsymbol{F})(\boldsymbol{r}) \tag{38}$$

$$\boldsymbol{\mathcal{K}}(\boldsymbol{F})(\boldsymbol{r}) = \nabla\times\boldsymbol{\mathcal{S}}_V(\boldsymbol{F})(\boldsymbol{r}) \tag{39}$$

3.2.1 Scaling

The system of equations in (35) and (36) is not well-balanced, because the operators have different scales and dimensions. We obtain better balanced systems by scaling the equations so that the quantities on both sides of the equations have the same dimensions [20].
Defining the bi-anisotropic parameters as

$$\begin{bmatrix} \boldsymbol{D} \\ \boldsymbol{B} \end{bmatrix} = \begin{bmatrix} \varepsilon_0\,\bar{\bar{\varepsilon}}_r & \sqrt{\varepsilon_0\mu_0}\,\bar{\bar{\xi}}_r \\ \sqrt{\varepsilon_0\mu_0}\,\bar{\bar{\zeta}}_r & \mu_0\,\bar{\bar{\mu}}_r \end{bmatrix} \begin{bmatrix} \boldsymbol{E} \\ \boldsymbol{H} \end{bmatrix} = \begin{bmatrix} \varepsilon_0\bar{\bar{I}} & 0 \\ 0 & \mu_0\bar{\bar{I}} \end{bmatrix} \begin{bmatrix} \bar{\bar{\varepsilon}}_r & \eta_0\,\bar{\bar{\xi}}_r \\ \frac{1}{\eta_0}\,\bar{\bar{\zeta}}_r & \bar{\bar{\mu}}_r \end{bmatrix} \begin{bmatrix} \boldsymbol{E} \\ \boldsymbol{H} \end{bmatrix} \tag{40}$$

with $\eta_0 = \sqrt{\mu_0/\varepsilon_0}$ and defining the scaled volume current densities as

$$\tilde{\boldsymbol{J}}_V = \frac{1}{\sqrt{\varepsilon_0}}\,\boldsymbol{J}_V = j\omega\bar{\bar{\tau}}_\varepsilon\cdot\tilde{\boldsymbol{E}} + j\omega\bar{\bar{\xi}}_r\cdot\tilde{\boldsymbol{H}} \tag{41}$$

$$\tilde{\boldsymbol{M}}_V = \frac{1}{\sqrt{\mu_0}}\,\boldsymbol{M}_V = j\omega\bar{\bar{\tau}}_\mu\cdot\tilde{\boldsymbol{H}} + j\omega\bar{\bar{\zeta}}_r\cdot\tilde{\boldsymbol{E}} \tag{42}$$

where

$$\tilde{\boldsymbol{E}} = \sqrt{\varepsilon_0}\,\boldsymbol{E} \quad \text{and} \quad \tilde{\boldsymbol{H}} = \sqrt{\mu_0}\,\boldsymbol{H} \tag{43}$$

The scaled volume integral equation representation for $\tilde{\boldsymbol{E}}$ and $\tilde{\boldsymbol{H}}$ read

$$\tilde{\boldsymbol{E}} = \frac{1}{j\omega}\boldsymbol{\mathcal{L}}(\tilde{\boldsymbol{J}}_V) - \sqrt{\varepsilon_0\mu_0}\,\boldsymbol{\mathcal{K}}(\tilde{\boldsymbol{M}}_V) + \tilde{\boldsymbol{E}}^i \tag{44}$$

$$\tilde{\boldsymbol{H}} = \frac{1}{j\omega}\boldsymbol{\mathcal{L}}(\tilde{\boldsymbol{M}}_V) + \sqrt{\varepsilon_0\mu_0}\,\boldsymbol{\mathcal{K}}(\tilde{\boldsymbol{J}}_V) + \tilde{\boldsymbol{H}}^i \tag{45}$$

where $\bar{\bar{\varepsilon}}, \bar{\bar{\mu}}, \bar{\bar{\xi}}, \bar{\bar{\zeta}}$ are the characteristic parameters of the material medium and

$$\bar{\bar{\tau}}_\varepsilon = \bar{\bar{\varepsilon}}_r - \bar{\bar{I}} \quad \text{and} \quad \bar{\bar{\tau}}_\mu = \bar{\bar{\mu}}_r - \bar{\bar{I}}. \tag{46}$$

3.3 Volume Integral Equation Representations

The representations in equations (35) and (36) or (44) and (45) have both fields and current densities and therefore the equations cannot be used directly. The currents $(\boldsymbol{J}_V, \boldsymbol{M}_V)$ can be represented in terms of fields $(\boldsymbol{E}, \boldsymbol{H})$ and fields can be represented in terms of fluxes $(\boldsymbol{D}, \boldsymbol{H})$ or potentials $(\boldsymbol{A}, V, \boldsymbol{F}, U)$ giving EH-, DB- and AVFU- formulations, respectively. Or the fields can be represented in terms of volume currents giving the JM-formulation. These formulations are discussed in detail in the following sections.
The EH- and DB- formulations presented in the next sections and those put by [1] and [2], respectively, are not the same. In [1] the total electric and magnetic fields are at first represented in terms of incident fields and scattered potentials, the scattered potentials are then defined in terms of equivalent polarization current densities and surface and volume charge densities that are then represented in terms of fields according to equations (28) and (29) to give the volume integral formulation for the fields. In [2] a volume integral formulation for the flux densities is obtained by representing the total fields in terms of flux densities and scattered field in terms of potentials, the potentials are then related to flux densities.

3.3.1 The EH-formulation

Using equations (28) and (29) in equations (35) and (36) we get the volume integral equations in terms of the fields.

$$\boldsymbol{E}(\boldsymbol{r}) = \frac{1}{\varepsilon_0}\boldsymbol{\mathcal{L}}\left((\bar{\bar{\varepsilon}} - \varepsilon_0\bar{\bar{I}})\cdot\boldsymbol{E} + \bar{\bar{\xi}}\cdot\boldsymbol{H}\right)(\boldsymbol{r}) - j\omega\boldsymbol{\mathcal{K}}\left((\bar{\bar{\mu}} - \mu_0\bar{\bar{I}})\cdot\boldsymbol{H} + \bar{\bar{\zeta}}\cdot\boldsymbol{E}\right)(\boldsymbol{r}) + \boldsymbol{E}^i(\boldsymbol{r})$$

$$= \frac{1}{\varepsilon_0}\boldsymbol{\mathcal{L}}\left(\varepsilon_0\bar{\bar{\tau}}_\varepsilon\cdot\boldsymbol{E}\right) + \frac{1}{\varepsilon_0}\boldsymbol{\mathcal{L}}\left(\bar{\bar{\xi}}\cdot\boldsymbol{H}\right)(\boldsymbol{r}) - j\omega\boldsymbol{\mathcal{K}}\left(\mu_0\bar{\bar{\tau}}_\mu\cdot\boldsymbol{H}\right) - j\omega\boldsymbol{\mathcal{K}}\left(\bar{\bar{\zeta}}\cdot\boldsymbol{E}\right)(\boldsymbol{r}) + \boldsymbol{E}^i(\boldsymbol{r}) \quad (47)$$

and

$$\boldsymbol{H}(\boldsymbol{r}) = \frac{1}{\mu_0}\boldsymbol{\mathcal{L}}\left((\bar{\bar{\mu}} - \mu_0\bar{\bar{I}})\cdot\boldsymbol{H} + \bar{\bar{\zeta}}\cdot\boldsymbol{E}\right)(\boldsymbol{r}) + j\omega\boldsymbol{\mathcal{K}}\left((\bar{\bar{\varepsilon}} - \varepsilon_0\bar{\bar{I}})\cdot\boldsymbol{E} + \bar{\bar{\xi}}\cdot\boldsymbol{H}\right)(\boldsymbol{r}) + \boldsymbol{H}^i(\boldsymbol{r})$$

$$= \frac{1}{\mu_0}\boldsymbol{\mathcal{L}}\left(\mu_0\bar{\bar{\tau}}_\mu \cdot \boldsymbol{H}\right) + \frac{1}{\mu_0}\boldsymbol{\mathcal{L}}\left(\bar{\bar{\zeta}} \cdot \boldsymbol{E}\right)(\boldsymbol{r}) + j\omega\boldsymbol{\mathcal{K}}\left(\varepsilon_0\bar{\bar{\tau}}_\varepsilon \cdot \boldsymbol{E}\right) + j\omega\boldsymbol{\mathcal{K}}\left(\bar{\bar{\xi}} \cdot \boldsymbol{H}\right)(\boldsymbol{r}) + \boldsymbol{H}^i(\boldsymbol{r}) \quad (48)$$

Substituting equations (41) and (42) into equations (44) and (45) we get the scaled equations for the fields.

$$\tilde{\boldsymbol{E}} = \boldsymbol{\mathcal{L}}\left(\bar{\bar{\tau}}_\varepsilon \cdot \tilde{\boldsymbol{E}}\right) - jk_0\,\boldsymbol{\mathcal{K}}\left(\bar{\bar{\zeta}}_r \cdot \tilde{\boldsymbol{E}}\right) + \boldsymbol{\mathcal{L}}\left(\bar{\bar{\xi}}_r \cdot \tilde{\boldsymbol{H}}\right) - jk_0\,\boldsymbol{\mathcal{K}}\left(\bar{\bar{\tau}}_\mu \cdot \tilde{\boldsymbol{H}}\right) + \tilde{\boldsymbol{E}}^i \quad (49)$$

$$\tilde{\boldsymbol{H}} = \boldsymbol{\mathcal{L}}\left(\bar{\bar{\tau}}_\mu \cdot \tilde{\boldsymbol{H}}\right) + jk_0\,\boldsymbol{\mathcal{K}}\left(\bar{\bar{\xi}}_r \cdot \tilde{\boldsymbol{H}}\right) + \boldsymbol{\mathcal{L}}\left(\bar{\bar{\zeta}}_r \cdot \tilde{\boldsymbol{E}}\right) + jk_0\,\boldsymbol{\mathcal{K}}\left(\bar{\bar{\tau}}_\varepsilon \cdot \tilde{\boldsymbol{E}}\right) + \tilde{\boldsymbol{H}}^i \quad (50)$$

3.3.2 The DB-formulation

The constitutive relations for bi-anisotropic medium can be re-written as,

$$\boldsymbol{E} = \bar{\bar{\alpha}}_1 \cdot \boldsymbol{D} + \bar{\bar{\alpha}}_2 \cdot \boldsymbol{B} \quad (51)$$

$$\boldsymbol{H} = \bar{\bar{\alpha}}_3 \cdot \boldsymbol{D} + \bar{\bar{\alpha}}_4 \cdot \boldsymbol{B} \quad (52)$$

where

$$\begin{bmatrix} \bar{\bar{\alpha}}_1 & \bar{\bar{\alpha}}_2 \\ \bar{\bar{\alpha}}_3 & \bar{\bar{\alpha}}_4 \end{bmatrix} = \begin{bmatrix} \bar{\bar{\varepsilon}} & \bar{\bar{\xi}} \\ \bar{\bar{\zeta}} & \bar{\bar{\mu}} \end{bmatrix}^{-1} \quad (53)$$

The equivalent polarization current densities can then be written in terms of flux densities as,

$$\boldsymbol{J}_V = j\omega(\bar{\bar{\beta}}_1 \cdot \boldsymbol{D} + \bar{\bar{\beta}}_2 \cdot \boldsymbol{B}) \quad (54)$$

$$\boldsymbol{M}_V = j\omega(\bar{\bar{\beta}}_3 \cdot \boldsymbol{B} + \bar{\bar{\beta}}_4 \cdot \boldsymbol{D}) \quad (55)$$

where

$$\begin{bmatrix} \bar{\bar{\beta}}_1 & \bar{\bar{\beta}}_2 \\ \bar{\bar{\beta}}_3 & \bar{\bar{\beta}}_4 \end{bmatrix} = \begin{bmatrix} \bar{\bar{I}} - \varepsilon_0\bar{\bar{\alpha}}_1 & -\varepsilon_0\bar{\bar{\alpha}}_2 \\ \bar{\bar{I}} - \mu_0\bar{\bar{\alpha}}_4 & -\mu_0\bar{\bar{\alpha}}_3 \end{bmatrix} \quad (56)$$

Equations (35) and (36) can now be written in terms of flux densities as,

$$\bar{\bar{\alpha}}_1 \cdot \boldsymbol{D} + \bar{\bar{\alpha}}_2 \cdot \boldsymbol{B} = \frac{1}{\varepsilon_1}\boldsymbol{\mathcal{L}}\left(\bar{\bar{\beta}}_1 \cdot \boldsymbol{D} + \bar{\bar{\beta}}_2 \cdot \boldsymbol{B}\right)(\boldsymbol{r}) - \boldsymbol{\mathcal{K}}\left(j\omega(\bar{\bar{\beta}}_3 \cdot \boldsymbol{B} + \bar{\bar{\beta}}_4 \cdot \boldsymbol{D})\right)(\boldsymbol{r}) + \boldsymbol{E}^i$$

Moving the incident electric field intensity to the left and rearranging we get,

$$\boldsymbol{E}^i = \bar{\bar{\alpha}}_1 \cdot \boldsymbol{D} - \frac{1}{\varepsilon_1}\boldsymbol{\mathcal{L}}\left(\bar{\bar{\beta}}_1 \cdot \boldsymbol{D}\right) + j\omega\boldsymbol{\mathcal{K}}\left(\bar{\bar{\beta}}_4 \cdot \boldsymbol{D}\right) + \bar{\bar{\alpha}}_2 \cdot \boldsymbol{B} - \frac{1}{\varepsilon_1}\boldsymbol{\mathcal{L}}\left(\bar{\bar{\beta}}_2 \cdot \boldsymbol{B}\right) + j\omega\boldsymbol{\mathcal{K}}\left(\bar{\bar{\beta}}_3 \cdot \boldsymbol{B}\right) \tag{57}$$

Similarly,

$$\bar{\bar{\alpha}}_3 \cdot \boldsymbol{D} + \bar{\bar{\alpha}}_4 \cdot \boldsymbol{B} = \frac{1}{\mu_1}\boldsymbol{\mathcal{L}}\left(\bar{\bar{\beta}}_3 \cdot \boldsymbol{B} + \bar{\bar{\beta}}_4 \cdot \boldsymbol{D}\right)(\boldsymbol{r}) + \boldsymbol{\mathcal{K}}\left(j\omega(\bar{\bar{\beta}}_1 \cdot \boldsymbol{D} + \bar{\bar{\beta}}_2 \cdot \boldsymbol{B})\right)(\boldsymbol{r}) + \boldsymbol{H}^i$$

Moving the incident magnetic field intensity to the left and rearranging we get,

$$\boldsymbol{H}^i = \bar{\bar{\alpha}}_3 \cdot \boldsymbol{D} - \frac{1}{\mu_1}\boldsymbol{\mathcal{L}}\left(\bar{\bar{\beta}}_4 \cdot \boldsymbol{D}\right) - j\omega\boldsymbol{\mathcal{K}}\left(\bar{\bar{\beta}}_1 \cdot \boldsymbol{D}\right) + \bar{\bar{\alpha}}_4 \cdot \boldsymbol{B} - \frac{1}{\mu_1}\boldsymbol{\mathcal{L}}\left(\bar{\bar{\beta}}_3 \cdot \boldsymbol{B}\right) - j\omega\boldsymbol{\mathcal{K}}\left(\bar{\bar{\beta}}_2 \cdot \boldsymbol{B}\right) \tag{58}$$

3.3.3 The JM-formulation

In order to have an equation for the electric current, equations (35) and (36) are multiplied with $j\omega(\bar{\bar{\varepsilon}}\varepsilon_0)\cdot$ and with $j\omega\bar{\bar{\xi}}\cdot$, respectively, and combined. An equation for the magnetic current is obtained similarly. The equations read

$$\boldsymbol{J}_V - \bar{\bar{\tau}}_\varepsilon \cdot \boldsymbol{\mathcal{L}}(\boldsymbol{J}_V) + j\omega\varepsilon_0\bar{\bar{\tau}}_\varepsilon \cdot \boldsymbol{\mathcal{K}}(\boldsymbol{M}_V) - \frac{\bar{\bar{\xi}}}{\mu_0} \cdot \boldsymbol{\mathcal{L}}(\boldsymbol{M}_V) - j\omega\bar{\bar{\xi}} \cdot \boldsymbol{\mathcal{K}}(\boldsymbol{J}_V) = j\omega\varepsilon_0\bar{\bar{\tau}}_\varepsilon \cdot \boldsymbol{E}^i + j\omega\bar{\bar{\xi}} \cdot \boldsymbol{H}^i \tag{59}$$

$$\boldsymbol{M}_V - \bar{\bar{\tau}}_\mu \cdot \boldsymbol{\mathcal{L}}(\boldsymbol{M}_V) - j\omega\mu_0\bar{\bar{\tau}}_\mu \cdot \boldsymbol{\mathcal{K}}(\boldsymbol{J}_V) - \frac{\bar{\bar{\zeta}}}{\varepsilon_0} \cdot \boldsymbol{\mathcal{L}}(\boldsymbol{J}_V) + j\omega\bar{\bar{\zeta}} \cdot \boldsymbol{\mathcal{K}}(\boldsymbol{M}) = j\omega\mu_0\bar{\bar{\tau}}_\mu \cdot \boldsymbol{H}^i + j\omega\bar{\bar{\zeta}} \cdot \boldsymbol{E}^i \tag{60}$$

Using (44) and (45) in (41) and (42), we get the scaled equations for the currents

$$\begin{bmatrix} \bar{\bar{I}} - \bar{\bar{\tau}}_\varepsilon \cdot \boldsymbol{\mathcal{L}} - jk_0\bar{\bar{\xi}}_r \cdot \boldsymbol{\mathcal{K}} & -\bar{\bar{\xi}}_r \cdot \boldsymbol{\mathcal{L}} + jk_0\bar{\bar{\tau}}_\varepsilon \cdot \boldsymbol{\mathcal{K}} \\ -\bar{\bar{\zeta}}_r \cdot \boldsymbol{\mathcal{L}} - jk_0\bar{\bar{\tau}}_\mu \cdot \boldsymbol{\mathcal{K}} & \bar{\bar{I}} - \bar{\bar{\tau}}_\mu \cdot \boldsymbol{\mathcal{L}} + jk_0\bar{\bar{\zeta}}_r \cdot \boldsymbol{\mathcal{K}} \end{bmatrix} \begin{bmatrix} \tilde{\boldsymbol{J}}_V \\ \tilde{\boldsymbol{M}}_V \end{bmatrix} = j\omega \begin{bmatrix} \bar{\bar{\tau}}_\varepsilon \cdot \tilde{\boldsymbol{D}}^i + \bar{\bar{\xi}}_r \cdot \tilde{\boldsymbol{B}}^i \\ \bar{\bar{\tau}}_\mu \cdot \tilde{\boldsymbol{B}}^i + \bar{\bar{\zeta}}_r \cdot \tilde{\boldsymbol{D}}^i \end{bmatrix} \tag{61}$$

Defining an integral operator $\boldsymbol{\mathcal{T}}(\boldsymbol{F})(\boldsymbol{r})$

$$\boldsymbol{\mathcal{T}}(\boldsymbol{F})(\boldsymbol{r}) = \nabla \times \nabla \times \boldsymbol{\mathcal{S}}(\boldsymbol{F})(\boldsymbol{r}) \tag{62}$$

So that $\boldsymbol{\mathcal{L}}(\boldsymbol{F})(\boldsymbol{r})$ can be written in terms of $\boldsymbol{\mathcal{T}}(\boldsymbol{F})(\boldsymbol{r})$ as

$$\boldsymbol{\mathcal{L}}(\boldsymbol{F})(\boldsymbol{r}) = \left(\boldsymbol{\mathcal{T}} - \boldsymbol{\mathcal{I}}\right)(\boldsymbol{F})(\boldsymbol{r}) \tag{63}$$

Thus, Eq. (61) can be written in terms of as $\boldsymbol{\mathcal{T}}$ operator as

$$\left[\begin{array}{cc} \bar{\bar{\varepsilon}}_r - \bar{\bar{\tau}}_\varepsilon \cdot \boldsymbol{\mathcal{T}} - jk_0\bar{\bar{\xi}}_r \cdot \boldsymbol{\mathcal{K}} & \bar{\bar{\xi}}_r - \bar{\bar{\xi}}_r \cdot \boldsymbol{\mathcal{T}} + jk_0\bar{\bar{\tau}}_\varepsilon \cdot \boldsymbol{\mathcal{K}} \\ \bar{\bar{\zeta}}_r - \bar{\bar{\zeta}}_r \cdot \boldsymbol{\mathcal{T}} - jk_0\bar{\bar{\tau}}_\mu \cdot \boldsymbol{\mathcal{K}} & \bar{\bar{\mu}}_r - \bar{\bar{\tau}}_\mu \cdot \boldsymbol{\mathcal{T}} + jk_0\bar{\bar{\zeta}}_r \cdot \boldsymbol{\mathcal{K}} \end{array}\right] \left[\begin{array}{c} \tilde{\boldsymbol{J}}_V \\ \tilde{\boldsymbol{M}}_V \end{array}\right] = j\omega \left[\begin{array}{c} \bar{\bar{\tau}}_\varepsilon \cdot \tilde{\boldsymbol{D}}^i + \bar{\bar{\xi}}_r \cdot \tilde{\boldsymbol{B}}^i \\ \bar{\bar{\tau}}_\mu \cdot \tilde{\boldsymbol{B}}^i + \bar{\bar{\zeta}}_r \cdot \tilde{\boldsymbol{D}}^i \end{array}\right] \tag{64}$$

3.3.4 The AVFU-formulation

In order to obtain a volume integral equation formulation for the potentials, let us define the electric and magnetic bound and surface charge densities with the polarization $(\boldsymbol{J}_V, \boldsymbol{M}_V)$ currents defined according to equations (28) and (29),

$$\rho_e = \left(\frac{j}{\omega}\right) \nabla \cdot \boldsymbol{J}_V, \tag{65}$$

$$\sigma_e = -\left(\frac{j}{\omega}\right) \boldsymbol{J}_V \cdot \hat{\boldsymbol{n}}, \tag{66}$$

$$\rho_m = \left(\frac{j}{\omega}\right) \nabla \cdot \boldsymbol{M}_V, \tag{67}$$

$$\sigma_m = -\left(\frac{j}{\omega}\right) \boldsymbol{M}_V \cdot \hat{\boldsymbol{n}}, \tag{68}$$

Where $\hat{\boldsymbol{n}}$ is the outward unit normal vector on the surface. With the charge and current densities defined, the scattered vector and scalar electric and magnetic potentials are defined, respectively, as

$$\boldsymbol{A}^s = \mu_0 \int_D \boldsymbol{J}_V(\boldsymbol{r}')G(\boldsymbol{r},\boldsymbol{r}')\,dv' \tag{69}$$

$$V^s = \frac{1}{\varepsilon_0}\int_D \rho_e G(\boldsymbol{r},\boldsymbol{r}')\,dv' + \frac{1}{\varepsilon_0}\int_S \sigma_e G(\boldsymbol{r},\boldsymbol{r}')\,ds' \tag{70}$$

$$\boldsymbol{F}^s = \varepsilon_0 \int_D \boldsymbol{M}_V(\boldsymbol{r}')G(\boldsymbol{r},\boldsymbol{r}')\,dv' \tag{71}$$

$$U^s = \frac{1}{\mu_0}\int_D \rho_m G(\boldsymbol{r},\boldsymbol{r}')\,dv' + \frac{1}{\mu_0}\int_S \sigma_m G(\boldsymbol{r},\boldsymbol{r}')\,ds' \tag{72}$$

The scalar and vector potentials are related to each other via the Lorenz Gauge

$$\nabla \cdot \boldsymbol{A} + j\omega\varepsilon_0\mu_0 V = 0 \tag{73}$$

$$\nabla \cdot \boldsymbol{F} + j\omega\varepsilon_0\mu_0 U = 0 \tag{74}$$

The electric and magnetic field intensities can be written in terms of potentials as

$$\boldsymbol{E} = -j\omega\boldsymbol{A} - \nabla V - \frac{1}{\varepsilon_0}\nabla \times \boldsymbol{F} \tag{75}$$

$$\boldsymbol{H} = -j\omega\boldsymbol{F} - \nabla U + \frac{1}{\mu_0}\nabla \times \boldsymbol{A} \tag{76}$$

So that the equivalent electric and magnetic current densities can be written as

$$\boldsymbol{J}_V = j\omega(\bar{\bar{\varepsilon}} - \varepsilon_0\bar{\bar{I}}) \cdot \left(-j\omega\boldsymbol{A} - \nabla V - \frac{1}{\varepsilon_0}\nabla \times \boldsymbol{F}\right) + j\omega\bar{\bar{\xi}} \cdot \left(-j\omega\boldsymbol{F} - \nabla U + \frac{1}{\mu_0}\nabla \times \boldsymbol{A}\right) \tag{77}$$

$$\boldsymbol{M}_V = j\omega(\bar{\bar{\mu}} - \mu_0\bar{\bar{I}}) \cdot \left(-j\omega\boldsymbol{F} - \nabla U + \frac{1}{\mu_0}\nabla \times \boldsymbol{A}\right) + j\omega\bar{\bar{\zeta}} \cdot \left(-j\omega\boldsymbol{A} - \nabla V - \frac{1}{\varepsilon_0}\nabla \times \boldsymbol{F}\right) \tag{78}$$

The vector electric potential can be written as

$$\boldsymbol{A}(\boldsymbol{r}) = \boldsymbol{A}^i(\boldsymbol{r}) + \boldsymbol{A}^s(\boldsymbol{r}), \tag{79}$$

Substituting the integral for $\boldsymbol{A}^s$ and moving $\boldsymbol{A}^i$ to the right we get,

$$\boldsymbol{A} - \mu_0 \int_D \Big[j\omega(\bar{\bar{\varepsilon}} - \varepsilon_0\bar{\bar{I}}) \cdot \left(-j\omega\boldsymbol{A} - \nabla V - \frac{1}{\varepsilon_0}\nabla \times \boldsymbol{F}\right) + j\omega\bar{\bar{\xi}} \cdot \left(-j\omega\boldsymbol{F} - \nabla U + \frac{1}{\mu_0}\nabla \times \boldsymbol{A}\right)\Big] G(\boldsymbol{r}, \boldsymbol{r}')\, dv' = \boldsymbol{A}^i, \tag{80}$$

Similarly the vector magnetic potential can be written as,

$$\boldsymbol{F}(\boldsymbol{r}) = \boldsymbol{F}^i(\boldsymbol{r}) + \boldsymbol{F}^s(\boldsymbol{r}) \tag{81}$$

Substituting the integral for $\boldsymbol{F}^s$ and moving $\boldsymbol{F}^i$ to the right we get,

$$\boldsymbol{F} - \varepsilon_0 \int_D \Big[j\omega(\bar{\bar{\mu}} - \mu_0\bar{\bar{I}}) \cdot \left(-j\omega\boldsymbol{F} - \nabla U + \frac{1}{\mu_0}\nabla \times \boldsymbol{A}\right) + j\omega\bar{\bar{\zeta}} \cdot \left(-j\omega\boldsymbol{A} - \nabla V - \frac{1}{\varepsilon_0}\nabla \times \boldsymbol{F}\right)\Big] G(\boldsymbol{r}, \boldsymbol{r}')\, dv' = \boldsymbol{F}^i \tag{82}$$

where, $\boldsymbol{A}^i$ and $\boldsymbol{F}^i$ are incident potentials, $\boldsymbol{A}$ and $\boldsymbol{F}$ are total potentials.

3.3.4.1 Scaled Equations In order to make the equations well balanced the parameters are redefined so that they have the same dimensions.

$$\tilde{\boldsymbol{A}}^s = j\eta_0 k_0 \int_D \boldsymbol{J}_V(\boldsymbol{r}')G(\boldsymbol{r},\boldsymbol{r}')\,dv', \tag{83}$$

$$\tilde{V}^s = \frac{k_0}{\varepsilon_0}\int_D \rho_e G(\boldsymbol{r},\boldsymbol{r}')\,dv' + \frac{k_0}{\varepsilon_0}\int_S \sigma_e G(\boldsymbol{r},\boldsymbol{r}')\,ds', \tag{84}$$

$$\tilde{\boldsymbol{F}}^s = j\frac{k_0}{\eta_0}\int_D \eta_0 \boldsymbol{M}_V(\boldsymbol{r}')G(\boldsymbol{r},\boldsymbol{r}')\,dv', \tag{85}$$

$$\tilde{U}^s = \frac{k_0}{\mu_0}\int_D \eta_0\rho_m G(\boldsymbol{r},\boldsymbol{r}')\,dv' + \frac{k_0}{\mu_0}\int_S \eta_0\sigma_m G(\boldsymbol{r},\boldsymbol{r}')\,ds', \tag{86}$$

The electric and magnetic field intensities can then be written in terms of potentials as

$$\boldsymbol{E} = -\tilde{\boldsymbol{A}} - \frac{1}{k_0}\nabla\tilde{V} + j\frac{1}{k_0}\nabla\times\tilde{\boldsymbol{F}}, \tag{87}$$

$$\eta_0\boldsymbol{H} = -\tilde{\boldsymbol{F}} - \frac{1}{k_0}\nabla\tilde{U} - j\frac{1}{k_0}\nabla\times\tilde{\boldsymbol{A}}, \tag{88}$$

Equations (87) and (88) hold for the incident, scattered and total fields. Thus the equivalent electric and magnetic current densities become

$$\begin{aligned}
\boldsymbol{J}_V &= j\omega\varepsilon_0(\bar{\bar{\varepsilon}}_r - \bar{\bar{I}})\cdot\left(-\tilde{\boldsymbol{A}} - \frac{1}{k_0}\nabla\tilde{V} + j\frac{1}{k_0}\nabla\times\tilde{\boldsymbol{F}}\right) + j\omega\frac{\bar{\bar{\xi}}}{\eta_0}\cdot\left(-\tilde{\boldsymbol{F}} - \frac{1}{k_0}\nabla\tilde{U} - j\frac{1}{k_0}\nabla\times\tilde{\boldsymbol{A}}\right),\\
&= j\omega\varepsilon_0\left[(\bar{\bar{\varepsilon}}_r - \bar{\bar{I}})\cdot\left(-\tilde{\boldsymbol{A}} - \frac{1}{k_0}\nabla\tilde{V} + j\frac{1}{k_0}\nabla\times\tilde{\boldsymbol{F}}\right) + \frac{\bar{\bar{\xi}}}{\sqrt{\varepsilon_0\mu_0}}\cdot\left(-\tilde{\boldsymbol{F}} - \frac{1}{k_0}\nabla\tilde{U} - j\frac{1}{k_0}\nabla\times\tilde{\boldsymbol{A}}\right)\right],\\
&= j\omega\varepsilon_0\left[(\bar{\bar{\varepsilon}}_r - \bar{\bar{I}})\cdot\left(-\tilde{\boldsymbol{A}} - \frac{1}{k_0}\nabla\tilde{V} + j\frac{1}{k_0}\nabla\times\tilde{\boldsymbol{F}}\right) + (\bar{\bar{\chi}}^T - j\bar{\bar{\kappa}}^T)\cdot\left(-\tilde{\boldsymbol{F}} - \frac{1}{k_0}\nabla\tilde{U} - j\frac{1}{k_0}\nabla\times\tilde{\boldsymbol{A}}\right)\right] \qquad (89)\\
\boldsymbol{M}_V &= j\omega\mu_0\frac{1}{\eta_0}(\bar{\bar{\mu}}_r - \bar{\bar{I}})\cdot\left(-\tilde{\boldsymbol{F}} - \frac{1}{k_0}\nabla\tilde{U} - j\frac{1}{k_0}\nabla\times\tilde{\boldsymbol{A}}\right) + j\omega\bar{\bar{\zeta}}\cdot\left(-\tilde{\boldsymbol{A}} - \frac{1}{k_0}\nabla\tilde{V} + j\frac{1}{k_0}\nabla\times\tilde{\boldsymbol{F}}\right),\\
\eta_0\boldsymbol{M}_V &= j\omega\mu_0\left[(\bar{\bar{\mu}}_r - \bar{\bar{I}})\cdot\left(-\tilde{\boldsymbol{F}} - \frac{1}{k_0}\nabla\tilde{U} - j\frac{1}{k_0}\nabla\times\tilde{\boldsymbol{A}}\right) + \frac{\bar{\bar{\zeta}}}{\sqrt{\varepsilon_0\mu_0}}\cdot\left(-\tilde{\boldsymbol{A}} - \frac{1}{k_0}\nabla\tilde{V} + j\frac{1}{k_0}\nabla\times\tilde{\boldsymbol{F}}\right)\right],\\
&= j\omega\mu_0\left[(\bar{\bar{\mu}}_r - \bar{\bar{I}})\cdot\left(-\tilde{\boldsymbol{F}} - \frac{1}{k_0}\nabla\tilde{U} - j\frac{1}{k_0}\nabla\times\tilde{\boldsymbol{A}}\right) + (\bar{\bar{\chi}} + j\bar{\bar{\kappa}})\cdot\left(-\tilde{\boldsymbol{A}} - \frac{1}{k_0}\nabla\tilde{V} + j\frac{1}{k_0}\nabla\times\tilde{\boldsymbol{F}}\right)\right] \qquad (90)
\end{aligned}$$

where the two new dyadics $\bar{\bar{\chi}}$ and $\bar{\bar{\kappa}}$ are defined as;

$$\bar{\bar{\chi}} = \frac{\bar{\bar{\zeta}} + \bar{\bar{\xi}}^T}{2} \tag{91}$$

$$\bar{\bar{\kappa}} = \frac{\bar{\bar{\zeta}} - \bar{\bar{\xi}}^T}{j2} \tag{92}$$

The scaled vector electric potential can be written as,

$$\tilde{\boldsymbol{A}}(\boldsymbol{r}) = \tilde{\boldsymbol{A}}^{i}(\boldsymbol{r}) + \tilde{\boldsymbol{A}}^{s}(\boldsymbol{r}), \tag{93}$$

Substituting the integral for $\tilde{\boldsymbol{A}}^{s}$ and moving $\tilde{\boldsymbol{A}}^{i}$ to the right we get,

$$\tilde{\boldsymbol{A}} - j\eta_0 k_0 \int_D j\omega\varepsilon_0 \Big[(\bar{\bar{\varepsilon}}_r - \bar{\bar{I}}) \cdot \left(-\tilde{\boldsymbol{A}} - \frac{1}{k_0}\nabla\tilde{V} + j\frac{1}{k_0}\nabla\times\tilde{\boldsymbol{F}}\right) + \left(\bar{\bar{\chi}}^T - j\bar{\bar{\kappa}}^T\right) \cdot \left(-\tilde{\boldsymbol{F}} - \frac{1}{k_0}\nabla\tilde{U} - j\frac{1}{k_0}\nabla\times\tilde{\boldsymbol{A}}\right)\Big] G(\boldsymbol{r},\boldsymbol{r}')\, dv' = \tilde{\boldsymbol{A}}^{i},$$

Multiplying the above equation by k_0 we get,

$$\tilde{\boldsymbol{A}} - \int_D \Big[(\bar{\bar{\varepsilon}}_r - \bar{\bar{I}}) \cdot \left(-k_0^2\tilde{\boldsymbol{A}} - k_0\nabla\tilde{V} + jk_0\nabla\times\tilde{\boldsymbol{F}}\right) + \left(\bar{\bar{\chi}}^T - j\bar{\bar{\kappa}}^T\right) \cdot \left(-k_0^2\tilde{\boldsymbol{F}} - k_0\nabla\tilde{U} - jk_0\nabla\times\tilde{\boldsymbol{A}}\right)\Big] G(\boldsymbol{r},\boldsymbol{r}')\, dv' = \tilde{\boldsymbol{A}}^{i} \tag{94}$$

Similarly, the scaled vector magnetic potential can be written as,

$$\tilde{\boldsymbol{F}}(\boldsymbol{r}) = \tilde{\boldsymbol{F}}^{i}(\boldsymbol{r}) + \tilde{\boldsymbol{F}}^{s}(\boldsymbol{r}), \tag{95}$$

Substituting the integral for $\tilde{\boldsymbol{F}}^{s}$ and moving $\tilde{\boldsymbol{F}}^{i}$ to the right we get,

$$\tilde{\boldsymbol{F}} - j\frac{k_0}{\eta_0}\int_D j\omega\mu_0 \Big[(\bar{\bar{\mu}}_r - \bar{\bar{I}}) \cdot \left(-\tilde{\boldsymbol{F}} - \frac{1}{k_0}\nabla\tilde{U} - j\frac{1}{k_0}\nabla\times\tilde{\boldsymbol{A}}\right) + (\bar{\bar{\chi}} + j\bar{\bar{\kappa}}) \cdot \left(-\tilde{\boldsymbol{A}} - \frac{1}{k_0}\nabla\tilde{V} + j\frac{1}{k_0}\nabla\times\tilde{\boldsymbol{F}}\right)\Big] G(\boldsymbol{r},\boldsymbol{r}')\, dv' = \tilde{\boldsymbol{F}}^{i},$$

Multiplying the above equation by k_0 we get,

$$\tilde{\boldsymbol{F}} + \int_D \Big[(\bar{\bar{\mu}}_r - \bar{\bar{I}}) \cdot \Big(-k_0^2 \tilde{\boldsymbol{F}} - k_0 \nabla \tilde{U} - j k_0 \nabla \times \tilde{\boldsymbol{A}} \Big) + (\bar{\bar{\chi}} + j\bar{\bar{\kappa}}) \cdot \Big(-k_0^2 \tilde{\boldsymbol{A}} - k_0 \nabla \tilde{V} + j k_0 \nabla \times \tilde{\boldsymbol{F}} \Big) \Big] G(\boldsymbol{r}, \boldsymbol{r}')\, dv' = \tilde{\boldsymbol{F}}^i \quad (96)$$

Similarly, scaling the Lorenz Gauge equations we get,

$$\nabla \cdot \tilde{\boldsymbol{A}} - k_0 \tilde{V} = 0 \quad (97)$$

$$\nabla \cdot \tilde{\boldsymbol{F}} - k_0 \tilde{U} = 0 \quad (98)$$

Equations (94), (96), (97) and (98) constitute the AVFU-formulation.
Defining the integral operators;

$$\boldsymbol{\mathcal{S}}_{\bar{\bar{\varepsilon}}}(\boldsymbol{X})(\boldsymbol{r}) = \int_D \Big[(\bar{\bar{\varepsilon}}_r - \bar{\bar{I}}) \cdot \boldsymbol{X} \Big] G(\boldsymbol{r}, \boldsymbol{r}')\, dv' \quad (99)$$

$$\boldsymbol{\mathcal{S}}_{\bar{\bar{\mu}}}(\boldsymbol{X})(\boldsymbol{r}) = \int_D \Big[(\bar{\bar{\mu}}_r - \bar{\bar{I}}) \cdot \boldsymbol{X} \Big] G(\boldsymbol{r}, \boldsymbol{r}')\, dv' \quad (100)$$

$$\boldsymbol{\mathcal{S}}_{\bar{\bar{\chi}}^T \bar{\bar{\kappa}}^T}(\boldsymbol{X})(\boldsymbol{r}) = \int_D \big[(\bar{\bar{\chi}}^T - \bar{\bar{\kappa}}^T) \cdot \boldsymbol{X} \big] G(\boldsymbol{r}, \boldsymbol{r}')\, dv' \quad (101)$$

$$\boldsymbol{\mathcal{S}}_{\bar{\bar{\chi}}\bar{\bar{\kappa}}}(\boldsymbol{X})(\boldsymbol{r}) = \int_D \left[(\bar{\bar{\chi}} + \bar{\bar{\kappa}}) \cdot \boldsymbol{X} \right] G(\boldsymbol{r}, \boldsymbol{r}')\, dv' \quad (102)$$

Equations (94), (96), (97) and (98) can be written in matrix form as,

$$\begin{bmatrix} \nabla \cdot \bar{\bar{I}} & -k_0 & 0 & 0 \\ 0 & 0 & \nabla \cdot \bar{\bar{I}} & -k_0 \\ \bar{\bar{I}} - {k_0}^2 \boldsymbol{\mathcal{S}}_{\bar{\bar{\varepsilon}}}(\bar{\bar{I}}) - j k_0 \boldsymbol{\mathcal{S}}_{\bar{\bar{\chi}}^T \bar{\bar{\kappa}}^T}(\nabla \times \bar{\bar{I}}) & -k_0 \boldsymbol{\mathcal{S}}_{\bar{\bar{\varepsilon}}}(\nabla) & j k_0 \boldsymbol{\mathcal{S}}_{\bar{\bar{\varepsilon}}}(\nabla \times \bar{\bar{I}}) - {k_0}^2 \boldsymbol{\mathcal{S}}_{\bar{\bar{\chi}}^T \bar{\bar{\kappa}}^T}(\bar{\bar{I}}) & -k_0 \boldsymbol{\mathcal{S}}_{\bar{\bar{\chi}}^T \bar{\bar{\kappa}}^T}(\nabla) \\ -j k_0 \boldsymbol{\mathcal{S}}_{\bar{\bar{\mu}}}(\nabla \times \bar{\bar{I}}) - {k_0}^2 \boldsymbol{\mathcal{S}}_{\bar{\bar{\chi}}\bar{\bar{\kappa}}}(\bar{\bar{I}}) & -k_0 \boldsymbol{\mathcal{S}}_{\bar{\bar{\chi}}\bar{\bar{\kappa}}}(\nabla) & \bar{\bar{I}} - {k_0}^2 \boldsymbol{\mathcal{S}}_{\bar{\bar{\mu}}}(\bar{\bar{I}}) + j k_0 \boldsymbol{\mathcal{S}}_{\bar{\bar{\chi}}\bar{\bar{\kappa}}}(\nabla \times \bar{\bar{I}}) & -k_0 \boldsymbol{\mathcal{S}}_{\bar{\bar{\mu}}}(\nabla) \end{bmatrix} \begin{bmatrix} \tilde{\boldsymbol{A}} \\ \tilde{V} \\ \tilde{\boldsymbol{F}} \\ \tilde{U} \end{bmatrix} = \begin{bmatrix} 0 \\ 0 \\ \tilde{\boldsymbol{A}}^i \\ \tilde{\boldsymbol{F}}^i \end{bmatrix} \quad (103)$$

Equation (103) is used in the numerical implementation of AVFU-formulation (4.2.2)

4 Numerical Solution of Volume Integral Equations

The numerical solution of volume integral equations is obtained by the *Method of Moments* (MoM). MoM is a mathematical concept by which the functional equations of field theory are reduced to matrix equations. The MoM technique was introduced by Roger F. Harrington in his 1967 seminal paper, "Matrix Methods for Field Problems" [21]. The MoM applies orthogonal projections to translate the integral equation statement into a system of linear equations. Basis functions are used to expand the unknowns (fields, flux densities, current densities or potentials), testing functions are used to enforce the equations hold in the weighted average sense and matrix methods are then used to solve for the expansion coefficients associated with the basis functions [22].

4.1 Method of Moments (MoM)

Consider the inhomogeneous equation,

$$L(f) = g \tag{104}$$

where L is a linear operator, g is a known excitation or forcing function, and f is the unknown quantity to be determined. Let f be expanded in a series of functions $f_1, f_2, f_3, \cdots$ in the domain of L, as

$$f = \sum_n \alpha_n f_n \tag{105}$$

where the α_n are constants. The f_n are called expansion functions or basis functions. Substituting (105) in (104), and using the linearity of L, we have

$$\sum_n \alpha_n L(f_n) = g \tag{106}$$

To determine α_n we choose another set of functions $w_1, w_2, w_3, \cdots$ in the range of L, and taking the inner product of (106) with each w_m, we get

$$\sum_n \alpha_n \langle w_m, L(f_n) \rangle = \langle w_m, g \rangle \tag{107}$$

The w_m, $m = 1, 2, 3, \cdots, M$ are referred to as the weighting or testing function. In practice, the number of basis and testing functions are equal, i.e. $N = M$.

Equation (107) can be written in matrix form as

$$[Z_{mn}]\,[\alpha_n] = [g_m] \tag{108}$$

where

$$[Z_{mn}] = \begin{bmatrix} \langle w_1, L(f_1)\rangle & \langle w_1, L(f_2)\rangle & \langle w_1, L(f_3)\rangle & \cdots \\ \langle w_2, L(f_1)\rangle & \langle w_2, L(f_2)\rangle & \langle w_2, L(f_3)\rangle & \cdots \\ \langle w_3, L(f_1)\rangle & \langle w_3, L(f_2)\rangle & \langle w_3, L(f_3)\rangle & \cdots \\ \vdots & \vdots & \vdots & \end{bmatrix} \tag{109}$$

$$[\alpha_n] = \begin{bmatrix} \alpha_1 \\ \alpha_2 \\ \alpha_3 \\ \vdots \end{bmatrix} \tag{110}$$

$$[g_m] = \begin{bmatrix} \langle w_1, g\rangle \\ \langle w_2, g\rangle \\ \langle w_3, g\rangle \\ \vdots \end{bmatrix} \tag{111}$$

If the matrix $[Z]$ is non-singular, i.e. its inverse $[Z^{-1}]$ exists and the unknown coefficients $\alpha_n, n = 1, 2, 3, \cdots, N$ are then given by

$$[\alpha_n] = [Z_{mn}]^{-1}[g_m] \tag{112}$$

and the solution for f is given by (105) [22].

Thus, the MoM uses orthogonal projections and linear algebra to reduce the integral equation problem to a system of linear equations. The unknown field, flux, current, or potential distribution is represented in terms of linearly independent set of basis functions. Then an inner product is formulated with a linearly independent set of testing functions forming a projection operator that forces the error to be orthogonal with respect to the space spanned. The expansion coefficients can be moved out of the linear operator; this permits

the evaluation of unknown functions. The expansion coefficients, the orthogonal projections of electromagnetic boundary conditions, and the loosely defined impedance's are gathered into a system of linear equations. This system of equations is solved to yield the expansion coefficients. The original distribution is then determined by introducing these coefficients back into the basis function expansion.

One of the main tasks in any particular problem is the choice of the basis (f_n) and testing (w_m) functions. Some of the factors that affect the choice of f_n and w_m are a) the accuracy of solution desired, b) the ease of evaluation of matrix elements, c) the size of system matrix that can be inverted [21].

4.1.1 Basis Functions

The MoM solution begins by defining the unknown distribution by a linearly independent set of basis functions. There are two types of basis functions, *sub-domain basis functions* and *entire domain basis functions*. Sub-domain basis functions subdivide the domain into small segments called *elements* and model the unknown distribution on each element or on a few adjacent elements by functions; $f_n, n = 1, 2, 3, \cdots, N$ that are typically low order polynomials. Whereas, the entire domain basis functions are defined over the entire domain and employ a more formal orthogonal expansion, such as a Fourier series, to represent the unknown distribution. Entire domain basis functions tend to yield more complicated calculations for the so-called impedances and, therefore, are less popular.

The choice of the basis functions depends on the (continuity) properties of the unknown function. Generally the basis function should satisfy the same physical (e.g., boundary) conditions as the original unknown. If the unknown quantity f is continuous, when it in many cases is advantageous that also the basis function approximation is continuous. This, however, is not necessary and it is possible to approximate a continuous function with discontinuous basis functions. On the other hand, if the function is discontinuous it should not be approximated with continuous functions. The basis functions should also be linearly independent to guarantee that the resulting linear system is non-singular and invertible. Moreover, the choice of basis functions is also effected by the nature of the unknown function, i.e. if the unknown function is a scalar or a vector. If the unknown function is a scalar or a vector whose coordinate components can be decoupled, than it can be expanded with continuous nodal basis functions (the degrees of freedom are related to the nodes of a mesh). If the unknown function is a vector whose coordinate components

cannot be decoupled than it is expanded with vector basis functions that are associated to the edges of a mesh or to the faces of elements in a mesh (degrees of freedom, DoF, is equal to the number of edges/faces).

- The EH-formulation is usually discretized with curl conforming functions, i.e. basis functions are curl conforming edge functions that keep the tangential continuity [23], [24]. The EH-formulation has also been discretized using piecewise constant and linear functions in order to obtain a non-conformal method, i.e. the continuity of the fields are not directly enforced but the solution approximately satisfies these conditions [25], [26].

- Normal components of the electric and magnetic flux densities must be continuous across material interfaces, therefore, the DB-formulation is usually discretized with divergence conforming face basis functions, known as the SWG functions or 3D RWG functions [27]. However, SWG are not divergence free (i.e. $\nabla \cdot \boldsymbol{D} \neq 0$ and $\nabla \cdot \boldsymbol{B} \neq 0$), therefore, fluxes should be expanded with solenoidal basis functions rather than SWG functions [28].

- In the JM-formulation, the equivalent volume current densities do not put any continuity requirements and it is necessary, therefore, that the basis functions do not enforce any continuity across material interfaces. The equivalent volume current densities are usually expanded with piecewise constant basis functions.

- The scalar and vector potentials in the AVFU-formulation are continuous functions in space and therefore can be expanded with scalar and components with scalar nodal basis functions [4], [5], [6].

4.1.2 Testing Functions

In order to convert an integral equation formulation into a matrix assembly, a set of weighting or testing functions are chosen. This set of functions should be approximately complete in the dual of the range of the integral operator if $\boldsymbol{\mathcal{L}}^2$ inner product is applied. There are a number of different ways of implementing the MoM technique depending on the choice of the testing functions. Two common approaches to formulating the orthogonal set of testing functions are the "Point Matching Technique" and the "Galerkin's Technique".

4.1.2.1 Point Matching The point matching or collocation technique defines the testing functions in terms of Dirac delta functions, i.e.

$$w_m(\boldsymbol{r}) = \delta(\boldsymbol{r} - \boldsymbol{r}_m) \tag{113}$$

where $\boldsymbol{r}_m$ are points in the domain at which the integral equations are enforced. The $\boldsymbol{r}_m$ (in a 3D case) are usually chosen to be the nodes of a tetrahedral mesh into which the structure is divided. One benefit of point matching is that in evaluating the matrix elements, no integral is required over the range of the testing function, only that of the source function. The primary disadvantage is that the equations are matched only at discrete locations throughout the solution domain, allowing them to assume a different value at points other than those used for testing.

4.1.2.2 Galerkin's Technique The second approach defines the testing function to be the same as the basis function and is formally known as the Galerkin's technique. Galerkins technique enforces the boundary conditions more rigorously and throughout the solution domain, instead of at discrete points as with the point-matching technique. But Galerkin's technique is more complicated from a computational perspective.

The choice of the testing functions is important in order to obtain an efficient numerical method. In [29] and [30] it is shown that the testing functions should span the dual space of the range of the integral operator to guarantee the convergence of the solution. In the case of Galerkin's Technique, where the basis and testing functions are the same, the technique works only if the range of the operator is dual to the space spanned by the basis function.

4.2 Method of Moments (MoM) Implementation of Volume Integral Equations

In this section MoM is applied to volume integral equation formulations. A complete MoM implementation of AVFU-formulation is discussed. For the MoM implementation of DB- and EH- formulations the interested reader is referred to [1] and [2], respectively.

4.2.1 MoM Implementation of the JM-formulation

Let us divide the object with linear tetrahedral elements N_T with N_V vertices (viz. nodes) and define basis $\boldsymbol{b}$ and testing $\boldsymbol{t}$ functions on the tetrahedral mesh. The equivalent volume currents are discontinuous if ε or μ are discontinuous; hence it is essential that the basis functions $\boldsymbol{b}_m$ do not enforce any continuity across the element interfaces. We use piecewise constant basis and testing functions (Galerkin's technique) to expand the unknowns (three functions in each tetrahedra).
Equation (64) can be written as;

$$\begin{bmatrix} A_{mn}^{11} & A_{mn}^{12} \\ A_{mn}^{21} & A_{mn}^{22} \end{bmatrix} \begin{bmatrix} x_m^1 \\ x_m^2 \end{bmatrix} = \begin{bmatrix} e_m^1 \\ e_m^2 \end{bmatrix} \tag{114}$$

for all $m = 1, \cdots, M$ and $n = 1, \cdots, N$.

$$\begin{aligned} A_{mn}^{11} &= \left\langle t_n, [\bar{\bar{\varepsilon}}_r - \bar{\bar{\tau}}_\varepsilon \cdot \nabla \times \nabla \times \boldsymbol{\mathcal{S}}(\boldsymbol{b}_m) - jk_0 \bar{\bar{\xi}}_r \cdot \nabla \times \boldsymbol{\mathcal{S}}(\boldsymbol{b}_n)] \right\rangle \\ &= \int_v \boldsymbol{t}_n \cdot \bar{\bar{\varepsilon}}_r \, dv - \int_s \boldsymbol{n} \times (\bar{\bar{\tau}}_\varepsilon^T \cdot \boldsymbol{t}_n) \cdot \int_v \nabla G \times \boldsymbol{b}_m \, dv' \, ds - jk_0 \int_v \boldsymbol{t}_n \cdot \bar{\bar{\xi}}_r \cdot \int_v \nabla G \times \boldsymbol{b}_m \, dv' \, dv \end{aligned} \tag{115}$$

Similarly,

$$A_{mn}^{12} = \int_v \boldsymbol{t}_n \cdot \bar{\bar{\xi}}_r \, dv - \int_s \boldsymbol{n} \times (\bar{\bar{\xi}}_r^T \cdot \boldsymbol{t}_n) \cdot \int_v \nabla G \times \boldsymbol{b}_m \, dv' \, ds - jk_0 \int_v \boldsymbol{t}_n \cdot \bar{\bar{\tau}}_\varepsilon \cdot \int_v \nabla G \times \boldsymbol{b}_m \, dv' \, dv \tag{116}$$

$$A_{mn}^{21} = \int_v \boldsymbol{t}_n \cdot \bar{\bar{\zeta}}_r \, dv - \int_s \boldsymbol{n} \times (\bar{\bar{\zeta}}_r^T \cdot \boldsymbol{t}_n) \cdot \int_v \nabla G \times \boldsymbol{b}_m \, dv' \, ds - jk_0 \int_v \boldsymbol{t}_n \cdot \bar{\bar{\tau}}_\mu \cdot \int_v \nabla G \times \boldsymbol{b}_m \, dv' \, dv \tag{117}$$

$$A_{mn}^{22} = \int_v \boldsymbol{t}_n \cdot \bar{\bar{\mu}}_r \, dv - \int_s \boldsymbol{n} \times (\bar{\bar{\tau}}_\mu^T \cdot \boldsymbol{t}_n) \cdot \int_v \nabla G \times \boldsymbol{b}_m \, dv' \, ds - jk_0 \int_v \boldsymbol{t}_n \cdot \bar{\bar{\zeta}}_r \cdot \int_v \nabla G \times \boldsymbol{b}_m \, dv' \, dv \tag{118}$$

$\bar{\bar{\tau}}_\varepsilon^T$,$\bar{\bar{\tau}}_\mu^T$,$\bar{\bar{\xi}}_r^T$,$\bar{\bar{\zeta}}_r^T$ are the transpose of $\bar{\bar{\tau}}_\varepsilon$,$\bar{\bar{\tau}}_\mu$,$\bar{\bar{\xi}}_r$ and $\bar{\bar{\zeta}}_r$, respectively.

$$x_m^1 = c_m \tag{119}$$

$$x_m^2 = d_m \tag{120}$$

c_m, d_m are the unknown coefficients.

$$e_m^1 = j\omega \left\langle \boldsymbol{t}_n, [\bar{\bar{\tau}}_\varepsilon \cdot \tilde{\boldsymbol{D}}^i + \bar{\bar{\xi}}_r \cdot \tilde{\boldsymbol{B}}^i] \right\rangle = j\omega \int_v \boldsymbol{t}_n \cdot [\bar{\bar{\tau}}_\varepsilon \cdot \tilde{\boldsymbol{D}}^i + \bar{\bar{\xi}} \cdot \tilde{\boldsymbol{B}}^i]\, dv \tag{121}$$

$$e_m^2 = j\omega \left\langle \boldsymbol{t}_n, [\bar{\bar{\tau}}_\mu \cdot \tilde{\boldsymbol{D}}^i + \bar{\bar{\zeta}}_r \cdot \tilde{\boldsymbol{B}}^i] \right\rangle = j\omega \int_v \boldsymbol{t}_n \cdot [\bar{\bar{\tau}}_\mu \cdot \tilde{\boldsymbol{D}}^i + \bar{\bar{\xi}}_r \cdot \tilde{\boldsymbol{B}}^i]\, dv \tag{122}$$

$n = 1, 2, 3, \cdots, N$ and $m = 1, 2, 3, \cdots, M$, $N = M$.

4.2.2 MoM Implementation of the AVFU-formulation

Dividing the scatterer in N_T discretization cells so that in an individual cell the characteristic parameters $(\bar{\bar{\varepsilon}}, \bar{\bar{\mu}}, \bar{\bar{\xi}}, \bar{\bar{\zeta}})$ are supposed to be constant; equation (103) can be written as,

$$\begin{bmatrix} B^{11} & B^{12} & B^{13} & B^{14} \\ B^{21} & B^{22} & B^{23} & B^{24} \\ B^{31} & B^{32} & B^{33} & B^{34} \\ B^{41} & B^{42} & B^{43} & B^{44} \end{bmatrix} \begin{bmatrix} y^1 \\ y^2 \\ y^3 \\ y^4 \end{bmatrix} = \begin{bmatrix} f^1 \\ f^2 \\ f^3 \\ f^4 \end{bmatrix} \tag{123}$$

The elements of the sub-matrices are defined below as;

$$B^{11} = \nabla \cdot \bar{\bar{I}} \tag{124}$$

$$B^{12} = -k_0 \tag{125}$$

$$B^{13} = 0 \tag{126}$$

$$B^{14} = 0 \tag{127}$$

$$B^{21} = 0 \tag{128}$$

$$B^{22} = 0 \tag{129}$$

$$B^{23} = \nabla \cdot \bar{\bar{I}} \tag{130}$$

$$B^{24} = -k_0 \tag{131}$$

$$B^{31} = \bar{\bar{I}} - {k_0}^2 \left[(\bar{\bar{\varepsilon}}_r - \bar{\bar{I}}) \boldsymbol{\mathcal{S}} (\bar{\bar{I}}) \right]_e - jk_0 \left[(\bar{\bar{\chi}}^T - \bar{\bar{\kappa}}^T) \boldsymbol{\mathcal{S}} (\nabla \times \bar{\bar{I}}) \right]_e \tag{132}$$

$$B^{32} = -k_0 \left[(\bar{\bar{\varepsilon}}_r - \bar{\bar{I}}) \boldsymbol{\mathcal{S}}(\nabla) \right]_e \tag{133}$$

$$B^{33} = jk_0 \left[(\bar{\bar{\varepsilon}}_r - \bar{\bar{I}}) \boldsymbol{\mathcal{S}}(\nabla \times \bar{\bar{I}}) \right]_e - {k_0}^2 \left[(\bar{\bar{\chi}}^T - \bar{\bar{\kappa}}^T) \boldsymbol{\mathcal{S}}(\bar{\bar{I}}) \right]_e \tag{134}$$

$$B^{34} = -k_0 \left[(\bar{\bar{\chi}}^T - \bar{\bar{\kappa}}^T) \boldsymbol{\mathcal{S}}(\nabla) \right]_e \tag{135}$$

$$B^{41} = -jk_0 \left[(\bar{\bar{\mu}}_r - \bar{\bar{I}}) \boldsymbol{\mathcal{S}}(\nabla \times \bar{\bar{I}}) \right]_e - {k_0}^2 \left[(\bar{\bar{\chi}} + \bar{\bar{\kappa}}) \boldsymbol{\mathcal{S}}(\bar{\bar{I}}) \right]_e \tag{136}$$

$$B^{42} = -k_0 \left[(\bar{\bar{\chi}} + \bar{\bar{\kappa}}) \boldsymbol{\mathcal{S}}(\nabla) \right]_e \tag{137}$$

$$B^{43} = \bar{\bar{I}} - {k_0}^2 \left[(\bar{\bar{\mu}}_r - \bar{\bar{I}}) \boldsymbol{\mathcal{S}}(\bar{\bar{I}}) \right]_e + jk_0 \left[(\bar{\bar{\chi}} + \bar{\bar{\kappa}}) \boldsymbol{\mathcal{S}}(\nabla \times \bar{\bar{I}}) \right]_e \tag{138}$$

$$B^{44} = -k_0 \left[(\bar{\bar{\mu}}_r - \bar{\bar{I}}) \boldsymbol{\mathcal{S}}(\nabla) \right]_e \tag{139}$$

where,

$$\boldsymbol{\mathcal{S}}(\boldsymbol{X})(\boldsymbol{r}) = \int_D XG(\boldsymbol{r}, \boldsymbol{r}')\, dv'$$

and

$$y^1 = \tilde{\boldsymbol{A}} \tag{140}$$

$$y^2 = \tilde{V} \tag{141}$$

$$y^3 = \tilde{\boldsymbol{F}} \tag{142}$$

$$y^4 = \tilde{U} \tag{143}$$

y^1 and y^3 are $1 \times 3N_n$ coefficient matrices (since each component of vector potentials is decoupled) and y^2 and y^4 are $1 \times N_n$ coefficient matrices.

$$f^1 = 0 \tag{144}$$

$$f^2 = 0 \tag{145}$$

$$f^3 = \tilde{\boldsymbol{A}}^i \tag{146}$$

$$f^4 = \tilde{\boldsymbol{F}}^i \tag{147}$$

f^1 and f^2 are $1 \times N_n$ zero matrices (the use of Lorenz gauge eliminates the requirement to specify the scalar potentials) and f^3 and f^4 are $1 \times 3N_n$ matrices defining the incident vector potentials.

The potentials are continuous functions in space which allows using scalar linear nodal basis functions (the AVFU-formulation involves gradients, divergence and curls of potential functions, therefore, piecewise constant basis functions cannot be used). Together with the scalar linear nodal basis functions, point matching testing procedure can be adopted so that the testing functions are delta functions. The potentials are expanded as;

$$\tilde{\boldsymbol{A}} = \sum_{n=1}^{N_V} \left(\hat{\boldsymbol{x}} A_{x,n} + \hat{\boldsymbol{y}} A_{y,n} + \hat{\boldsymbol{z}} A_{z,n}\right) b_n = \sum_{n=1}^{N_V} \boldsymbol{A}_n b_n, \tag{148}$$

$$\tilde{V} = \sum_{n=1}^{N_V} V_n b_n, \tag{149}$$

$$\tilde{\boldsymbol{F}} = \sum_{n=1}^{N_V} \left(\hat{\boldsymbol{x}} F_{x,n} + \hat{\boldsymbol{y}} F_{y,n} + \hat{\boldsymbol{z}} F_{z,n}\right) b_n = \sum_{n=1}^{N_V} \boldsymbol{F}_n b_n, \tag{150}$$

$$\tilde{U} = \sum_{n=1}^{N_V} U_n b_n. \tag{151}$$

If $N_i^e, i = 1, \ldots, 4$ are linear nodal shape functions of the e^{th} tetrahedron, then the above defined potentials can be rewritten as,

$$\tilde{\boldsymbol{A}} = \sum_{e=1}^{N_T} \sum_{i=1}^{4} \left(\hat{\boldsymbol{x}} A_{x,i}^e + \hat{\boldsymbol{y}} A_{y,i}^e + \hat{\boldsymbol{z}} A_{z,i}^e\right) N_i^e, \tag{152}$$

$$\tilde{V} = \sum_{e=1}^{N_T} \sum_{i=1}^{4} V_i^e N_i^e, \tag{153}$$

$$\tilde{\boldsymbol{F}} = \sum_{e=1}^{N_T} \sum_{i=1}^{4} \left(\hat{\boldsymbol{x}} F_{x,i}^e + \hat{\boldsymbol{y}} F_{y,i}^e + \hat{\boldsymbol{z}} F_{z,i}^e\right) N_i^e, \tag{154}$$

$$\tilde{U} = \sum_{e=1}^{N_T} \sum_{i=1}^{4} U_i^e N_i^e. \tag{155}$$

4.2.2.1 Evaluation of Unknown Integral Terms Using the Local Matrices By using the concept of local matrices the matrix assembly is simplified as will be demonstrated

later. From equation (103) we have the following unknown terms;

$$1.\ \langle t_m, b_n \rangle = \int_v t_m b_n \, dv, \tag{156}$$

$$2.\ \langle \boldsymbol{t}_m, \nabla \cdot \boldsymbol{b}_n \rangle = \int_v \boldsymbol{t}_m \cdot \nabla \cdot \boldsymbol{b}_n \, dv, \tag{157}$$

$$3.\ \left\langle \boldsymbol{t}_m, \bar{\bar{P}} \cdot \boldsymbol{\mathcal{S}}(b_n) \right\rangle = \int_v \boldsymbol{t}_m \cdot \bar{\bar{P}} \cdot \int_v \boldsymbol{b}_n G(\boldsymbol{r}, \boldsymbol{r}') \, dv' \, dv, \tag{158}$$

$$4.\ \left\langle \boldsymbol{t}_m, \bar{\bar{P}} \cdot \boldsymbol{\mathcal{S}}(\nabla b_n) \right\rangle = \int_v \boldsymbol{t}_m \cdot \bar{\bar{P}} \cdot \int_v (\nabla b_n) G(\boldsymbol{r}, \boldsymbol{r}') \, dv' \, dv, \tag{159}$$

$$5.\ \left\langle \boldsymbol{t}_m, \bar{\bar{P}} \cdot \boldsymbol{\mathcal{S}}(\nabla \times \boldsymbol{b}_n) \right\rangle = \int_v \boldsymbol{t}_m \cdot \bar{\bar{P}} \cdot \int_v (\nabla \times \boldsymbol{b}_n) G(\boldsymbol{r}, \boldsymbol{r}') \, dv' \, dv, \tag{160}$$

where $\bar{\bar{P}}$ represents a material dyadic. Using the shape functions define the following local matrices;

$$alok_{ij}^{(0,1)} = \int_{E_d} \delta(\boldsymbol{r}_i) N_j^e(\boldsymbol{r}') \, dv = 1 \qquad if \ \ i = j \ \ (0 \ \text{ otherwise}), \tag{161}$$

$$alok_{ij}^{(0,x)} = \int_{E_d} \delta(\boldsymbol{r}_i) \frac{\partial N_j^e(\boldsymbol{r}')}{\partial x} \, dv = \frac{\partial N_j^e(\boldsymbol{r}')}{\partial x} \qquad for\ all \qquad (i \in E_d) == (j \in E_e), \tag{162}$$

$$alok_{ij}^{(0,y)} = \int_{E_d} \delta(\boldsymbol{r}_i) \frac{\partial N_j^e(\boldsymbol{r}')}{\partial y} \, dv = \frac{\partial N_j^e(\boldsymbol{r}')}{\partial y} \qquad for\ all \qquad (i \in E_d) == (j \in E_e), \tag{163}$$

$$alok_{ij}^{(0,z)} = \int_{E_d} \delta(\boldsymbol{r}_i) \frac{\partial N_j^e(\boldsymbol{r}')}{\partial z} \, dv = \frac{\partial N_j^e(\boldsymbol{r}')}{\partial z} \qquad for\ all \qquad (i \in E_d) == (j \in E_e), \tag{164}$$

$$\begin{aligned} alok_{ij}^{(1)} &= \int_{E_d} \delta(\boldsymbol{r}_i) \int_{E_e} G(\boldsymbol{r}, \boldsymbol{r}') N_j^e(\boldsymbol{r}') \, dv' \, dv \\ &= \left| \det(J_{\boldsymbol{\mathcal{F}}_e}) \right| \sum_{p=1}^{P} w_p G(\boldsymbol{r}_d, \boldsymbol{r}'_e) \hat{N}_j^e(\alpha, \beta, \gamma) \qquad (\boldsymbol{r}_d \in E_d \ \ \& \ \ \boldsymbol{r}'_e \in E_e) \end{aligned} \tag{165}$$

$$alok_{ij}^{(2)} = \int_{E_d} \delta(\boldsymbol{r}_i) \int_{E_e} G(\boldsymbol{r}, \boldsymbol{r}') \, dv' \, dv = \int_{E_e} G(\boldsymbol{r}, \boldsymbol{r}') \, dv' = \sum_{j=1}^{4} alok_{ij}^{(1)} \tag{166}$$

$$i = j = 1, \ldots, 4$$

where $alok^{(0,1)}, alok^{(0,x)}, alok^{(0,y)}, alok^{(0,z)}$ and $alok^{(1)}$ are $[4 \times 4]$ matrices and $alok^{(2)}$

is a scalar. So, the above unknown integrals can be written in terms of the local matrices and scalar as;

$$1.\left\langle \delta(\boldsymbol{r}_i), N_j^e(\boldsymbol{r}')\right\rangle = \int_{E_d} \delta(\boldsymbol{r}_i) N_j^e(\boldsymbol{r}')\, dv = alok_{ij}^{(0,1)},$$

$$2.\left\langle \delta(\boldsymbol{r}_i), \nabla\cdot(\hat{\boldsymbol{x}} f_{x,j}^e + \hat{\boldsymbol{y}} f_{y,j}^e + \hat{\boldsymbol{z}} f_{z,j}^e) N_j^e\right\rangle = \int_{E_d} \delta(\boldsymbol{r}_i)\left(f_{x,j}^e \frac{\partial N_j^e}{\partial x} + f_{y,j}^e \frac{\partial N_j^e}{\partial y} + f_{z,j}^e \frac{\partial N_j^e}{\partial z}\right) dv,$$
$$= f_{x,j}^e alok_{ij}^{(0,x)} + f_{y,j}^e alok_{ij}^{(0,y)} + f_{z,j}^e alok_{ij}^{(0,z)},$$

$$3.\left\langle \boldsymbol{\delta}(\boldsymbol{r}_i), \bar{\bar{P}}\cdot\boldsymbol{\mathcal{S}}\left((\hat{\boldsymbol{x}} f_{x,j}^e + \hat{\boldsymbol{y}} f_{y,j}^e + \hat{\boldsymbol{z}} f_{z,j}^e) N_j^e\right)\right\rangle$$
$$= \int_{E_d} \boldsymbol{\delta}(\boldsymbol{r}_i)\cdot\bar{\bar{P}}\cdot\int_{E_e} (\hat{\boldsymbol{x}} f_{x,j}^e + \hat{\boldsymbol{y}} f_{y,j}^e + \hat{\boldsymbol{z}} f_{z,j}^e) N_j^e G(\boldsymbol{r},\boldsymbol{r}')\, dv'\, dv$$
$$= f_{x,j}^e\left(\hat{\boldsymbol{x}}\cdot\bar{\bar{P}}\cdot\hat{\boldsymbol{x}} alok_{ij}^{(1)} + \hat{\boldsymbol{y}}\cdot\bar{\bar{P}}\cdot\hat{\boldsymbol{x}} alok_{ij}^{(1)} + \hat{\boldsymbol{z}}\cdot\bar{\bar{P}}\cdot\hat{\boldsymbol{x}} alok_{ij}^{(1)}\right)$$
$$+ f_{y,j}^e\left(\hat{\boldsymbol{x}}\cdot\bar{\bar{P}}\cdot\hat{\boldsymbol{y}} alok_{ij}^{(1)} + \hat{\boldsymbol{y}}\cdot\bar{\bar{P}}\cdot\hat{\boldsymbol{y}} alok_{ij}^{(1)} + \hat{\boldsymbol{z}}\cdot\bar{\bar{P}}\cdot\hat{\boldsymbol{y}} alok_{ij}^{(1)}\right)$$
$$+ f_{z,j}^e\left(\hat{\boldsymbol{x}}\cdot\bar{\bar{P}}\cdot\hat{\boldsymbol{z}} alok_{ij}^{(1)} + \hat{\boldsymbol{y}}\cdot\bar{\bar{P}}\cdot\hat{\boldsymbol{z}} alok_{ij}^{(1)} + \hat{\boldsymbol{z}}\cdot\bar{\bar{P}}\cdot\hat{\boldsymbol{z}} alok_{ij}^{(1)}\right)$$

$$4.\left\langle \boldsymbol{\delta}(\boldsymbol{r}_i), \bar{\bar{P}}\cdot\boldsymbol{\mathcal{S}}(\nabla N_j^e(\boldsymbol{r}'))\right\rangle$$
$$= \int_{E_d} \boldsymbol{\delta}(\boldsymbol{r}_i)\cdot\bar{\bar{P}}\cdot\int_{E_e} \nabla N_j^e(\boldsymbol{r}') G(\boldsymbol{r},\boldsymbol{r}')\, dv'\, dv,$$
$$= \hat{\boldsymbol{x}}\cdot\bar{\bar{P}}\cdot\nabla N_j^e(\boldsymbol{r}') alok_{ij}^{(2)} + \hat{\boldsymbol{y}}\cdot\bar{\bar{P}}\cdot\nabla N_j^e(\boldsymbol{r}') alok_{ij}^{(2)} + \hat{\boldsymbol{z}}\cdot\bar{\bar{P}}\cdot\nabla N_j^e(\boldsymbol{r}') alok_{ij}^{(2)},$$

$$5.\left\langle \boldsymbol{\delta}(\boldsymbol{r}_i), \bar{\bar{P}}\cdot\boldsymbol{\mathcal{S}}(\nabla\times(\hat{\boldsymbol{x}} f_{x,j}^e + \hat{\boldsymbol{y}} f_{y,j}^e + \hat{\boldsymbol{z}} f_{z,j}^e) N_j^e)\right\rangle$$
$$= \int_{E_d} \boldsymbol{\delta}(\boldsymbol{r}_i)\cdot\bar{\bar{P}}\cdot\int_{E_e}\Big[f_{x,j}^e\left(\hat{\boldsymbol{y}}\frac{\partial N_j^e}{\partial z} - \hat{\boldsymbol{z}}\frac{\partial N_j^e}{\partial y}\right) + f_{y,j}^e\left(-\hat{\boldsymbol{x}}\frac{\partial N_j^e}{\partial z} + \hat{\boldsymbol{z}}\frac{\partial N_j^e}{\partial x}\right) +$$
$$f_{z,j}^e\left(\hat{\boldsymbol{x}}\frac{\partial N_j^e}{\partial y} - \hat{\boldsymbol{y}}\frac{\partial N_j^e}{\partial x}\right)\Big] G(\boldsymbol{r},\boldsymbol{r}')\, dv'\, dv$$
$$= f_{x,j}^e\left[\hat{\boldsymbol{x}}\cdot\bar{\bar{P}}\cdot\left(\hat{\boldsymbol{y}}\frac{\partial N_j^e}{\partial z} - \hat{\boldsymbol{z}}\frac{\partial N_j^e}{\partial y}\right) + \hat{\boldsymbol{y}}\cdot\bar{\bar{P}}\cdot\left(\hat{\boldsymbol{y}}\frac{\partial N_j^e}{\partial z} - \hat{\boldsymbol{z}}\frac{\partial N_j^e}{\partial y}\right) + \hat{\boldsymbol{z}}\cdot\bar{\bar{P}}\cdot\left(\hat{\boldsymbol{y}}\frac{\partial N_j^e}{\partial z} - \hat{\boldsymbol{z}}\frac{\partial N_j^e}{\partial y}\right)\right] alok_{ij}^{(2)}$$
$$+ f_{y,j}^e\left[\hat{\boldsymbol{x}}\cdot\bar{\bar{P}}\cdot\left(\hat{\boldsymbol{z}}\frac{\partial N_j^e}{\partial x} - \hat{\boldsymbol{x}}\frac{\partial N_j^e}{\partial z}\right) + \hat{\boldsymbol{y}}\cdot\bar{\bar{P}}\cdot\left(\hat{\boldsymbol{z}}\frac{\partial N_j^e}{\partial x} - \hat{\boldsymbol{x}}\frac{\partial N_j^e}{\partial z}\right) + \hat{\boldsymbol{z}}\cdot\bar{\bar{P}}\cdot\left(\hat{\boldsymbol{z}}\frac{\partial N_j^e}{\partial x} - \hat{\boldsymbol{x}}\frac{\partial N_j^e}{\partial z}\right)\right] alok_{ij}^{(2)}$$
$$+ f_{z,j}^e\left[+\hat{\boldsymbol{x}}\cdot\bar{\bar{P}}\cdot\left(\hat{\boldsymbol{x}}\frac{\partial N_j^e}{\partial y} - \hat{\boldsymbol{y}}\frac{\partial N_j^e}{\partial x}\right)\hat{\boldsymbol{y}}\cdot\bar{\bar{P}}\cdot\left(\hat{\boldsymbol{x}}\frac{\partial N_j^e}{\partial y} - \hat{\boldsymbol{y}}\frac{\partial N_j^e}{\partial x}\right) + \hat{\boldsymbol{z}}\cdot\bar{\bar{P}}\cdot\left(\hat{\boldsymbol{x}}\frac{\partial N_j^e}{\partial y} - \hat{\boldsymbol{y}}\frac{\partial N_j^e}{\partial x}\right)\right] alok_{ij}^{(2)}$$

4.2.2.2 Numerical Evaluation of Integrals Let us define a reference 3D element (tetrahedron) $\hat{E}$ with vertices $(0,0,0),(1,0,0),(0,1,0),(0,0,1)$ and let $p_j^e, j = 1,2,3,4$ be the vertices of a tetrahedron E_e. Linear mapping $\boldsymbol{\mathcal{F}}_e : \hat{E} \to E_e$ is defined as,

$$\boldsymbol{\mathcal{F}}_e(\alpha,\beta,\gamma) := \sum_{i=1}^{4} \boldsymbol{p}_j^e \hat{N}_i(\alpha,\beta,\gamma) = (\boldsymbol{p}_2^e - \boldsymbol{p}_1^e)\alpha + (\boldsymbol{p}_3^e - \boldsymbol{p}_1^e)\beta + (\boldsymbol{p}_4^e - \boldsymbol{p}_1^e)\gamma + \boldsymbol{p}_1^e \quad (167)$$

Above $\hat{N}_i, i = 1,\ldots,4$ are the nodal shape functions on $\hat{E}$

$$\hat{N}_1(\alpha,\beta,\gamma) = 1 - \alpha - \beta - \gamma, \quad (168)$$

$$\hat{N}_2(\alpha,\beta,\gamma) = \alpha, \quad (169)$$

$$\hat{N}_3(\alpha,\beta,\gamma) = \beta, \quad (170)$$

$$\hat{N}_4(\alpha,\beta,\gamma) = \gamma \quad (171)$$

Using mapping $\boldsymbol{\mathcal{F}}_e$ we can write

$$\int_{T_e} b(x,y,z)\, dv = \left|\det(J_{\boldsymbol{\mathcal{F}}_e})\right| \int_{\hat{T}} b\left(\boldsymbol{\mathcal{F}}_e(\alpha,\beta,\gamma)\right)\, d\alpha d\beta d\gamma \quad (172)$$

Here $J_{\boldsymbol{\mathcal{F}}_e}$ is the Jacobian of $\boldsymbol{\mathcal{F}}_e$, given as

$$J_{\boldsymbol{\mathcal{F}}_e} = \left[\frac{\partial \boldsymbol{\mathcal{F}}_e}{\partial\alpha}, \frac{\partial \boldsymbol{\mathcal{F}}_e}{\partial\beta}, \frac{\partial \boldsymbol{\mathcal{F}}_e}{\partial\gamma}\right] = \begin{bmatrix} x_2 - x_1 & x_3 - x_1 & x_4 - x_1 \\ y_2 - y_1 & y_3 - y_1 & y_4 - y_1 \\ z_2 - z_1 & z_3 - z_1 & z_4 - z_1 \end{bmatrix} \quad (173)$$

The shape functions on the real element can be expressed as

$$N_i^e = \hat{N}_i\left(\boldsymbol{\mathcal{F}}_e^{-1}(\boldsymbol{r})\right) = \hat{N}_i(\hat{\boldsymbol{r}}) \quad (174)$$

where $\boldsymbol{\mathcal{F}}_e^{-1}$: $T_e \to \hat{T}$ is the inverse of $\boldsymbol{\mathcal{F}}_e$, $\boldsymbol{r} = (x,y,z)$ is a point in T_e and $\hat{\boldsymbol{r}} = (\alpha,\beta,\gamma)$ a point in $\hat{T}$.
Given a function $f(x,y,z)$ the gradient in the transformed coordinates is of the form

$$\nabla^t f = \begin{bmatrix} \frac{\partial f}{\partial\alpha} & \frac{\partial f}{\partial\beta} & \frac{\partial f}{\partial\gamma} \end{bmatrix}^T \quad (175)$$

where the derivatives are calculated via the chain rule as

$$\frac{\partial f}{\partial \alpha} = \frac{\partial f}{\partial x}\frac{\partial x}{\partial \alpha} + \frac{\partial f}{\partial y}\frac{\partial y}{\partial \alpha} + \frac{\partial f}{\partial z}\frac{\partial z}{\partial \alpha}, \tag{176}$$

$$\frac{\partial f}{\partial \beta} = \frac{\partial f}{\partial x}\frac{\partial x}{\partial \beta} + \frac{\partial f}{\partial y}\frac{\partial y}{\partial \beta} + \frac{\partial f}{\partial z}\frac{\partial z}{\partial \beta}, \tag{177}$$

$$\frac{\partial f}{\partial \gamma} = \frac{\partial f}{\partial x}\frac{\partial x}{\partial \gamma} + \frac{\partial f}{\partial y}\frac{\partial y}{\partial \gamma} + \frac{\partial f}{\partial z}\frac{\partial z}{\partial \gamma} \tag{178}$$

The above equations can be written in matrix notation as

$$\begin{bmatrix} \frac{\partial f}{\partial \alpha} \\ \frac{\partial f}{\partial \beta} \\ \frac{\partial f}{\partial \gamma} \end{bmatrix} = \begin{bmatrix} \frac{\partial x}{\partial \alpha} & \frac{\partial y}{\partial \alpha} & \frac{\partial z}{\partial \alpha} \\ \frac{\partial x}{\partial \beta} & \frac{\partial y}{\partial \beta} & \frac{\partial z}{\partial \beta} \\ \frac{\partial x}{\partial \gamma} & \frac{\partial y}{\partial \gamma} & \frac{\partial z}{\partial \gamma} \end{bmatrix} \begin{bmatrix} \frac{\partial f}{\partial x} \\ \frac{\partial f}{\partial y} \\ \frac{\partial f}{\partial z} \end{bmatrix} \tag{179}$$
$$\nabla^t f = J^T \nabla f$$

where J^T is the transpose of the Jacobian matrix. Thus, the gradient in the original coordinate system can be calculated using the transformed coordinates as

$$\nabla f = (J^T)^{-1} \nabla^t f \tag{180}$$

The gradients of the scalar nodal shape functions defined on the reference tetrahedron $\hat{E}$ are

$$\nabla \hat{N}_1(\alpha, \beta, \gamma) = [-1, -1, -1], \tag{181}$$

$$\nabla \hat{N}_2(\alpha, \beta, \gamma) = [1, 0, 0], \tag{182}$$

$$\nabla \hat{N}_3(\alpha, \beta, \gamma) = [0, 1, 0], \tag{183}$$

$$\nabla \hat{N}_4(\alpha, \beta, \gamma) = [0, 0, 1] \tag{184}$$

Now, the other problem that remains is to calculate the divergence and curl of the basis function. The divergence and curl of a vector function are defined, respectively, as

$$\nabla \cdot \boldsymbol{f} = \left(\hat{\boldsymbol{x}} \frac{\partial}{\partial x} + \hat{\boldsymbol{y}} \frac{\partial}{\partial y} + \hat{\boldsymbol{z}} \frac{\partial}{\partial z} \right) \cdot (\hat{\boldsymbol{x}} f_x + \hat{\boldsymbol{y}} f_y + \hat{\boldsymbol{z}} f_z) = \left(\frac{\partial f_x}{\partial x} + \frac{\partial f_y}{\partial y} + \frac{\partial f_z}{\partial z} \right), \tag{185}$$

$$\nabla \times \boldsymbol{f} = \begin{vmatrix} \hat{\boldsymbol{x}} & \hat{\boldsymbol{y}} & \hat{\boldsymbol{z}} \\ \frac{\partial}{\partial x} & \frac{\partial}{\partial y} & \frac{\partial}{\partial z} \\ f_x & f_y & f_z \end{vmatrix} = \hat{\boldsymbol{x}} \left(\frac{\partial f_z}{\partial y} - \frac{\partial f_y}{\partial z} \right) - \hat{\boldsymbol{y}} \left(\frac{\partial f_z}{\partial x} - \frac{\partial f_x}{\partial z} \right) + \hat{\boldsymbol{z}} \left(\frac{\partial f_y}{\partial x} - \frac{\partial f_x}{\partial y} \right) \tag{186}$$

When $\boldsymbol{f}$ is defined using scalar nodal shape functions then each component of $\boldsymbol{f}$ is approximated by individual nodal shape functions, i.e.

$$\boldsymbol{f} = \sum_{e=1}^{N_T} \sum_{i=1}^{4} \left(\hat{\boldsymbol{x}} f_{x,i}^e + \hat{\boldsymbol{y}} f_{y,i}^e + \hat{\boldsymbol{z}} f_{z,i}^e \right) N_i^e \tag{187}$$

where, $f_{x,i}^e, f_{y,i}^e, f_{z,i}^e$ are the unknown coefficients. Thus the divergence and curl of $\boldsymbol{f}$ can be obtained as,

$$\begin{aligned} \nabla \cdot \boldsymbol{f} &= \sum_{e=1}^{N_T} \sum_{i=1}^{4} \left(f_{x,i}^e \nabla \cdot \hat{\boldsymbol{x}} + f_{y,i}^e \nabla \cdot \hat{\boldsymbol{y}} + f_{z,i}^e \nabla \cdot \hat{\boldsymbol{z}} \right) N_i^e, \\ &= \sum_{e=1}^{N_T} \sum_{i=1}^{4} \left(f_{x,i}^e \frac{\partial N_i^e}{\partial x} + f_{y,i}^e \frac{\partial N_i^e}{\partial y} + f_{z,i}^e \frac{\partial N_i^e}{\partial z} \right), \end{aligned} \tag{188}$$

Similarly,

$$\begin{aligned} \nabla \times \boldsymbol{f} &= \sum_{e=1}^{N_T} \sum_{i=1}^{4} \left(f_{x,i}^e \begin{vmatrix} \hat{\boldsymbol{x}} & \hat{\boldsymbol{y}} & \hat{\boldsymbol{z}} \\ \frac{\partial}{\partial x} & \frac{\partial}{\partial y} & \frac{\partial}{\partial z} \\ N_i^e & 0 & 0 \end{vmatrix} + f_{y,i}^e \begin{vmatrix} \hat{\boldsymbol{x}} & \hat{\boldsymbol{y}} & \hat{\boldsymbol{z}} \\ \frac{\partial}{\partial x} & \frac{\partial}{\partial y} & \frac{\partial}{\partial z} \\ 0 & N_i^e & 0 \end{vmatrix} + f_{z,i}^e \begin{vmatrix} \hat{\boldsymbol{x}} & \hat{\boldsymbol{y}} & \hat{\boldsymbol{z}} \\ \frac{\partial}{\partial x} & \frac{\partial}{\partial y} & \frac{\partial}{\partial z} \\ 0 & 0 & N_i^e \end{vmatrix} \right), \\ &= \sum_{e=1}^{N_T} \sum_{i=1}^{4} \left[f_{x,i}^e \left(\hat{\boldsymbol{y}} \frac{\partial N_i^e}{\partial z} - \hat{\boldsymbol{z}} \frac{\partial N_i^e}{\partial y} \right) + f_{y,i}^e \left(-\hat{\boldsymbol{x}} \frac{\partial N_i^e}{\partial z} + \hat{\boldsymbol{z}} \frac{\partial N_i^e}{\partial x} \right) + f_{z,i}^e \left(\hat{\boldsymbol{x}} \frac{\partial N_i^e}{\partial y} - \hat{\boldsymbol{y}} \frac{\partial N_i^e}{\partial x} \right) \right] \end{aligned} \tag{189}$$

Once we know the gradient of the basis function, the $\hat{x}, \hat{y}, \hat{z}$ components of the gradient give us $\frac{\partial N_i^e}{\partial x}, \frac{\partial N_i^e}{\partial y}, \frac{\partial N_i^e}{\partial z}$ respectively, from which $\nabla \cdot \boldsymbol{f}$ and $\nabla \times \boldsymbol{f}$ can be calculated. Next, using the point matching technique, testing functions are delta functions and inner product defined as

$$\begin{aligned} \langle f, g \rangle &= \int_v f g \, dv \\ \langle \boldsymbol{f}, \boldsymbol{g} \rangle &= \int_v \boldsymbol{f} \cdot \boldsymbol{g} \, dv \end{aligned} \tag{190}$$

where v is the volume of the object.

4.2.2.3 Matrix Assembly In this section the idea is to demonstrate how the matrix assembly is done using local matrices in the case of a pure dielectric scatterer. In this

case, equation (103) simplifies to

$$\begin{bmatrix} \nabla \cdot \bar{\bar{I}} & -k_0 \\ \bar{\bar{I}} - {k_0}^2 \sum_{e=1}^{N_T} \left[(\bar{\bar{\varepsilon}}_r - \bar{\bar{I}}) \boldsymbol{\mathcal{S}}(\bar{\bar{I}}) \right]_e & -k_0 \sum_{e=1}^{N_T} \left[(\bar{\bar{\varepsilon}}_r - \bar{\bar{I}}) \boldsymbol{\mathcal{S}}(\nabla) \right]_e \end{bmatrix} \begin{bmatrix} \boldsymbol{A} \\ V \end{bmatrix} = \begin{bmatrix} 0 \\ \boldsymbol{A}^{inc} \end{bmatrix} \tag{191}$$

Next, approximating the potentials with linear nodal basis functions and testing with delta function we get a system of linear equations where i goes through all the nodes in the mesh and $j = 1, \ldots, 4$ for each tetrahedron e in the mesh.

$$\left\langle \boldsymbol{\delta}(\boldsymbol{r}_i), \begin{bmatrix} \nabla \cdot [\hat{\boldsymbol{x}} + \hat{\boldsymbol{y}} + \hat{\boldsymbol{z}}] N_j^e & -k_0 N_j^e \\ [\hat{\boldsymbol{x}} + \hat{\boldsymbol{y}} + \hat{\boldsymbol{z}}] N_j^e - {k_0}^2 (\bar{\bar{\varepsilon}}_r - \bar{\bar{I}}) \boldsymbol{\mathcal{S}}([\hat{\boldsymbol{x}} + \hat{\boldsymbol{y}} + \hat{\boldsymbol{z}}] N_j^e) & -k_0 (\bar{\bar{\varepsilon}}_r - \bar{\bar{I}}) \boldsymbol{\mathcal{S}}(\nabla N_j^e) \end{bmatrix} \begin{bmatrix} A_{x,j} \\ A_{y,j} \\ A_{z,j} \\ V \end{bmatrix} \right\rangle = \left\langle \boldsymbol{\delta}(\boldsymbol{r}_i), \begin{bmatrix} 0 \\ \boldsymbol{A}^{inc} \end{bmatrix} \right\rangle \tag{192}$$

Thus, we have

$$\begin{bmatrix} S_x & S_y & S_z & S_V \\ Z_{xx} & Z_{xy} & Z_{xz} & Z_A \\ Z_{yx} & Z_{yy} & Z_{yz} & Z_B \\ Z_{zx} & Z_{zy} & Z_{zz} & Z_C \end{bmatrix} \begin{bmatrix} A_{x,j} \\ A_{y,j} \\ A_{z,j} \\ V \end{bmatrix} = \begin{bmatrix} 0 \\ b_x \\ b_y \\ b_z \end{bmatrix} \tag{193}$$

where $S_{x,y,z}$ are $N_V \times N_V$ sparse matrices that represent the Lorenz gauge differential operators and their only non-vanishing entries are defined at the nodes that belong to elements adjacent to a given node. S_V is a sparse $N_V \times N_V$ matrix that is essentially free-space wavenumber times $N_V \times N_V$ identity matrix.

$Z_{xx,yy,zz}$ are dense $N_V \times N_V$ matrices representing difference of identity matrix and the integrals from the basis functions to the delta testing functions for the vector potential. $Z_{xy,xz,yx,yz,zx,zy}$ are $N_V \times N_V$ matrices with vanishing entries. $Z_{A,B,C}$ are dense $N_V \times N_V$ matrices denoting the integrals from the $x-$, $y-$, $z-$ component of the gradient of the basis functions to the delta testing functions. And b_x, b_y, b_z are $N_V \times 1$ vectors defining

the components of the incident potentials at the vertices of a mesh.

$$
\begin{aligned}
S_x(i,n_j^e) &= alok_{ij}^{(0,x)} \\
S_y(i,n_j^e) &= alok_{ij}^{(0,y)} \\
S_z(i,n_j^e) &= alok_{ij}^{(0,z)} \\
S_V(i,n_j^e) &= -k_0 alok_{ij}^{(0,1)} \\
Z_{xx}(i,n_j^e) &= \left[alok_{ij}^{(0,1)} - k_0^2 \hat{\boldsymbol{x}} \cdot (\bar{\bar{\varepsilon}}_r - \bar{\bar{I}}) \cdot \hat{\boldsymbol{x}} alok_{ij}^{(1)}\right] \\
Z_{xy}(i,n_j^e) &= -k_0^2 \hat{\boldsymbol{x}} \cdot (\bar{\bar{\varepsilon}}_r - \bar{\bar{I}}) \cdot \hat{\boldsymbol{y}} alok_{ij}^{(1)} \\
Z_{xz}(i,n_j^e) &= -k_0^2 \hat{\boldsymbol{x}} \cdot (\bar{\bar{\varepsilon}}_r - \bar{\bar{I}}) \cdot \hat{\boldsymbol{z}} alok_{ij}^{(1)} \\
Z_{yx}(i,n_j^e) &= -k_0^2 \hat{\boldsymbol{y}} \cdot (\bar{\bar{\varepsilon}}_r - \bar{\bar{I}}) \cdot \hat{\boldsymbol{x}} alok_{ij}^{(1)} \\
Z_{yy}(i,n_j^e) &= alok_{ij}^{(0,1)} - k_0^2 \hat{\boldsymbol{y}} \cdot (\bar{\bar{\varepsilon}}_r - \bar{\bar{I}}) \cdot \hat{\boldsymbol{y}} alok_{ij}^{(1)} \\
Z_{yz}(i,n_j^e) &= -k_0^2 \hat{\boldsymbol{y}} \cdot (\bar{\bar{\varepsilon}}_r - \bar{\bar{I}}) \cdot \hat{\boldsymbol{z}} alok_{ij}^{(1)} \\
Z_{zx}(i,n_j^e) &= -k_0^2 \hat{\boldsymbol{z}} \cdot (\bar{\bar{\varepsilon}}_r - \bar{\bar{I}}) \cdot \hat{\boldsymbol{x}} alok_{ij}^{(1)} \\
Z_{zy}(i,n_j^e) &= -k_0^2 \hat{\boldsymbol{z}} \cdot (\bar{\bar{\varepsilon}}_r - \bar{\bar{I}}) \cdot \hat{\boldsymbol{y}} alok_{ij}^{(1)} \\
Z_{zz}(i,n_j^e) &= alok_{ij}^{(0,1)} - k_0^2 \hat{\boldsymbol{z}} \cdot (\bar{\bar{\varepsilon}}_r - \bar{\bar{I}}) \cdot \hat{\boldsymbol{z}} alok_{ij}^{(1)} \\
Z_A(i,n_j^e) &= -k_0 \hat{\boldsymbol{x}} \cdot (\bar{\bar{\varepsilon}}_r - \bar{\bar{I}}) \cdot \nabla N_j^e alok_{ij}^{(2)} \\
Z_B(i,n_j^e) &= -k_0 \hat{\boldsymbol{y}} \cdot (\bar{\bar{\varepsilon}}_r - \bar{\bar{I}}) \cdot \nabla N_j^e alok_{ij}^{(2)} \\
Z_C(i,n_j^e) &= -k_0 \hat{\boldsymbol{z}} \cdot (\bar{\bar{\varepsilon}}_r - \bar{\bar{I}}) \cdot \nabla N_j^e alok_{ij}^{(2)} \\
b^x(i) &= \left\langle \delta(\boldsymbol{r}_i), A_x^{inc} \right\rangle \\
b^y(i) &= \left\langle \delta(\boldsymbol{r}_i), A_y^{inc} \right\rangle \\
b^z(i) &= \left\langle \delta(\boldsymbol{r}_i), A_z^{inc} \right\rangle
\end{aligned}
$$

where i runs from $1, 2, \ldots, N_V$, $j = 1, \ldots, 4$ and n_j^e are the global node numbers of an element e.

The extension of the above equations to the bi-anisotropic case is straight forward but cumbersome. The only additional terms arise from the integral of the curl of vector potential and is explained before to deal with. The final system matrix consists of 64 elements that are $N_V \times N_V$ matrices.

5 Numerical Results

For easy implementation a MATLAB programme is developed for the AVFU-formulation to set up the MoM matrix equations. Solution to the MoM matrix equations gives the unknown coefficients associated with the basis function approximation of potentials ($\boldsymbol{A}, V, \boldsymbol{F}$, U for the AVFU-formulation). From these coefficients; the scattered fields, potentials, charge distribution, polarization current distribution etc. can be obtained. Singular integrals are calculated using the singularity subtraction technique [31].

5.1 Excitation Dependence

In this section the excitation dependence associated with the AVFU-formulation is discussed. The governing equations that define the incident potentials when the electric and magnetic field intensities are specified are (87), (88), (97) and (98). Any choice of incident potentials should satisfy these equations. There are a number of different combinations that can be specified for a given electric and magnetic field intensities combination. It is found that different specification of the incident potentials is limited by the nature of the scatterer.

If the electric and magnetic field intensities are specified respectively as $\boldsymbol{E}^i = E_0 e^{-jk_0 z}\hat{\boldsymbol{x}}$ and $\eta_0 \boldsymbol{H}^i = H_0 e^{-jk_0 z}\hat{\boldsymbol{y}}$, the following combinations are possible that satisfy (87), (88), (97) and (98).

1. $\tilde{A}_x^i = -e^{-jkz}$ & $\tilde{A}_y^i = \tilde{A}_z^i = 0$
   $\tilde{V}^i = 0$
   $\tilde{\boldsymbol{F}}^i = 0,$ i.e. $\tilde{F}_x^i = \tilde{F}_y^i = \tilde{F}_z^i = 0$
   $\tilde{U}^i = 0$

2. $\tilde{\boldsymbol{A}}^i = 0,$ i.e. $\tilde{A}_x^i = \tilde{A}_y^i = \tilde{A}_z^i = 0$
   $\tilde{V}^i = 0$
   $\tilde{F}_y^i = -e^{-jkz}$ & $\tilde{F}_x^i = \tilde{F}_z^i = 0$
   $\tilde{U}^i = 0$

3. $\tilde{A}_z^i = -jkxe^{-jkz}$ & $\tilde{A}_x^i = \tilde{A}_y^i = 0$
   $\tilde{V}^i = -kxe^{-jkz}$
   $\tilde{\boldsymbol{F}}^i = 0,$ i.e. $\tilde{F}_x^i = \tilde{F}_y^i = \tilde{F}_z^i = 0$
   $\tilde{U}^i = 0$

4. $\tilde{\boldsymbol{A}}^i = 0,$ i.e. $\tilde{A}_x^i = \tilde{A}_y^i = \tilde{A}_z^i = 0$
   $\tilde{V}^i = 0$
   $\tilde{F}_x^i = -jkye^{-jkz}$ & $\tilde{F}_y^i = \tilde{F}_z^i = 0$
   $\tilde{U}^i = -kye^{-jkz}$

5. $\tilde{A}_x^i = -0.5e^{-jkz}$ & $\tilde{A}_y^i = \tilde{A}_z^i = 0$
   $\tilde{V}^i = 0$
   $\tilde{F}_y^i = -0.5e^{-jkz}$ & $\tilde{F}_x^i = \tilde{F}_z^i = 0$
   $\tilde{U}^i = 0$

Choice 1 works well in the case of dielectric spheres or when the permittivity dyadic takes values other than unity and the permeability dyadic is an identity dyadic. Choice 2 works for the magnetic spheres or when the permeability dyadic is different from free-space permeability and the permittivity dyadic is an identity dyadic. In the case of complex scatterers when both permittivity and permeability dyadic are complex and also $\bar{\bar{\xi}}$ and $\bar{\bar{\zeta}}$ are specified, then choice 5 gives the correct results. Choice 3 and 4 though satisfy the governing equations (87), (88), (97),(98) are not found to produce any correct results.
Actually, the choice of incident scalar potentials does not directly effect the AVFU-formulation (since incident potentials do not appear in (103)), but instead this choice affects the choice of the vector potentials. A choice of potentials that specifies all the scalar and vector potentials could not be investigated. This unique choice of scalar and vector potential is supposed to work for all cases but the in time-frame of this master thesis work is not selected.

5.2 Calculating the Scattering Cross Section (SCS)

In this section a demonstration is given on how to calculate the scattered fields when the coefficients associated with the basis function approximation of volume currents (ob-

tained using the JM-formulation), or the potentials (obtained using the AVFU-formulation) are known. If the scattered field is known for a given incident angle then the SCS can be calculated by using (15) or (16). In this section a demonstration is given on how to calculate the scattered fields from unknowns of the AVFU-formulation.
From equations (13) and (14) we have;

$$\boldsymbol{E}_s(\boldsymbol{r}) \approx \frac{e^{-jkr}}{4\pi r}\int\limits_{\Omega}\left\{j\omega\mu_0\hat{\boldsymbol{r}}\times[\hat{\boldsymbol{r}}\times\boldsymbol{J}(\boldsymbol{r}')]+jk_0\hat{\boldsymbol{r}}\times\boldsymbol{M}(\boldsymbol{r}')\right\}e^{jk\hat{\boldsymbol{r}}\cdot\boldsymbol{r}'}\,d\Omega', \quad (194)$$

$$\boldsymbol{H}_s(\boldsymbol{r}) \approx \frac{e^{-jkr}}{4\pi r}\int\limits_{\Omega}\left\{j\omega\varepsilon_0\hat{\boldsymbol{r}}\times[\hat{\boldsymbol{r}}\times\boldsymbol{M}(\boldsymbol{r}')]-jk_0\hat{\boldsymbol{r}}\times\boldsymbol{J}(\boldsymbol{r}')\right\}e^{jk\hat{\boldsymbol{r}}\cdot\boldsymbol{r}'}\,d\Omega' \quad (195)$$

where $\boldsymbol{J}$ and $\boldsymbol{M}$ are given by (89) and (90). If the unknown coefficients associated with the basis function approximation of potentials are known, then (89) and (90) can be written as,

$$\boldsymbol{J}_V = j\omega\varepsilon_0\left[(\bar{\bar{\varepsilon}}_r-\bar{\bar{I}})\cdot\boldsymbol{X}+\left(\bar{\bar{\chi}}^T-j\bar{\bar{\kappa}}^T\right)\cdot\boldsymbol{Y}\right] \quad (196)$$

$$\eta_0\boldsymbol{M}_V = j\omega\mu_0\left[(\bar{\bar{\mu}}_r-\bar{\bar{I}})\cdot\boldsymbol{Y}+(\bar{\bar{\chi}}+j\bar{\bar{\kappa}})\cdot\boldsymbol{X}\right] \quad (197)$$

where

$$\boldsymbol{X} = \begin{bmatrix} -\sum_{i=1}^{N_v}A_{x,i}N_i-\frac{1}{k_0}\sum_{i=1}^{N_v}\frac{\partial N_i}{\partial x}V_i+j\frac{1}{k_0}\sum_{i=1}^{N_v}\left(F_{z,i}\frac{\partial N_i}{\partial y}-F_{y,i}\frac{\partial N_i}{\partial z}\right)\\ -\sum_{i=1}^{N_v}A_{y,i}N_i-\frac{1}{k_0}\sum_{i=1}^{N_v}\frac{\partial N_i}{\partial y}V_i+j\frac{1}{k_0}\sum_{i=1}^{N_v}\left(F_{z,i}\frac{\partial N_i}{\partial x}-F_{x,i}\frac{\partial N_i}{\partial z}\right)\\ -\sum_{i=1}^{N_v}A_{z,i}N_i-\frac{1}{k_0}\sum_{i=1}^{N_v}\frac{\partial N_i}{\partial z}V_i+j\frac{1}{k_0}\sum_{i=1}^{N_v}\left(F_{y,i}\frac{\partial N_i}{\partial x}-F_{x,i}\frac{\partial N_i}{\partial y}\right)\end{bmatrix} \quad (198)$$

$$\boldsymbol{Y} = \begin{bmatrix} -\sum_{i=1}^{N_v}F_{x,i}N_i-\frac{1}{k_0}\sum_{i=1}^{N_v}\frac{\partial N_i}{\partial x}U_i-j\frac{1}{k_0}\sum_{i=1}^{N_v}\left(A_{z,i}\frac{\partial N_i}{\partial y}-A_{y,i}\frac{\partial N_i}{\partial z}\right)\\ -\sum_{i=1}^{N_v}F_{y,i}N_i-\frac{1}{k_0}\sum_{i=1}^{N_v}\frac{\partial N_i}{\partial y}U_i-j\frac{1}{k_0}\sum_{i=1}^{N_v}\left(A_{z,i}\frac{\partial N_i}{\partial x}-A_{x,i}\frac{\partial N_i}{\partial z}\right)\\ -\sum_{i=1}^{N_v}F_{z,i}N_i-\frac{1}{k_0}\sum_{i=1}^{N_v}\frac{\partial N_i}{\partial z}U_i-j\frac{1}{k_0}\sum_{i=1}^{N_v}\left(A_{y,i}\frac{\partial N_i}{\partial x}-A_{x,i}\frac{\partial N_i}{\partial y}\right)\end{bmatrix} \quad (199)$$

Substituting (196) and (197) in (194) and (195) we get the numerically implementable equations for scattered fields once the unknown coefficients associated with the basis

function approximation of potentials are known;

$$\boldsymbol{E}_s(\boldsymbol{r}) \approx -k_0^2 \frac{e^{-jkr}}{4\pi r} \int_{\Omega} \Big\{ \hat{\boldsymbol{r}} \times \Big[\hat{\boldsymbol{r}} \times \Big[(\bar{\bar{\varepsilon}}_r - \bar{\bar{I}}) \cdot \boldsymbol{X} + \big(\bar{\bar{\chi}}^T - j\bar{\bar{\kappa}}^T\big) \cdot \boldsymbol{Y} \Big] \Big] + \hat{\boldsymbol{r}} \times \Big[(\bar{\bar{\mu}}_r - \bar{\bar{I}}) \cdot \boldsymbol{Y} + (\bar{\bar{\chi}} + j\bar{\bar{\kappa}}) \cdot \boldsymbol{X} \Big] \Big\} e^{jk\hat{\boldsymbol{r}}\cdot\boldsymbol{r}'} \, d\Omega' \quad (200)$$

$$\boldsymbol{H}_s(\boldsymbol{r}) \approx -\frac{k_0^2}{\eta_0} \frac{e^{-jkr}}{4\pi r} \int_{\Omega} \Big\{ \hat{\boldsymbol{r}} \times \Big[\hat{\boldsymbol{r}} \times \Big[(\bar{\bar{\mu}}_r - \bar{\bar{I}}) \cdot \boldsymbol{Y} + (\bar{\bar{\chi}} + j\bar{\bar{\kappa}}) \cdot \boldsymbol{X} \Big] \Big] - \hat{\boldsymbol{r}} \times \Big[(\bar{\bar{\varepsilon}}_r - \bar{\bar{I}}) \cdot \boldsymbol{X} + \big(\bar{\bar{\chi}}^T - j\bar{\bar{\kappa}}^T\big) \cdot \boldsymbol{Y} \Big] \Big\} e^{jk\hat{\boldsymbol{r}}\cdot\boldsymbol{r}'} \, d\Omega' \quad (201)$$

5.3 Study of Scattering from Different Materials

In this section, the scattering cross section is presented for several test objects that are either isotropic, anisotropic, bi-isotropic or bi-anisotropic. The basic geometry in nearly all test problems is a sphere, but some results are also presented for structures with cubical geometry. A comparison is made between the solutions obtained using the JM- and AVFU- formulations and those that already exist, such as Mie series solutions for dielectric or chiral spheres, and numerical solutions obtained by [1] (EH-formulation) and [2] (DB-formulation).
Since GMRES and MLMFA are not implemented with the AVFU-formulation, the problem domain that can be analysed is limited and analysis of complex structures is not presented in all cases but some results for complex scatterers are shown for the AVFU-formulation to show the validity of the method.

5.3.1 Isotropic Sphere

As a first example, the scattering from a homogeneous isotropic sphere is studied. The sphere is of size $k_0 r = 0.05$ and is illuminated by a plane electromagnetic wave propagating in the z direction with electric field oriented along the $x-$axis, i.e. $\boldsymbol{E}^i = E_0 e^{-jk_0 z}\hat{\boldsymbol{x}}$ and $\eta_0 \boldsymbol{H}^i = H_0 e^{-jk_0 z}\hat{\boldsymbol{y}}$, where $E_0 = 1\,[V/m]$. The sphere is descritized into 348 tetrahedrons for the AVFU-formulation and 8279 tetrahedrons for the JM-formulation. Three cases are presented; a lossless dielectric sphere ($\varepsilon_{real} > 1, \varepsilon_{img} = 0, \mu_r = 1$), a lossless magnetic sphere ($\mu_{real} > 1, \mu_{img} = 0, \varepsilon_r = 1$) and a lossy dielectric sphere ($\varepsilon_{real} > 1, \varepsilon_{img} > 0, \mu_r = 1$).

Since the size of the sphere is very small ($k_0 r << 1$), The far-field scattering converges

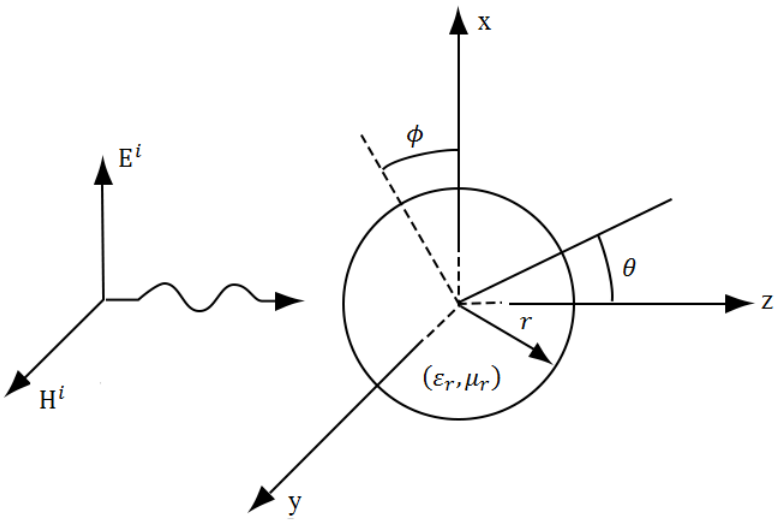

Figure 5: Geometry of isotropic dielectric/magnetic and "metamaterial" spheres.

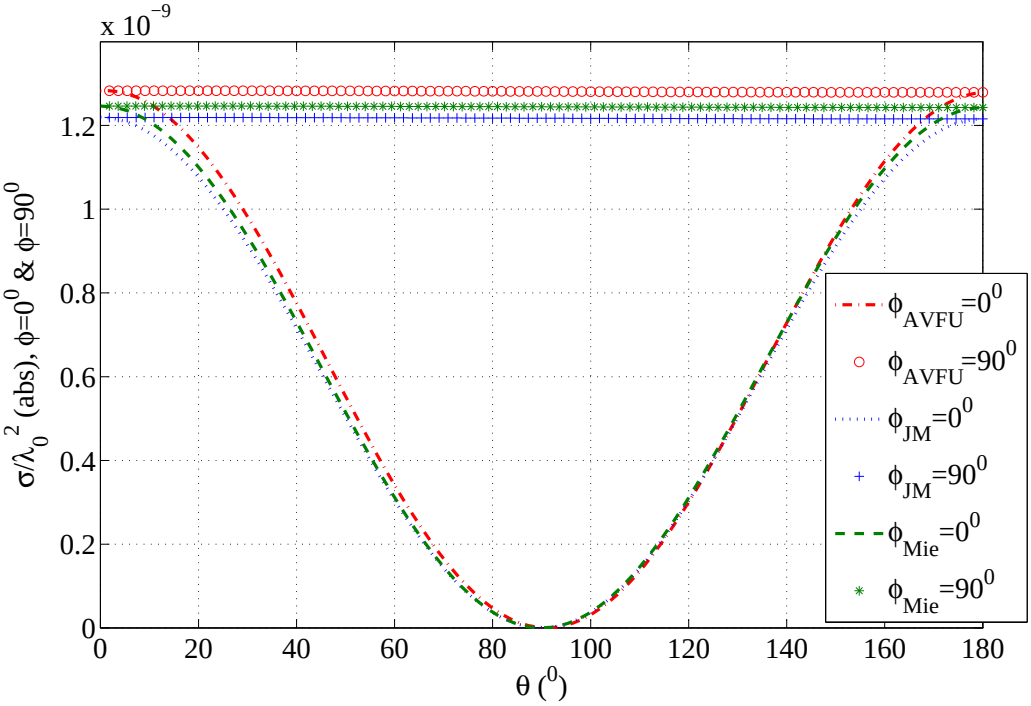

Figure 6: Bistatic SCS $\phi = 0^0$ (E-plane) and $\phi = 90^0$ (H-plane) of an isotropic dielectric sphere, $k_0 r = 0.05$ and $\varepsilon_r = 4$, $\mu_r = 1$.

to Rayleigh regime, this means that the electric and magnetic fields can be calculated from the dipole moments induced in the scatterer [32]. The absolute amplitude of the differential scattering cross-section σ of a very small sphere can be calculated according to the

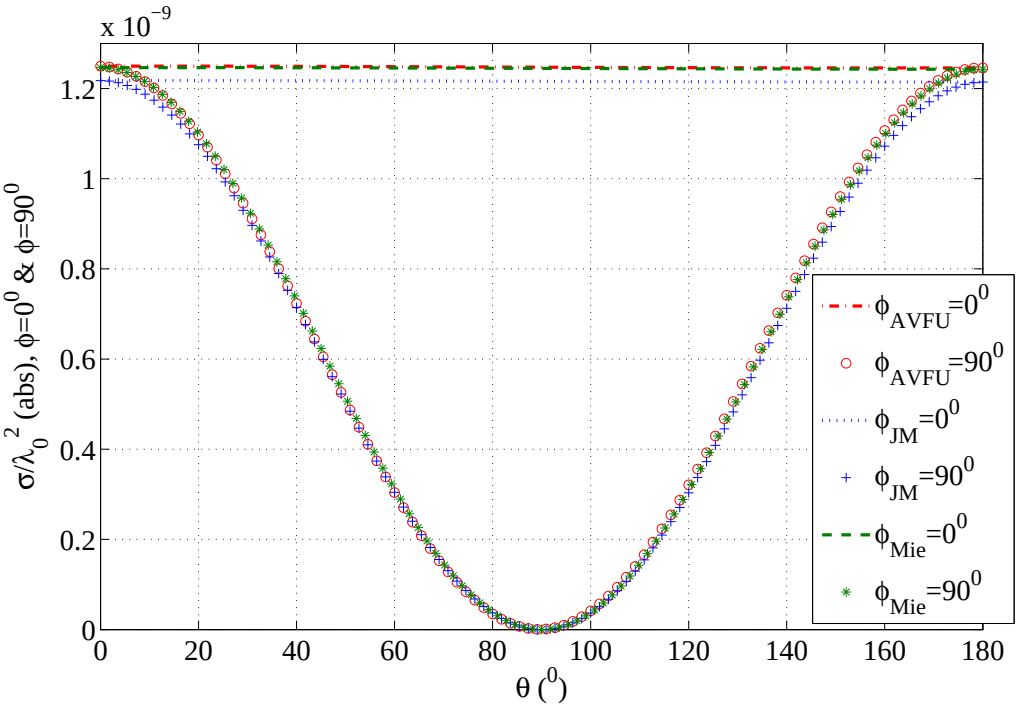

Figure 7: Bistatic SCS $\phi = 0^0$ (E-plane) and $\phi = 90^0$ (H-plane) of an isotropic magnetic sphere, $k_0 r = 0.05$ and $\varepsilon_r = 1$, $\mu_r = 4$.

Rayleigh theory as,

$$\frac{\sigma(\theta,\phi)}{\lambda^2} = \frac{(k_0 a)^6}{9\pi}|\boldsymbol{F}(\theta,\phi)|^2 \tag{202}$$

where

$$\boldsymbol{F}(\theta,\phi) = (\boldsymbol{p}_e \times \hat{\boldsymbol{r}} - \boldsymbol{p}_m) \times \hat{\boldsymbol{r}} \tag{203}$$

and

$$p_e = 3\frac{\varepsilon_r - 1}{\varepsilon + 2} \tag{204}$$

$$p_m = 3\frac{\mu_r - 1}{\mu + 2} \tag{205}$$

$$\boldsymbol{r} = \sin\theta\cos\phi\hat{\boldsymbol{x}} + \sin\theta\sin\phi\hat{\boldsymbol{y}} + \cos\theta\hat{\boldsymbol{z}} \tag{206}$$

The electric and magnetic dipoles are oriented along the direction of the incident electric and magnetic fields.

Fig. 6 shows the bistatic SCS of a dielectric sphere with permittivity $\varepsilon = 4$, $\mu = 1$ and Fig. 7 shows the bistatic SCS of a magnetic sphere with permeability $\mu = 4$, $\varepsilon = 1$ in linear scale. It is observed that the bistatic SCS of a dielectric and magnetic sphere

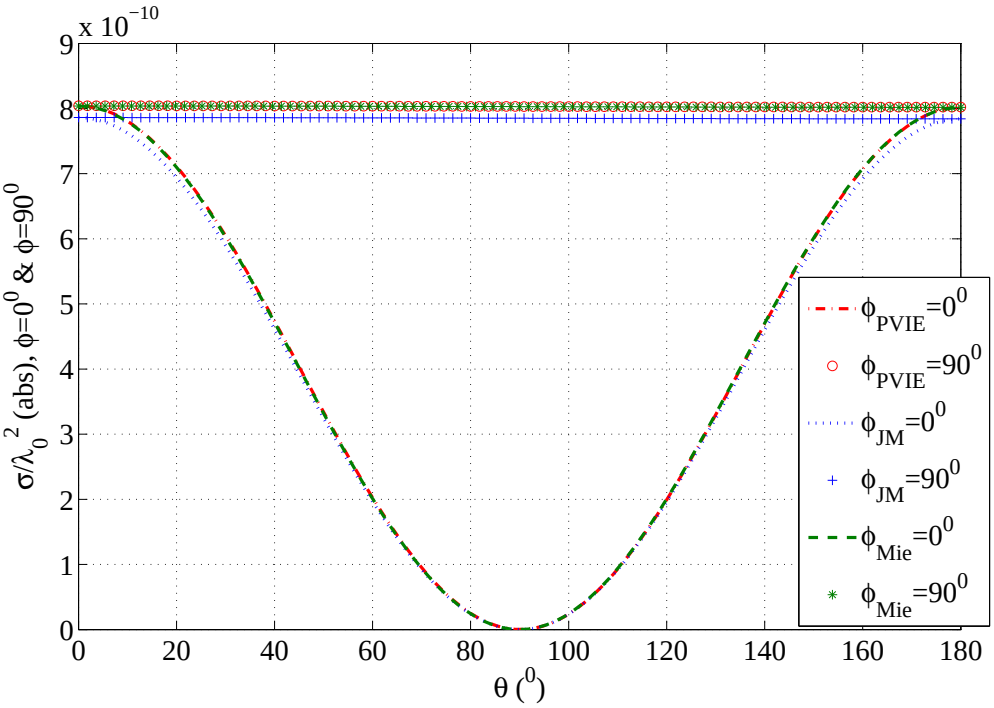

Figure 8: Bistatic SCS $\phi = 0^0$ (E-plane) and $\phi = 90^0$ (H-plane) of an isotropic lossy dielectric sphere, $k_0 r = 0.05$ and $\varepsilon_r = 3 - j0.2$, $\mu_r = 1$.

of same size and permittivity and permeability switched are same in magnitude but the SCS in the $\phi = 0^0(E - plane)$ and $\phi = 90^0(H - plane)$ plane's are exchanged. Fig. 8 shows the bistatic SCS of a lossy dielectric sphere with permittivity $\varepsilon = 3 - j0.2$, $\mu = 1$ in linear scale, it can be seen from Fig. 8 that the bistatic SCS has decreased in the $\phi = 0^0(E - plane)$ and $\phi = 90^0(H - plane)$ plane's compared to lossless cases.
It is seen that the results match well to the Mie-series solution for a fairly small number of tetrahedrons for all the three cases.

5.3.2 Double Negative Sphere

Mie-series solution for electromagnetic scattering by a double negative sphere is discussed in [33]. One of the two examples in [33] is presented here, the other example has a size parameter $k_0 r > 10$ and due to computational limitations, solution cannot be obtained.

The double negative sphere has a radius $r = 0.015$ m and is discretized into 139302 tetrahedrons. It is illuminated by a plane electromagnetic wave of frequency 9.375 GHz and propagating in the z direction with electric field oriented along the $x-$axis, i.e.

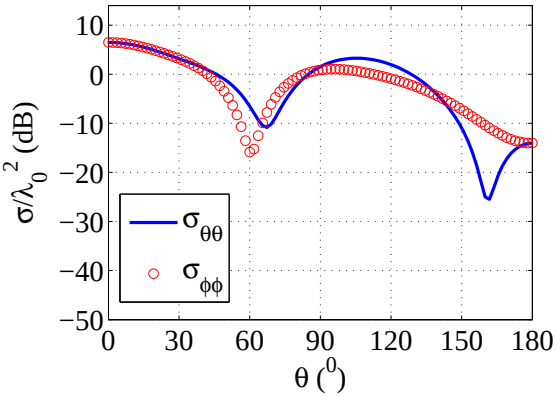

Figure 9: Bistatic SCS $\sigma_{\theta\theta}$ and $\sigma_{\phi\phi}$ of double negative sphere.

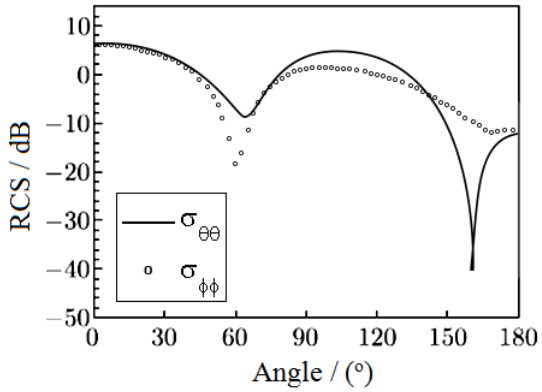

Figure 10: Bistatic SCS $\sigma_{\theta\theta}$ and $\sigma_{\phi\phi}$ of double negative sphere from [33].

$\boldsymbol{E}^i = E_0 e^{-jk_0 z}\hat{\boldsymbol{x}}$ and $\eta_0 \boldsymbol{H}^i = H_0 e^{-jk_0 z}\hat{\boldsymbol{y}}$, where $E_0 = 1\ [V/m]$. The permittivity and permeability of the metamaterial sphere are $\bar{\bar{\varepsilon}}_r = [-4+j0.001]\bar{\bar{I}}$ and $\bar{\bar{\mu}}_r = [-1+j0.001]\bar{\bar{I}}$, respectively.
The numerical results produced using the JM-formulation are found to be in good agreement with the Mie-series solution presented in [33] as shown in Figs. 9 and 10.

5.3.3 Layered Sphere

Next, the scattering from two different layered dielectric spheres is investigated. One of the layered spheres has different permittivities for the inner and outer spheres and is a model problem discussed in [1] and the other layered sphere is a magnetic sphere inside an electric sphere and a comparison is made between the JM-formulation and AVFU-formulation.

5.3.3.1 Two-Layered Sphere 1 The E-plane ($\phi = 0^0$) and H-plane ($\phi = 90^0$) bistatic scattering cross-sections of a two-layered dielectric sphere are shown in Fig. 12. The sphere has a size $k_0 r_2 = 0.408$ and contains two-layers of dielectric materials of different permittivities. The outer layer has a radius r_2 and the inner sphere has a radius $r_1 = 0.5 r_2$. The relative permittivity of outer layer is $\varepsilon_{r_2} = 9$ and that of the inner sphere is $\varepsilon_{r_1} = 4$. The sphere is meshed into 8095 tetrahedrons and is illuminated by a plane electromagnetic wave propagating in the z direction with electric field oriented along the $x-$axis, i.e. $\boldsymbol{E}^i = E_0 e^{-jk_0 z}\hat{\boldsymbol{x}}$ and $\eta_0 \boldsymbol{H}^i = H_0 e^{-jk_0 z}\hat{\boldsymbol{y}}$, where $E_0 = 1\ [V/m]$.
It is seen that both the JM- and AVFU- formulations give similar results that agree well with the Mie-series solution. It should be mentioned that numerical results associated with

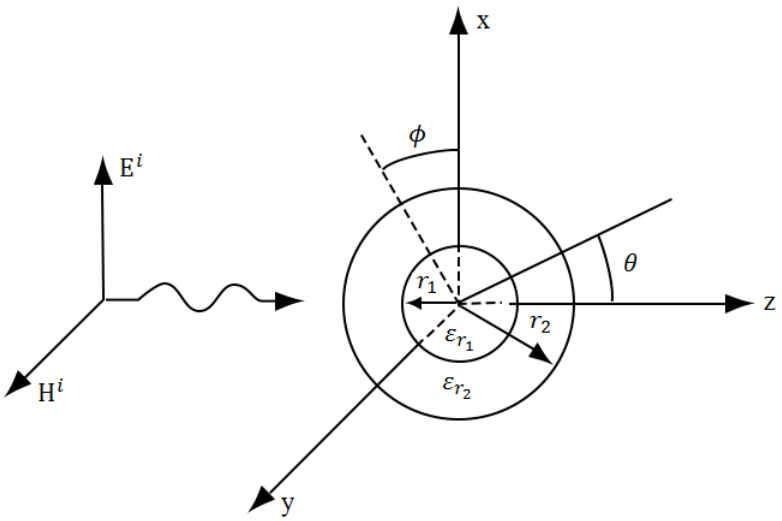

Figure 11: Geometry of layered sphere.

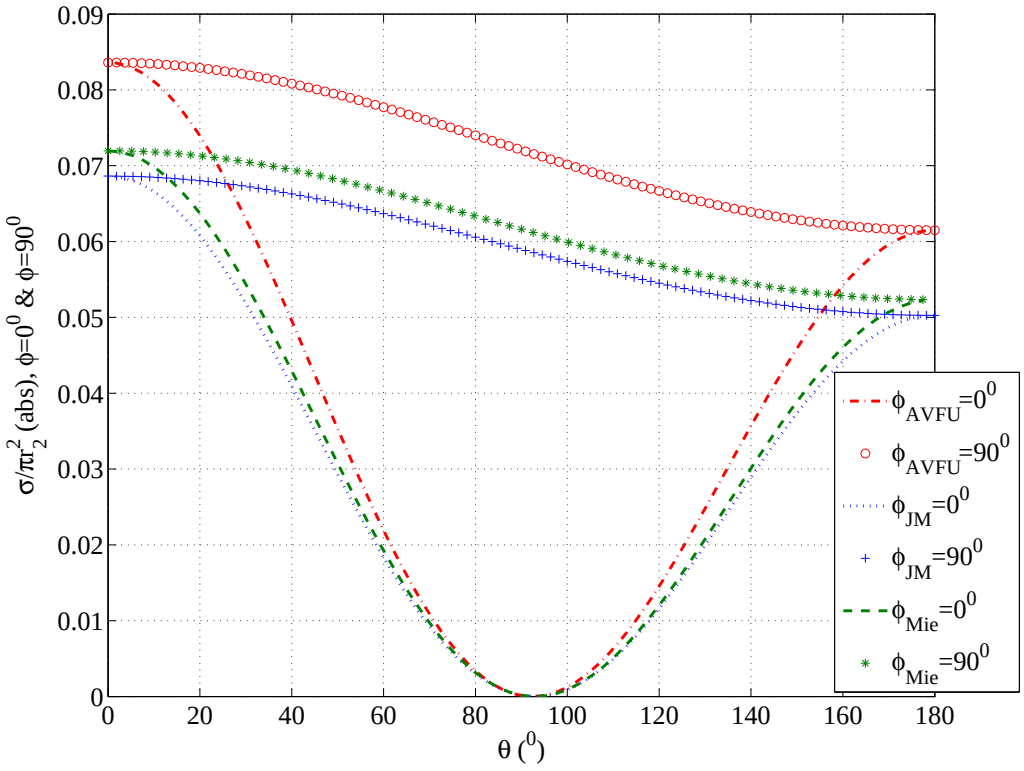

Figure 12: Bistatic SCS $\phi = 0^0$ (E-plane) and $\phi = 90^0$ (H-plane) of a two-layered dielectric sphere, $k_0 r_2 = 0.408$, $r_2/r_1 = 0.5$ and $\varepsilon_{r_1} = 4$, $\varepsilon_{r_2} = 9$.

scattering from layered or multilayered structures are more prone to the discretization limitations.

5.3.3.2 Two-Layered Sphere 2 The second layered sphere is an electric sphere inside a magnetic sphere. The sphere has a size of $k_0 r_2 = 0.1$ and contains a magnetic layer of permeability $\mu_{r_2} = 10$ on top of a dielectric sphere of permittivity $\varepsilon_{r_1} = 10$. The outer layer has a radius r_2 and the inner sphere has a radius $r_1 = 0.5 r_2$. The sphere is meshed into 8095 tetrahedrons and is illuminated by a plane electromagnetic wave propagating in the z direction with electric field oriented along the $x-$axis, i.e. $\boldsymbol{E}^i = E_0 e^{-jk_0 z}\hat{\boldsymbol{x}}$ and $\eta_0 \boldsymbol{H}^i = H_0 e^{-jk_0 z}\hat{\boldsymbol{y}}$, where $E_0 = 1\ [V/m]$.

Fig. 13 shows the E-plane ($\phi = 0^0$) and H-plane ($\phi = 90^0$) bistatic SCS obtained using

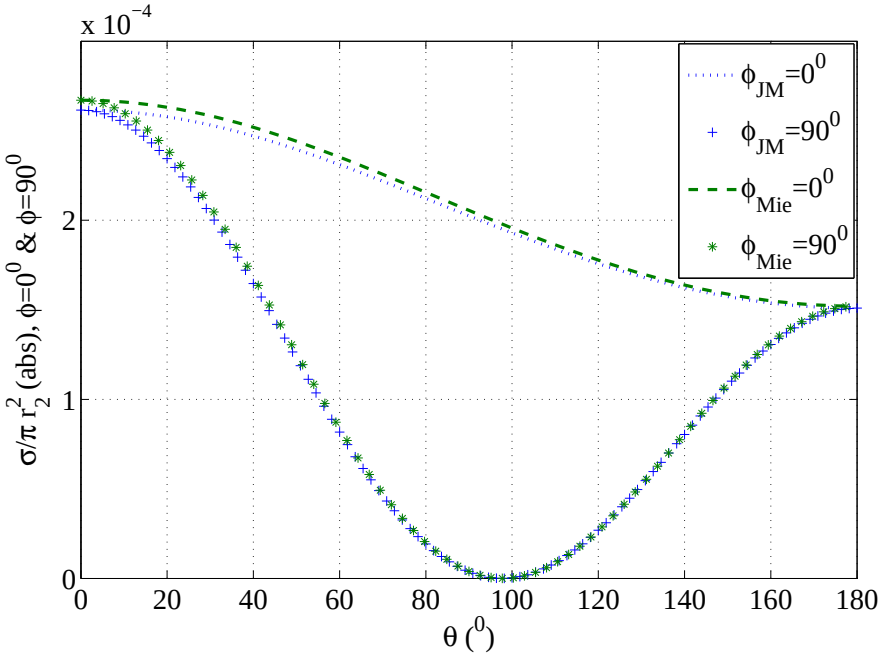

Figure 13: Bistatic SCS $\phi = 0^0$ (E-plane) and $\phi = 90^0$ (H-plane) of a two-layered sphere, $k_0 r_2 = 0.1$, $r_2/r_1 = 0.5$ and $\varepsilon_{r_1} = 1$, $\varepsilon_{r_2} = 10$, $\mu_{r_1} = 10$, $\mu_{r_2} = 1$.

the JM-formulation and Mie-series code. The results are found to be similar. The results produced by the AVFU-formulation for 8095 domain elements were not accurate and are not mentioned here.

5.3.4 DB Sphere

The scattering cross section (SCS) of a homogeneous sphere with $\varepsilon_r = 0$ and $\mu_r = 0$ mimicking DB boundary condition (i.e. normal component of electric $\boldsymbol{D}$ and magnetic $\boldsymbol{B}$ flux densities vanish at the boundary surface) is presented in this section. Spheres with DB boundary condition do not scatter in the back-scattering direction and the scattering diagram is rotationally symmetric [32] [28]. Consider a homogeneous sphere of size

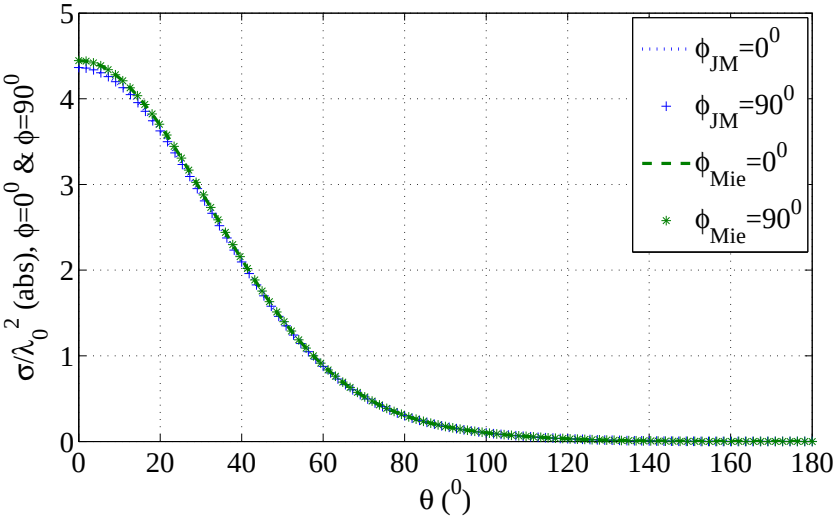

Figure 14: Bistatic SCS $\phi = 0^0$ (E-plane) and $\phi = 90^0$ (H-plane) of homogeneous sphere of size $k_0 r = 2$ and $\varepsilon_r = 1e^{-10}$, $\mu_r = 1e^{-10}$.

parameter $k_0 a = 2$ that is discretized into 8279 tetrahedrons. Let's define the constitutive parameters of the sphere as, $\varepsilon = \mu = 1e^{-10}$. Next, the sphere is illuminated by a plane electromagnetic wave propagating in the z direction with electric field oriented along the $x-$axis, i.e. $\boldsymbol{E}^i = E_0 e^{-jk_0 z}\hat{\boldsymbol{x}}$ and $\eta_0 \boldsymbol{H}^i = H_0 e^{-jk_0 z}\hat{\boldsymbol{y}}$, where $E_0 = 1\ [V/m]$.
The numerical results for the JM-formulation are found to be in good agreement with the Mie-series solution. The results from the AVFU-formulation are not presented in this section as an error of around $1.7e^{-3}$ (-3 dB) is associated to the results produced but the results are found to follow the same pattern.

5.3.5 PEC Sphere

A perfect electric conductor (PEC) condition requires the tangential components of the electric field intensity to be zero at a PEC boundary. The scattering from a PEC material is obtained if the material parameters are defined as $\varepsilon_r = \infty$ and $\mu_r = 0$. Scattering from

PEC objects is one common problem investigated in electromagnetics.

Consider a homogeneous sphere of size parameter $k_0 a = 2$. The sphere is discretized

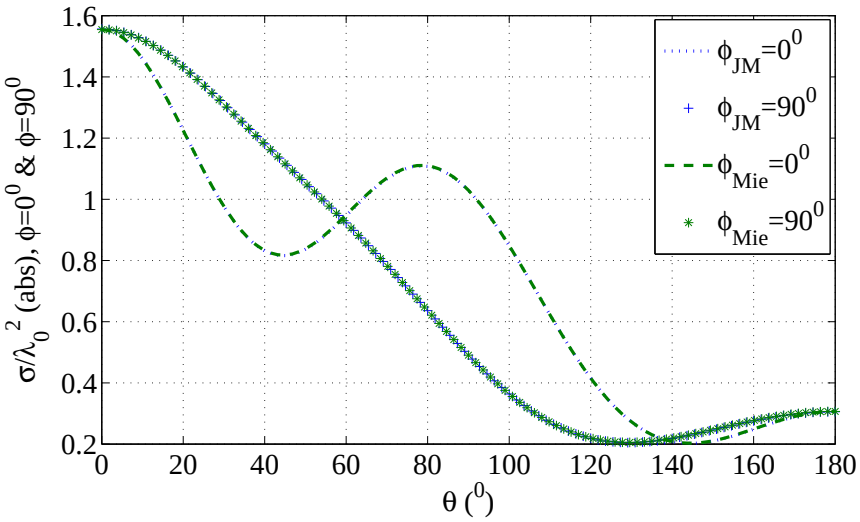

Figure 15: Bistatic SCS $\phi = 0^0$ (E-plane) and $\phi = 90^0$ (H-plane) of a homogeneous sphere of size $k_0 r = 2$ and $\varepsilon_r = 100$, $\mu_r = 1e^{-10}$.

into 53124 domain elements. The constitutive parameters of the sphere are defined as, $\varepsilon = 100$, $\mu = 1e^{-10}$. The sphere is illuminated by a plane electromagnetic wave propagating in the z direction with electric field oriented along the $x-$axis, i.e. $\boldsymbol{E}^i = E_0 e^{-jk_0 z}\hat{\boldsymbol{x}}$ and $\eta_0 \boldsymbol{H}^i = H_0 e^{-jk_0 z}\hat{\boldsymbol{y}}$, where $E_0 = 1\ [V/m]$.

It is found that the PEC condition is numerically difficult to implement and requires a very fine meshing of the domain. The numerical results for the JM-formulation are found to be in good agreement with the Mie-series solution. The results from the AVFU-formulation for a maximum mesh density of 8279 tetrahedrons are not acceptable.

5.3.6 Chiral Sphere

Scattering from chiral spheres has been studied extensively in [1], [2] and [33] etc. The important property of chiral media is that the existence of chirality $\bar{\bar{\xi}}$ of chiral material spheres decreases the bistatic SCS compared with normal dielectric or magnetic spheres. The scattering from chiral spheres is studied in this section. The spheres are illuminated by a plane electromagnetic wave propagating in the z direction with electric field oriented along the $x-$axis, i.e. $\boldsymbol{E}^i = E_0 e^{-jk_0 z}\hat{\boldsymbol{x}}$ and $\eta_0 \boldsymbol{H}^i = H_0 e^{-jk_0 z}\hat{\boldsymbol{y}}$, where $E_0 = 1\ [V/m]$.

The Chiral Sphere is a model problem that is discussed in [2], the radius of the sphere is $0.8\lambda_0$ and the constitutive parameters are $\bar{\bar{\varepsilon}}_r = 1.5\bar{\bar{I}}$, $\bar{\bar{\mu}}_r = 1.5\bar{\bar{I}}$, $\bar{\bar{\xi}}_r = -\bar{\bar{\zeta}}_r = -j0.2\bar{\bar{I}}$.

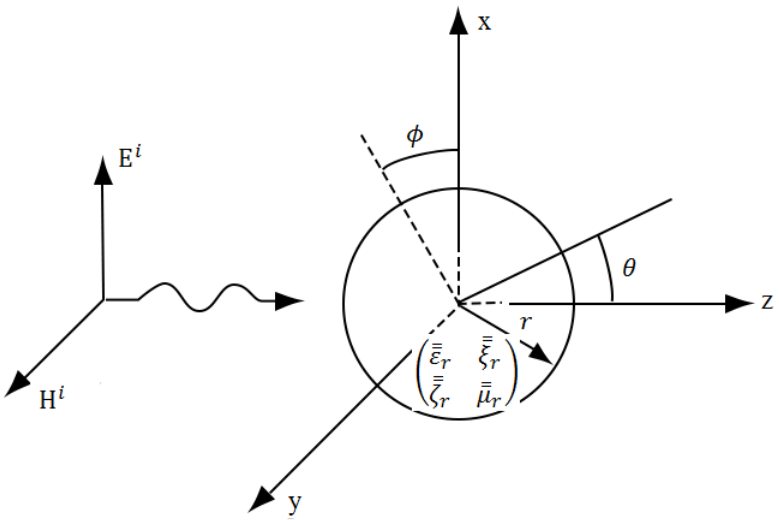

Figure 16: Geometry of chiral sphere.

The numerical results produced using the JM-formulation are found to be in good agreement with the Mie-series solution presented in [2], the solutions produced using AVFU-formulation also agree well but due to discretization limitations some numerical error is associated as shown in Figs 17 and 18.

Next, the scattering from a chiral sphere of radius $r = 0.015$ m is investigated [33]. The

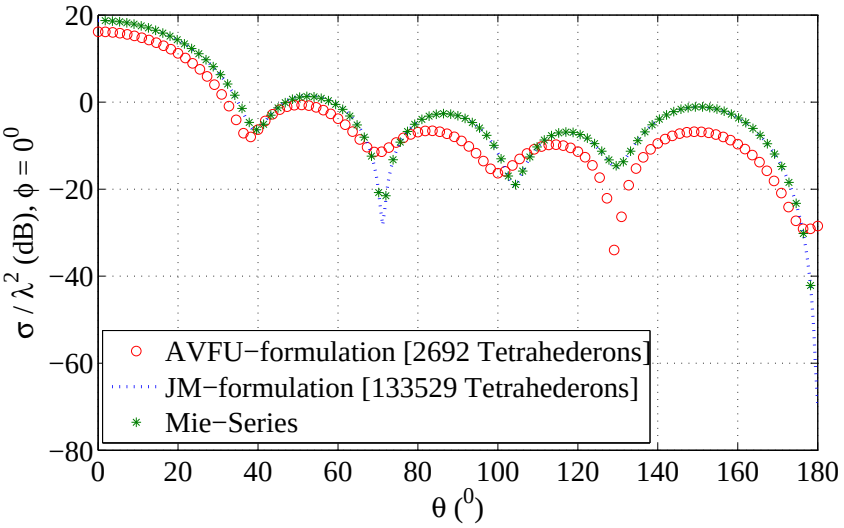

Figure 17: Co-polarized bistatic SCS $\sigma_{\theta\theta}$ of a chiral sphere, $r = 0.8\lambda_0$ and $\bar{\bar{\varepsilon}}_r = 1.5\bar{\bar{I}}$, $\bar{\bar{\mu}}_r = 1.5\bar{\bar{I}}$, $\bar{\bar{\xi}}_r = -\bar{\bar{\zeta}}_r = -j0.2\bar{\bar{I}}$.

constitutive parameters of the sphere are $\bar{\bar{\varepsilon}}_r = [4 + j0.001]\bar{\bar{I}}$, $\bar{\bar{\mu}}_r = [1 + j0.001]\bar{\bar{I}}$ and

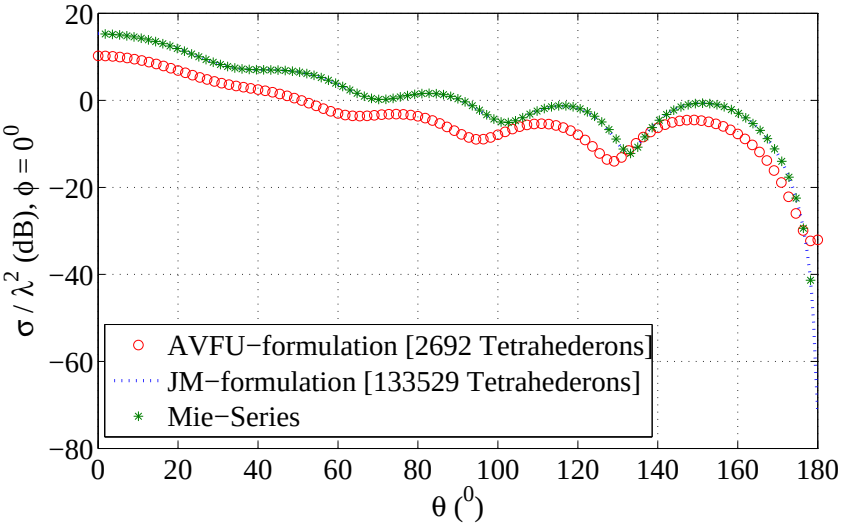

Figure 18: Co-polarized bistatic SCS $\sigma_{\theta\phi}$ of a chiral sphere, $r = 0.8\lambda_0$ and $\bar{\bar{\varepsilon}}_r = 1.5\bar{\bar{I}}$, $\bar{\bar{\mu}}_r = 1.5\bar{\bar{I}}$, $\bar{\bar{\xi}}_r = -\bar{\bar{\zeta}}_r = -j0.2\bar{\bar{I}}$.

$\bar{\bar{\xi}}_r = [0.1 + j0.001]\bar{\bar{I}}$. The frequency of the incident electromagnetic radiation is 9.375 GHz.

The co- and cross-polarized bistatic SCS produced using the JM-formulation are found to be in good agreement with the Mie-series solution presented in [33] as shown in Figs 19 $-$ 22.

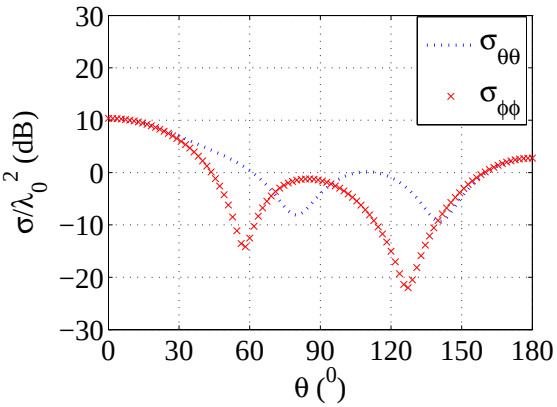

Figure 19: Co-polarized bistatic SCS $\sigma_{\theta\theta}$ and $\sigma_{\phi\phi}$ of chiral sphere.

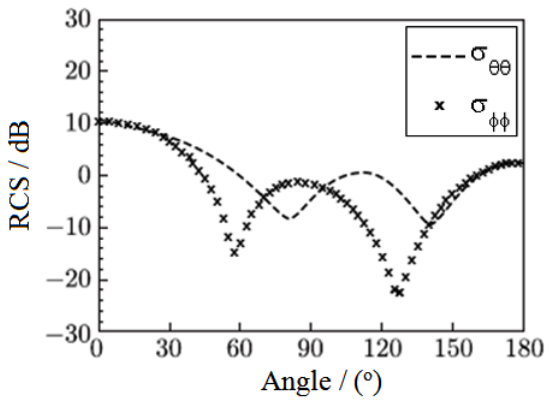

Figure 20: Co-polarized bistatic SCS $\sigma_{\theta\theta}$ and $\sigma_{\phi\phi}$ of chiral sphere from [33].

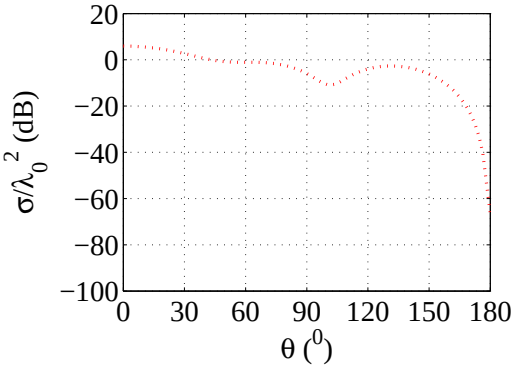

Figure 21: Cross-polarized bistatic SCS $\sigma_{\theta\phi} = \sigma_{\phi\theta}$ of chiral sphere.

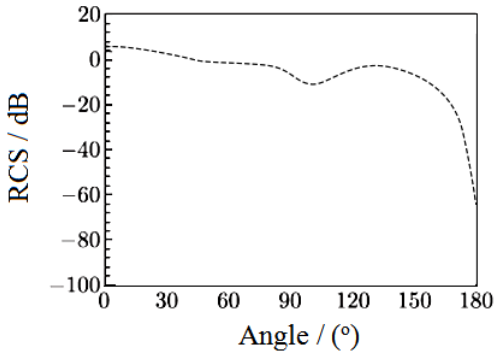

Figure 22: Cross-polarized bistatic SCS $\sigma_{\theta\phi} = \sigma_{\phi\theta}$ of chiral sphere from [33].

5.3.7 Chiral Double Negative Sphere

The scattering from chiral double negative sphere is discussed in [33], the sphere has a radius of 0.015 m , the constitutive parameters are $\bar{\bar{\varepsilon}}_r = [-4.0 + j0.001]\bar{\bar{I}}$, $\bar{\bar{\mu}}_r = [-1.0 + j0.001]\bar{\bar{I}}$, $\bar{\bar{\xi}}_r = -\bar{\bar{\zeta}}_r = [0.1 + j0.001]\bar{\bar{I}}$ and the frequency of incident plane electromagnetic wave is 9.375 GHz.

As shown in Figs $23 - 26$ the co- and cross-polarized SCS produced using the JM-formulation are in good agreement with the Mie-series solution presented in [33].

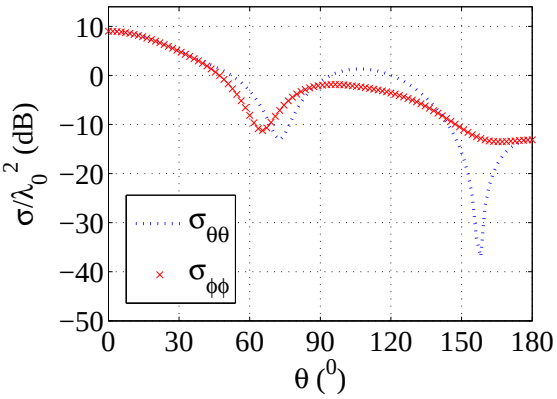

Figure 23: Co-polarized bistatic SCS $\sigma_{\theta\theta}$ and $\sigma_{\phi\phi}$ of a chiral metamaterial sphere.

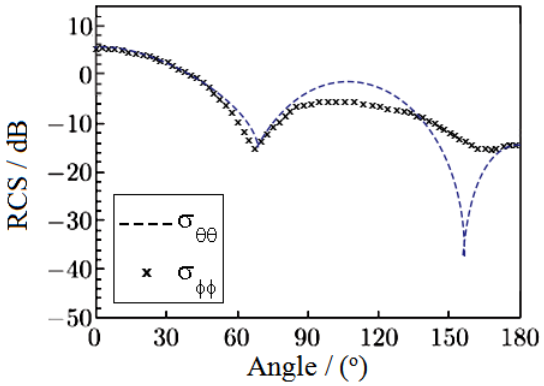

Figure 24: Co-polarized bistatic SCS $\sigma_{\theta\theta}$ and $\sigma_{\phi\phi}$ of a chiral double negative sphere from [33].

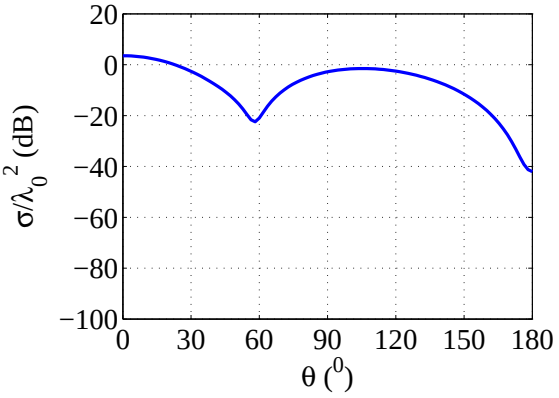

Figure 25: Cross-polarized bistatic SCS $\sigma_{\theta\phi} = \sigma_{\phi\theta}$ of a chiral double negative sphere.

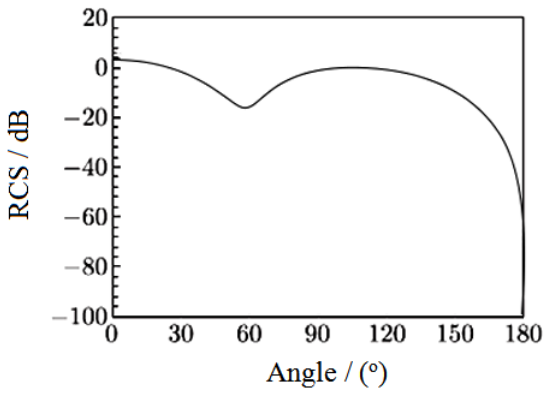

Figure 26: Cross-polarized bistatic SCS $\sigma_{\theta\phi} = \sigma_{\phi\theta}$ of a chiral double negative sphere from [33].

5.3.8 Gyroelectric Sphere

Consider a homogeneous gyroelectric sphere $k_0 r = 0.5$ that has a relative permittivity dyadic defined as $\bar{\bar{\varepsilon}}_r = \begin{bmatrix} 5 & j & 0 \\ -j & 5 & 0 \\ 0 & 0 & 7 \end{bmatrix}$ and relative permeability $\bar{\bar{\mu}}_r = \bar{\bar{I}}$.
The sphere is discretized into 2613 and 8257 domain elements for the JM-formulation

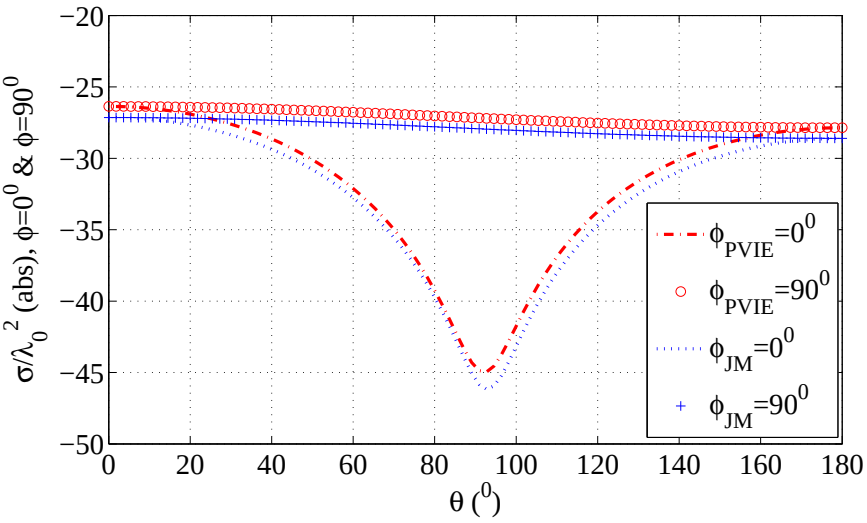

Figure 27: Bistatic scattering cross section $\phi = 0^0$ (E-plane) and $\phi = 90^0$ (H-plane) of a gyroelectric sphere, $k_0 r = 0.5$ and $\varepsilon_{r_{xx}} = \varepsilon_{r_{yy}} = 5$, $\varepsilon_{r_{zz}} = 7$, $\varepsilon_{r_{xy}} = -\varepsilon_{r_{yx}} = j$, $\mu_r = 1$.

and AVFU-formulation, respectively. The sphere is then illuminated by a plane electromagnetic wave propagating in the z direction with electric field oriented along the $x-$axis,

i.e. $\boldsymbol{E}^i = E_0 e^{-jk_0 z}\hat{\boldsymbol{x}}$ and $\eta_0 \boldsymbol{H}^i = H_0 e^{-jk_0 z}\hat{\boldsymbol{y}}$, where $E_0 = 1\ [V/m]$.
The numerical results produced using the JM-formulation and AVFU-formulation are found to be near exact to the solutions presented in [1].

5.3.9 Gyroelectric Shell

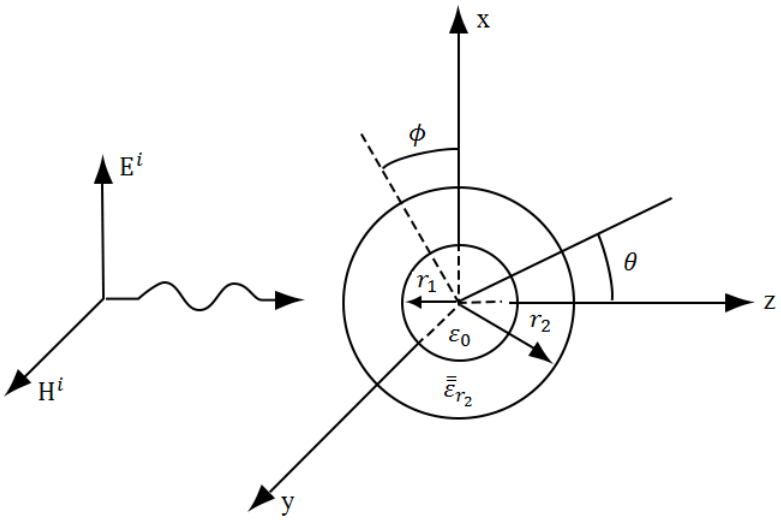

Figure 28: Geometry of gyroelectric spherical shell.

In this section the SCS of a gyroelectric shell is presented. The shell has an outer layer of gyroelectric material and inside is air. The radius of the outer layer is $r_2 = 0.6\lambda_0$ and $r_2/r_1 = 2$. The gyroelectricty of the outer layer is defined as $\bar{\bar{\varepsilon}}_{r_2} = \begin{bmatrix} 5 & j & 0 \\ -j & 5 & 0 \\ 0 & 0 & 7 \end{bmatrix}$ and relative permeability is $\bar{\bar{\mu}}_{r_2} = \bar{\bar{I}}$.

The shell is discretized into 8151 tetrahedrons and is illuminated by a plane electromagnetic wave propagating in the z direction with electric field oriented along the $x-$axis, i.e. $\boldsymbol{E}^i = E_0 e^{-jk_0 z}\hat{\boldsymbol{x}}$ and $\eta_0 \boldsymbol{H}^i = H_0 e^{-jk_0 z}\hat{\boldsymbol{y}}$, where $E_0 = 1\ [V/m]$.
The numerical results produced using the JM-formulation and AVFU-formulation are found to be in great agreement with the solutions presented in [2] as can been seen from Figs $29 - 31$.

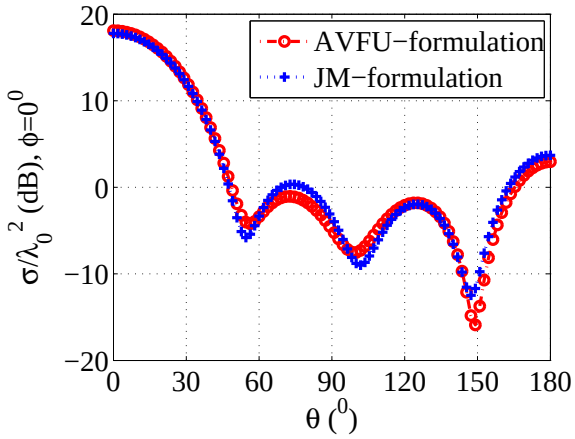

Figure 29: Bistatic scattering cross section $\phi = 0^0$ (E-plane) of gyroelectric shell.

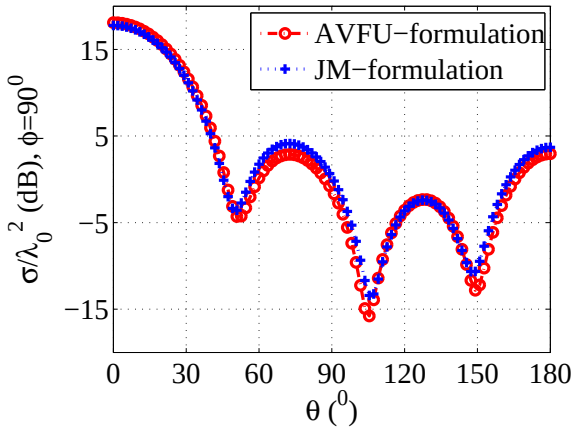

Figure 30: Bistatic scattering cross section $\phi = 90^0$ (H-plane) of gyroelectric shell.

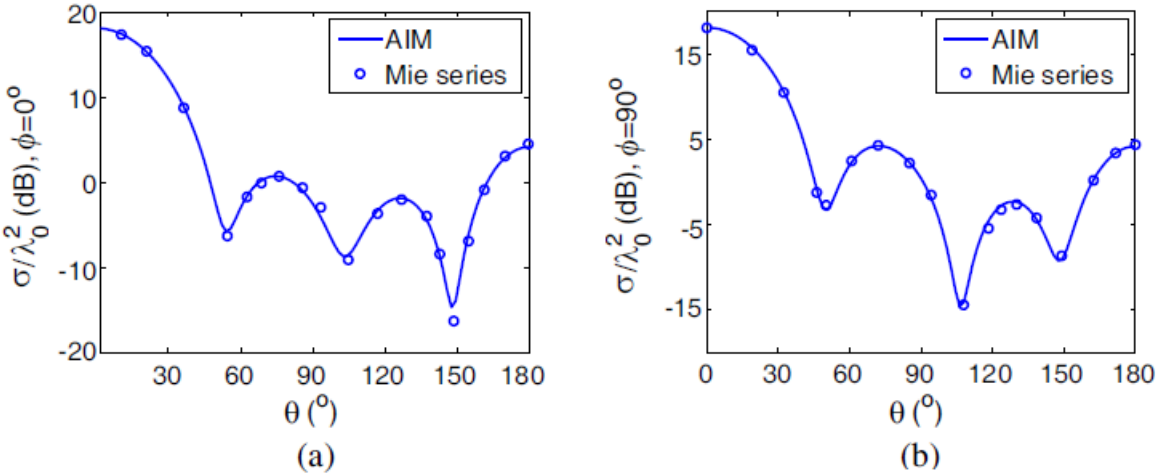

Figure 31: Reference [2] bistatic scattering cross section (a) $\phi = 0^0$ (E-plane) and (b) $\phi = 90^0$ (H-plane) of gyroelectric shell of inner radius $r_1 = 0.3\lambda_0$, outer radius $r_2 = 0.6\lambda_0$, $\varepsilon_{r_{xx}} = \varepsilon_{r_{yy}} = 2.5$, $\varepsilon_{r_{zz}} = 1.5$, $\varepsilon_{r_{xy}} = -\varepsilon_{r_{yx}} = j$, $\mu_r = 1$.

5.4 Solution Accuracy vs Mesh Density Analysis

In this section the aim is to study the solution accuracy as function of mesh density. The scatterer under study is a cube ($k_0 l = 0.5$). Two cases are investigated, a Gyroelectric cube with material parameters $\bar{\bar{\varepsilon}}_r = \begin{bmatrix} 2.5 & j & 0 \\ -j & 2.5 & 0 \\ 0 & 0 & 1.5 \end{bmatrix}$ and relative permeability $\bar{\bar{\mu}}_r = \bar{\bar{I}}$ and a chiral cube with material parameters $\bar{\bar{\varepsilon}}_r = 4\bar{\bar{I}}$, $\bar{\bar{\mu}}_r = \bar{\bar{I}}$, $\bar{\bar{\xi}}_r = -\bar{\bar{\zeta}}_r = j0.2\bar{\bar{I}}$. The cube is illuminated by a plane electromagnetic wave propagating in the z direction with

electric field oriented along the $x-$axis, i.e. $\boldsymbol{E}^i = E_0 e^{-jk_0 z}\hat{\boldsymbol{x}}$ and $\eta_0 \boldsymbol{H}^i = H_0 e^{-jk_0 z}\hat{\boldsymbol{y}}$, where $E_0 = 1\ [V/m]$.

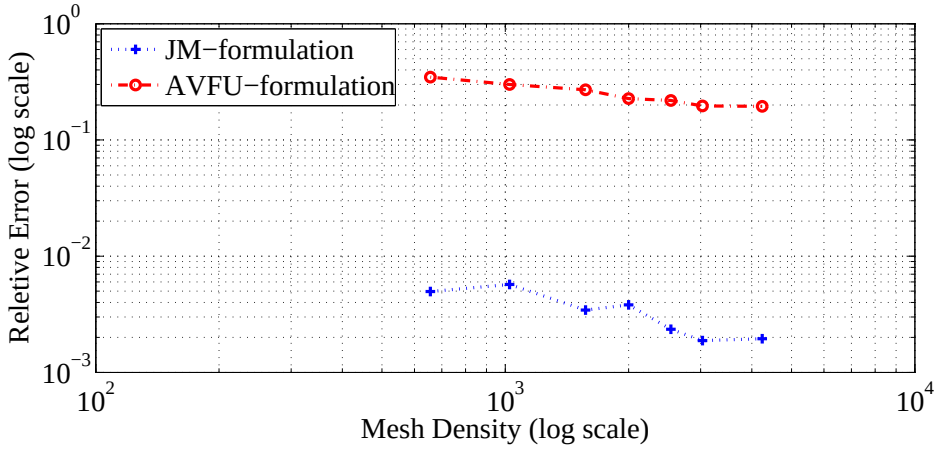

Figure 32: Relative error vs mesh density analysis of a chiral cube ($k_0 l = 0.5$) and $\bar{\bar{\varepsilon}}_r = 4\bar{\bar{I}}$, $\bar{\bar{\mu}}_r = \bar{\bar{I}}$, $\bar{\bar{\xi}}_r = -\bar{\bar{\zeta}}_r = j0.2\bar{\bar{I}}$.

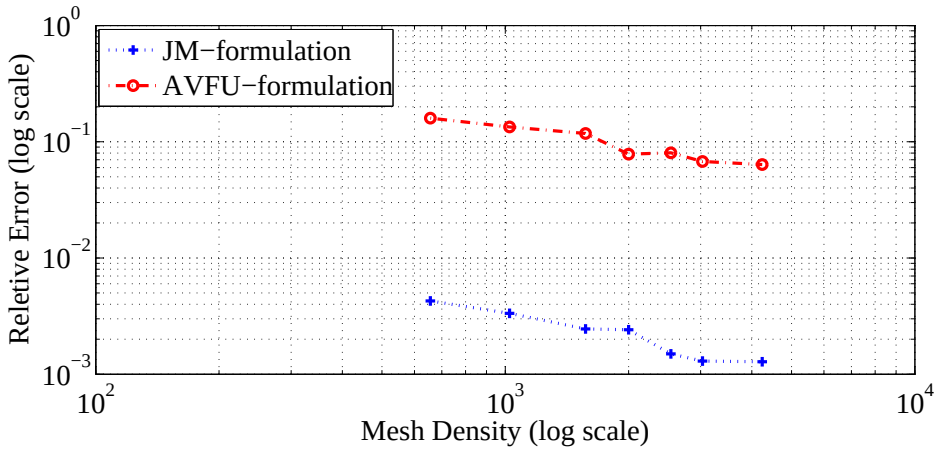

Figure 33: Relative error vs mesh density analysis of a gyroelectric cube ($k_0 l = 0.5$) and $\varepsilon_{r_{xx}} = \varepsilon_{r_{yy}} = 2.5$, $\varepsilon_{r_{zz}} = 1.5$, $\varepsilon_{r_{xy}} = -\varepsilon_{r_{yx}} = j$, $\mu_r = 1$.

Figures 32 and 33 show the relative error as a function of mesh density of a chiral and gyroelectric cube, respectively. Reference results are produced using the JM-formulation with the cube descritized into 41000 tetrahedrons. It is observed that the JM-formulation gives better accuracy than the AVFU-formulation in both the cases. The relative error decreases as the mesh density is increased in both cases but for the chiral cube the relative error with the JM-formulation is found to be oscillating.

6 Conclusion

In this master thesis work, volume integral equations formulated in terms of the current densities ($\boldsymbol{J}$ and $\boldsymbol{M}$) and potentials ($\boldsymbol{A}$, V, $\boldsymbol{F}$ and U) are investigated. The validation of the JM-formulation is checked and a CEM model is developed for the AVFU-formulation. A general description is also given on formulating and implementing volume integral equations for the DB- and EH- formulations. The AVFU-formulation is coded in Matlab. The scattering cross section of simple isotropic spheres to complex bianisotropic spheres is investigated and the obtained results are found to be in good agreement with the available results in literature and analytical Mie-series solutions. The only numerical property that is investigated is the convergence of the solutions as a function of mesh density for a gyroelectric and a chiral cube of size parameter $k_0 l = 0.5$. Since GMRES and MLFMA are not applied to the AVFU-formulation, the size of the scatterer and complexity in terms of material parameters is limited. The document is put so that it can be easily followed to develop and implement volume integral equations based on fields ($\boldsymbol{E}$ and $\boldsymbol{H}$), flux densities ($\boldsymbol{D}$ and $\boldsymbol{B}$), current densities ($\boldsymbol{J}$ and $\boldsymbol{M}$) or potentials ($\boldsymbol{A}$, V, $\boldsymbol{F}$ and U).

The implementation of GRMES and MLFMA to the AVFU-formulation will help analyzing the scattering from more complex and large scatterers, as the available results in literature or analytical solutions are available for simple geometries such as spheres only and with very limited material complexity. In this master thesis the AVFU-formulation is formulated such that the surface integrals are avoided by using the Lorenz Gauge. Preliminary research with AVFU-formulation that includes surface integrals ([4] and [5]) proves to provide much better accuracy then the current implemented formulation and is to be investigated further. The excitation problem associated with the AVFU-formulation is to be solved as well. The numerical characteristics of the JM- and AVFU- formulations such as the solution accuracy as a function of size and material parameters, the conditioning of the matrices and eigenvalue value analysis are to be studied in the future. It has been found that Galerkin's technique does not work with AVFU-formulation if linear nodal basis functions are used to expand the unknowns, as a next step the Galerkin's technique is to be applied to the AVFU-formulation by using higher order basis functions. Further, the properties of the JM-formulation are also to be investigated when higher-order basis functions are implemented.

References

[1] C. Mei, M. Hasanovic, J. K. Lee, and E. Arvas, "Comprehensive solution to scattering by bianisotropic objects of arbitrary shape," Progress in Electromagnetic Research B, Vol.42, pp. 335-362, 2012. doi:10.2528/PIERB12062009 http://www.jpier.org/pierb/pier.php?paper=12062009

[2] L. Hu, L.-W. Li, and T.-S Yeo, "Analysis of scattering by large inhomogeneous bianisotropic objects using AIM," Progress in Electromagnetic Research, PIER 99, pp. 21-36, 2009.

[3] J. Markkanen, P. Ylä-Oijala, A. Sihvola, "Discretization of volume integral equation formulations for extremely anisotropic materials," *IEEE Trans. Antennas Propagat.,* vol. 60, no. 11, pp. 5195-5202, Nov. 2012.

[4] P. De Doncker, "A potential integral equations method for electromagnetic scattering by penetrable bodies,"*IEEE Trans. Antennas Propagat.,* vol. 49, no. 7, pp. 779-782, July 2001.

[5] P. De Doncker, "A volume/surface potential formulation of the method of moments applied to electromagnetic scattering," Engineering Analysis with Boundary Elements, Elsevier 27 (2003), pp. 325-331.

[6] R. Chang and V. Lomakin, "Potential-based volume integral equations," *IEEE Int. Symp. on Antennas and Propagat. (APSURSI),* pp. 2712-2715, 2011.

[7] W. C. Chew, J. M. Jin, E. Michielssen, J. M. Song, "*Fast and Efficient Algorithms in Computational Electromagnetics*," UK: Artech House, 2001.

[8] D. B. Davidson, "*Computational Electromagnetics for RF and Microwave Engineering*," UK: Cambridge University press, 2011.

[9] E. K. Miller, "A selective survey of computational electromagnetics," *IEEE Trans. Antennas Propagat.,* vol. 36, no. 9, pp. 1281-1305, September 1988.

[10] C. A. Balanis, "*Advanced Engineering Electromagnetics*," USA: John Wiley & Sons, Inc., 1989.

[11] D. K. Cheng, "*Field and Wave Electromagnetics*," USA: Addison-Wesley Publishing Company, Inc., 1989.

[12] J. A. Kong, "*Theory of Electromagnetic waves*," New York, USA: Wiley Interscience, 1975.

[13] A. Sihvola, "Chiral and bi-anisotropic mixtures," in *Electromagnetic Mixing Formulas and Applications,* IEE Electromagnetic Wave Series 47. Hertfordshire, United Kingdom: IEE, 1999, ch. 6, pp. 113-130.

[14] J. L. Volakis, K. Sertel, "*Integral Equation Methods for Electromagnetics*," USA: SciTech Publishing, Inc., 2012.

[15] C. F. Bohren, D. R. Huffman, "*Absorption and Scattering of Light by Small Particles*," Germany: WILEY-VCH, 2004.

[16] M. Gouda, "The method of moment for the electromagnetic scattering from bodies of revolution," Master's thesis, University of Boras, Sweden, 2008.

[17] J.-M. Jin, "*The Finite Element Method in Electromagnetics*," New York, USA: John Wiley & Sons, Inc., 2002.

[18] A. J. Burton and G. F. Miller, "The application of integral equation methods to the numerical solution of some exterior boundary-value problems," *Proc. Roy. Soc. Lond.,* vol. 323, no. 1553, pp. 201-210, June 1971.

[19] R. F. Harrington, "*Time-Harmonic Electromagnetic Fields*," New York, USA: MaGraw-Hill, 1961.

[20] M. Taskinen and P. Ylä-Oijala, "Current and charge integral equation formulation," *IEEE Trans. Antennas Propagat.,* vol. 54, no. 1, pp. 58-67, Jan. 2006.

[21] R.F. Harrington, "Matrix methods for field problems,"*IEEE Proc.,* vol. 55, pp. 136-49, Feb. 1967.

[22] R.F. Harrington, "*Field Computation by Moment Methods*," NewYork:The Macmillan Company, 1968.

[23] L. E. Sun and W. C. Chew, "A novel formulation of the volume integral equation for electromagnetic scattering," *Waves in Random and Complex Media,* vol. 19, no. 1, pp. 162-180 2009.

[24] J. P. Webb, "Hierarchal vector basis functions of arbitrary order for triangular and tetrahedral finite elements," *IEEE Trans. Antennas Propag.,* vol. 47, no. 8, pp. 1244-1253 1999.

[25] N. A. Ozdemir and J.-F. Lee, "A nonconformal volume integral equation for electromagnetic scattering from penetrable objects," *IEEE Trans. Magn.,* vol. 43, no. 4, pp. 1369-1372 2007.

[26] K. Sertel and J. L. Volakis, "Multilevel fast multipole method solution of volume integral equations using parametric geometry modeling," *IEEE Trans. Antennas Propag.,* vol. 52, no. 7, pp. 1686-1692 2004.

[27] D. Schaubert, D. Wilton, A. Glisson, "A tetrahedral modeling method for electromagnetic scattering by arbitrarily shaped inhomogeneous dielectric bodies," *IEEE Trans. Antennas Propag.,* vol. 32, no.1, pp. 77-85, January 1984.

[28] J. Markkanen, P. Ylä-Oijala, A. Sihvola, "Computation of scattering by DB objects with surface integral equation method ," *IEEE Trans. Antennas Propagat.,* vol. 59, no. 1, pp. 154-161, Jan. 2011.

[29] M. C. van Beurden and S. J. L. van Eijndhoven, "Gaps in present discretization schemes for domain integral equations," *International Conference on Electromagnetics in Advanced Application, ICEAA,* 2007, Torino.

[30] M. C. van Beurden and S. J. L. van Eijndhoven, "Well-posedness of domain integral equations for a dielectric object in homogenous background," *J Eng Math,* 62:289-302, 2008.

[31] S. Järvenpää, M. Taskinen, P. Ylä-oijala, "Singularity subtraction technique for high-order polynomial vector basis functions on planar triangles," *IEEE Trans. Ant. Propag.,* vol. 54, no. 1 pp. 42-49, Jan 2006.

[32] A. Sihvola, et al., "Scattering by DB Spheres," *IEEE Antennas and Wireless Propagat. Letters,* vol. 8, pp. 542-545, May 2009.

[33] M. Wang, et al., "Mie series for electromagnetic scattering of chiral metamaterials sphere," *Journal of Systems Engineering and Electronics,* vol. 22, no. 6, pp. 885-891, Dec. 2011